



THE HONG KONG  
POLYTECHNIC UNIVERSITY

香港理工大學

Pao Yue-kong Library

包玉剛圖書館

---

## Copyright Undertaking

This thesis is protected by copyright, with all rights reserved.

**By reading and using the thesis, the reader understands and agrees to the following terms:**

1. The reader will abide by the rules and legal ordinances governing copyright regarding the use of the thesis.
2. The reader will use the thesis for the purpose of research or private study only and not for distribution or further reproduction or any other purpose.
3. The reader agrees to indemnify and hold the University harmless from and against any loss, damage, cost, liability or expenses arising from copyright infringement or unauthorized usage.

### IMPORTANT

If you have reasons to believe that any materials in this thesis are deemed not suitable to be distributed in this form, or a copyright owner having difficulty with the material being included in our database, please contact [lbsys@polyu.edu.hk](mailto:lbsys@polyu.edu.hk) providing details. The Library will look into your claim and consider taking remedial action upon receipt of the written requests.

**RISK- AND RESILIENCE-BASED LIFE-CYCLE  
ANALYSIS OF ENGINEERING STRUCTURES UNDER  
MULTIPLE HAZARDS**

**YAOHAN LI**

**The Hong Kong Polytechnic University**

**2022**

The Hong Kong Polytechnic University

Department of Civil and Environmental Engineering

**Risk- and Resilience-Based Life-Cycle Analysis of  
Engineering Structures under Multiple Hazards**

**Yaohan LI**

A thesis submitted in partial fulfilment of the requirements for the degree  
of Doctor of Philosophy

Jun 2021

## **CERTIFICATE OF ORIGINALITY**

I hereby declare that this thesis is my own work and that, to the best of my knowledge and belief, it reproduces no material previously published or written, nor material that has been accepted for the award of any other degree or diploma, except where due acknowledgement has been made in the text.

\_\_\_\_\_ (Signed)

\_\_\_\_\_ LI Yaohan (Name of student)

*This thesis is dedicated to my family  
for their love and support*

## **ABSTRACT**

In recent decades, the devastating effects that hazards have on societies worldwide have intermittently raised the attention of governments and the public to hazard risk assessment and management. For civil infrastructure, various hazards (e.g., earthquakes, hurricanes, and progressive deterioration) can lead to damage and failure of the system. They may impair structural functionality and result in severe social disruption and economic losses. Additionally, due to various sources of uncertainty, multiple hazards may interact and cause amplification of the adverse effects on the system. In a life-cycle context, the hazard-induced losses can be accumulated, thus resulting in a considerable reduction in the resilience of civil infrastructure. Therefore, it is of paramount importance to assess the risk and enhance the resilience of civil infrastructure subjected to multi-hazard scenarios in a life-cycle context. This thesis aims to develop a risk- and resilience-based life-cycle analysis framework for engineering structures under multiple hazards. The proposed framework consists of different segments: scenario-based multi-hazard analysis, structural vulnerability assessment, quantification of long-term loss and resilience, and life-cycle management of civil infrastructure subjected to multiple hazards. The uncertainties springing from each segment are considered and evaluated.

The probabilistic hazard analysis and structural vulnerability assessment play fundamental roles in the life-cycle analysis. Most previous studies paid attention to the impact of the single hazard and neglected the compound effects of multi-hazard effects. For instance, neglecting the compounding effect of hurricane events may lead to

underestimation of the structural vulnerability and provide inappropriate inputs for the life-cycle analysis. In this thesis, a copula-based multivariate approach is proposed to model the correlation between hazard parameters based on historical records. By identifying the correlation between hazard parameters, the structural vulnerability subjected to the multi-hazard scenarios can be assessed.

Given the hazard analysis and structural vulnerability, risk and resilience can be employed to assess the performance of the engineering structures under hazards. Different from previous studies focusing on a single hazard, this thesis proposes two indicators (i.e., long-term resilience and loss) to assess the long-term performance of systems under stationary and nonstationary hazards. A general approach is developed to quantify long-term loss (i.e., damage cost) and resilience considering uncertainties associated with hazard frequency and intensity. Specifically, the renewal theory is used to assess the performance under stationary hazards, and the moment generating function approach is developed to address uncertainty resulting from the nonstationary occurrence.

In addition to uncertainties of hazards, uncertainties in terms of long-term loss cannot be ignored. Though the minimum expectation of long-term loss has been applied as a standard criterion, uncertainties associated with the other statistical moments, especially the higher-order moments (i.e., skewness and kurtosis) have been neglected in previous research. Therefore, in addition to the lower-order moments (i.e., mean and standard deviation), this thesis provides a higher-order analysis for the long-term loss assessment. The higher-order moments can be significant parameters in the decision-making process during life-cycle management.

Subsequently, a probabilistic life-cycle management framework can be proposed to incorporate various performance indicators and uncertainties. As the performance of civil infrastructure degrades with time due to exposure to multiple hazards, a reliability-based approach is proposed to describe structural performance. Gradual deterioration caused by environmental exposure and extreme events are taken into account. The combined effects and the interaction between different deterioration processes are also explored in the proposed life-cycle framework. Based on the time-dependent reliability assessment, the maintenance policy can be developed. Herein, the impact of correlated maintenance interval and cost on the life-cycle cost is highlighted. Such correlation has been commonly neglected in previous studies. A copula-based renewal model is proposed to quantify statistical moments of the life-cycle maintenance cost analytically and numerically. The proposed model delivers an effective approach for data-based decision-making and life-cycle management of ageing engineering structures. Illustrative examples are presented to demonstrate the proposed framework. Results reveal the significance of considering interactions among deterioration processes, correlated maintenance interval and cost, and higher-order moments during the life-cycle analysis.

Overall, this thesis provides methodologies to address risk- and resilience-based life-cycle assessment and management of engineering structures. A life-cycle analysis framework of ageing civil infrastructure under multiple hazards is proposed. Multi-hazard effects are considered in the proposed framework including continuous deterioration and external extreme hazards (e.g., earthquakes and hurricanes). The proposed framework is applied and illustrated by several engineering applications focusing on highway bridges. The proposed framework can be applied to assist

decision-makers in planning risk mitigation strategies and enhancing infrastructural resilience in a life-cycle context.

# LIST OF PUBLICATIONS

## Journal articles

- Li, Y.**, Dong, Y. \*, and Qian, J. (2020). Higher-order analysis of probabilistic long-term loss under nonstationary hazards. *Reliability Engineering & System Safety*, 203, 107092.
- Li, Y.**, Dong, Y. \*, Frangopol, D. M., and Gautam, D. (2020). Long-term resilience and loss assessment of highway bridges under multiple natural hazards. *Structure and Infrastructure Engineering*, 16(4), 626-641.
- Li, Y.**, Dong, Y. \*, and Zhu, D. (2020). Copula-based vulnerability analysis of civil infrastructure subjected to hurricanes. *Frontiers in Built Environment*, 6, 571911.
- Li, Y.**, Dong, Y. \*, and Guo, H. (2021). Copula-based multivariate renewal model for life-cycle analysis considering multiple dependent deterioration processes. (under review).
- Zhu, D., **Li, Y.**, Dong, Y. \*, and Yuan, P. (2021). Long-term loss assessment of coastal bridges from hurricanes incorporating overturning failure mode. *Advances in Bridge Engineering*, 2(10), 1-15.
- Zhu, D., **Li, Y.**, and Dong, Y. \* (2021). Reliability-based retrofit assessment of coastal bridges subjected to wave forces using 3D CFD simulation and metamodeling. *Civil Engineering and Environmental Systems*, 38(1), 59-83.

- Wu, J. \*, Zhang, L., **Li, Y.**, and Dong, Y. (2021). Prediction of dry shrinkage deformation for partially enclosed steel reinforced concrete columns. *Journal of Building Engineering*, 44, 102675.
- Anwar, G. A., Dong, Y. \*, and **Li, Y.** (2020). Performance-based decision-making of buildings under seismic hazard considering long-term loss, sustainability, and resilience. *Structure and Infrastructure Engineering*, 17(4), 454-470.
- Zheng, Y., Dong, Y. \*, and **Li, Y.** (2018). Resilience and life-cycle performance of smart bridges with shape memory alloy (SMA)-cable-based bearings. *Construction and Building Materials*, 158, 389-400.

## Conference papers

- Li, Y.,** Dong, Y.\* , and Frangopol, D. M. (2021). Probabilistic Long-Term Loss Assessment of Highway Bridges under Hurricanes considering Stochastic Dependence using Copulas. *Proceedings of the 13th International Conference on Structural Safety and Reliability (ICOSSAR 2021)*, Shanghai, P.R. China, Jun 21-25, 2021.
- Li, Y.** and Dong, Y.\* (2021). Life-Cycle Management Considering Correlation, *The 2nd ZHITU Symposium on Advances in Civil Engineering*, Ulsan, South Korea (Virtual Event), Sep 28-29, 2021.
- Li, Y.** and Dong, Y.\* (2021). Probabilistic maintenance cost over life cycle of deteriorating bridges considering stochastic dependence, *Engineering Mechanics Institute Conference and Probabilistic Mechanics & Reliability Conference*, Maryland, USA (Virtual Event), May 25-28, 2021.
- Li, Y.,** and Dong, Y.\* (2020). Life-Cycle Probabilistic Loss and Resilience Quantification of Civil Infrastructure Under Extreme Events. *Proceedings of IABSE Conference: Risk Intelligence of Infrastructures*, Seoul, South Korea, Nov 9-10, 2020.
- Li, Y.,** and Dong, Y.\* (2019). Risk-Informed Hazard Loss of Bridges in a Life-Cycle Context. *Proceedings of the 13th International Conference on Applications of Statistics and Probability in Civil Engineering (ICASPI3)*, Seoul, South Korea, May 26-30, 2019.

**Li, Y.** and Dong, Y.\* (2018). Risk-Informed Assessment of Climate Change on Bridges by Considering Structural Deterioration and Hazards. *Proceedings of 9th International Conference on Bridge Maintenance, Safety and Management (IABMAS 2018)*, Melbourne, Australia, Jul 9-13, 2018.

Dong, Y.\*, Zheng, Y., and **Li, Y.** (2018). Resilience Assessment of Highway Bridges using SAM-based Isolation Bearings. *Proceedings of 9th International Conference on Bridge Maintenance, Safety and Management (IABMAS 2018)*, Melbourne, Australia, Jul 9-13, 2018.

## **ACKNOWLEDGMENTS**

I would like to express my deepest gratitude to my advisor, Dr. You Dong, for his patience, endless support, and excellent guidance during my PhD study at the Hong Kong Polytechnic University. He is always supportive and helpful when I encounter difficulties during my research. His patience and supervision have constantly encouraged me to challenge myself and achieve my goals. Also, I am extremely grateful for his tremendous help during the hard and extraordinary year of the COVID-19 pandemic. I am so fortunate to be his first PhD student and have the opportunity to study under his guidance.

Besides, I would like to express my sincere thanks to my co-supervisor, Prof. Yuhong Wang, for his encouragement and generous support during my study. I would also like to extend my appreciation to Prof. Songye Zhu for his recommendations and assistance during the application of PhD Programme and invaluable comments during my PhD candidature. Additionally, I thank all the professors who shared their thoughts and constructive comments during this process.

My heartfelt thanks should be extended to my current colleagues in Dr. Dong's group including Dr. Peng Yuan, Mses. Menghan Zhao, Qian Wu, and Messrs. Hongyuan Guo, Ghazanfar Ali Anwar, Jing Qian, Deming Zhu, Fuhao Deng, Li Lai, Jiixin Zhang, as well as former colleagues Dr. Bing Tu and Dr. Anastasios Giouvanidis, for their warm support and friendship. Thanks for listening and providing advice throughout the entire study process. In addition, I would like to thank my former and current office mates: Prof. Bin Wang, Dr. Jinli Cui, Dr. Zuolei Du, Dr. Peichen Wu,

Mr. Yu Pan, and Mr. Ang Li for creating a pleasant working environment and inspiring ideas. I am also grateful to express my thanks to my dear friends at the Hong Kong Polytechnic University: Mses. Zimo Zhu, Fei Xu, Zhihang Xue, Qiuhan Meng, Dr. Linhao Zhang, Dr. Lei Huang, Dr. Xiaoyi Lan, Dr. Meng Xiao, Dr. Junbo Chen, Dr. Yishu Yan, Dr. Jinyang Li, Dr. Rongrong Hou, and many others. They have provided valuable suggestions and comments for this work.

Finally, I am forever grateful to my parents Mr. Li and Ms. Gao, who have raised me and taught me to be an independent thinker. Their unconditional love and encouragement have become a driving force of my life. This work would never be possible without their support.

# CONTENTS

<b>CERTIFICATE OF ORIGINALITY .....</b>	<b>i</b>
<b>ABSTRACT .....</b>	<b>iii</b>
<b>LIST OF PUBLICATIONS.....</b>	<b>vii</b>
<b>ACKNOWLEDGMENTS .....</b>	<b>xi</b>
<b>CONTENTS.....</b>	<b>xiii</b>
<b>LIST OF FIGURES.....</b>	<b>xviii</b>
<b>LIST OF TABLES.....</b>	<b>xxiv</b>
<b>CHAPTER 1 INTRODUCTION.....</b>	<b>1</b>
1.1 Overview and background .....	1
1.2 Objectives and scope .....	4
1.3 Thesis organizations .....	5
1.4 Contributions.....	7
<b>CHAPTER 2 LITERATURE REVIEW .....</b>	<b>10</b>
2.1 Introduction.....	10
2.2 Multiple hazards and multivariate analysis .....	10
2.2.1 Evaluation of natural hazards for highway bridges .....	11
2.2.2 Multivariate analysis and copula model .....	22
2.3 Risk and resilience assessment under hazards .....	25

2.3.1 Risk assessment .....	25
2.3.2 Resilience assessment .....	29
2.4. Deterioration modeling and maintenance policy .....	38
2.4.1 Interaction among deterioration processes.....	38
2.4.2 Condition-based maintenance .....	40
2.5 Research Gaps .....	41
<b>CHAPTER 3 PROBABILISTIC HAZARD ANALYSIS AND STRUCTURAL PERFORMANCE UNDER SINGLE HAZARD .....</b>	<b>43</b>
3.1 Introduction.....	43
3.2 Structural performance under earthquakes .....	44
3.2.1 Probabilistic seismic hazard analysis.....	44
3.2.2 Structural vulnerability assessment of highway bridge .....	48
3.3 Structural performance under hurricanes.....	51
3.3.1 Hazard parameters .....	52
3.3.2 Structural vulnerability assessment under hurricanes .....	53
3.4 Summary.....	60
<b>CHAPTER 4 MULTIVARIATE ANALYSIS AND VULNERABILITY ASSESSMENT UNDER COMPOUND EXTREME EVENTS .....</b>	<b>61</b>
4.1 Introduction.....	61
4.2 Multivariate dependence model .....	62
4.3 Multivariate hazard analysis under hurricanes.....	68

4.4 Illustrative example .....	73
4.5 Summary .....	86
<b>CHAPTER 5 LONG-TERM RESILIENCE AND LOSS UNDER STATIONARY HAZARDS USING RENEWAL APPROACH .....</b>	<b>88</b>
5.1 Introduction.....	88
5.2 Stationary hazard model: homogeneous Poisson process .....	89
5.3 Long-term assessment under stationary hazards.....	90
5.4 Renewal approach for long-term loss and resilience.....	92
5.4.1 Renewal function.....	92
5.4.2 Other applications of renewal approach .....	96
5.4.3 Validation by using Monte Carlo simulation .....	98
5.5 Illustrative example .....	99
5.6 Summary.....	108
<b>CHAPTER 6 HIGHER-ORDER ANALYSIS UNDER NONSTATIONARY HAZARDS IN A LIFE-CYCLE CONTEXT .....</b>	<b>111</b>
6.1 Introduction.....	111
6.2 Nonstationary arrival models .....	113
6.2.1 Non-Poisson renewal process.....	114
6.2.2 Non-homogeneous Poisson process .....	115
6.2.3 Mixed Poisson process.....	116
6.3 Long-term loss under nonstationary hazards .....	117

6.4 Higher-order analysis using moment generating function.....	118
6.4.1 Moment generating function approach.....	119
6.4.2 Moment generating function for homogeneous Poisson case.....	120
6.4.3 Moment generating function for non-homogeneous Poisson case	124
6.4.4 Moment generating function for mixed Poisson case .....	126
6.5 Higher-order moments for renewal case .....	127
6.5.1 Higher-order moments using moment generating function .....	127
6.5.2 Comparison between renewal approach and moment generating function approach.....	131
6.6 Illustrative example .....	132
6.7 Summary.....	140

**CHAPTER 7 LIFE-CYCLE ANALYSIS SUBJECTED TO MULTIPLE  
DEPENDENT DETERIORATION PROCESSES..... 142**

7.1 Introduction.....	142
7.2 Structural deterioration over life-cycle.....	143
7.2.1 Gradual deterioration .....	143
7.2.2 Shock deterioration: external shock and fatal shock .....	144
7.3 System reliability analysis .....	145
7.3.1 Stochastic demand and capacity.....	146
7.3.2 Failure mechanisms and limit state function.....	148
7.3.3 Dependence between deterioration processes .....	149

7.4 Illustrative example .....	151
7.5 Summary .....	158
<b>CHAPTER 8 A COPULA-BASED LIFE-CYCLE MANAGEMENT FRAMEWORK OF DETERIORATING SYSTEMS .....</b>	<b>160</b>
8.1 Introduction .....	160
8.2 A copula-based life-cycle analysis framework .....	161
8.2.1 Maintenance policy .....	162
8.2.2 Life-cycle maintenance cost .....	164
8.3 Analytical case: life-cycle analysis with FGM copula .....	171
8.3.1 Expectation and variance of life-cycle maintenance cost .....	172
8.3.2 Higher-order moments of life-cycle maintenance cost .....	178
8.4 Illustrative examples .....	179
8.4.1 Data-based decision making and higher-order moments .....	179
8.4.2 Effect of copulas on life-cycle maintenance cost .....	186
8.5 Summary .....	192
<b>CHAPTER 9 CONCLUSIONS AND FUTURE WORK .....</b>	<b>194</b>
9.1 Conclusions .....	194
9.2 Suggestions for future research .....	196
<b>REFERENCES .....</b>	<b>198</b>

## LIST OF FIGURES

Figure 1-1 Organization of the thesis and the proposed life-cycle analysis framework. .....	7
Figure 2-1 Computational framework integrating resilience and loss assessment. ....	12
Figure 2-2 (a) Collapsed and washed away bridge due to 2017 flood in Nepal and (b) scouring observed in a bridge in Nepal after the 2017 central Nepal flash flood (photos adapted from (Li <i>et al.</i> 2020a)). .....	15
Figure 2-3 Resilience assessment framework (adapted from ISO (2009))......	31
Figure 3-1 Seismic hazard curve under the investigated seismic scenario.....	48
Figure 3-2 The three-dimensional bridge model with dimensions (unit: meter). .....	49
Figure 3-3 Fragility curves associated with four damage states. ....	50
Figure 3-4 A process diagram to assess the structural performance of highway bridges subjected to hurricanes. ....	52
Figure 3-5 (a) Geometry of bridge superstructure and (b) numerical diagram of computation domain of the FEM model.....	54
Figure 3-6 An illustrated 2D CFD model showing wave behavior acting upon a bridge superstructure changing with time (unit: second).....	56

Figure 3-7 Comparison between numerical and experimental results of the maximum total uplift force acting on the bridge superstructure. ....	57
Figure 4-1 The bridge in Escambia Bay, Florida, and tracks of historical tropical cyclones, including Hurricane Ivan (adapted from NOAA 2020). ....	74
Figure 4-2 (a) Geometry of the bridge deck; (b) The three-dimensional model of the bridge deck; and (c) Diagram of the computational domain of the numerical model. ....	75
Figure 4-3 An illustrative diagram of the wave-air-structure interaction effects in the three-dimensional CFD model. ....	77
Figure 4-4 Scatter plot of observed and simulated maximum wave height and peak water level based on the selected Clayton copula. ....	81
Figure 4-5 Samples of correlated $H$ and $W$ in the copula domain using Hüsler-Reiss, Gaussian, and Clayton copula functions considering Kendall's tau equal to 0.1, 0.5, and 0.9. ....	82
Figure 5-1 The long-term resilience and loss framework based on the stochastic renewal process. ....	92
Figure 5-2 System-level fragility curves for the bridge at different damage stages (adapted from Nielson and DesRoches (2007)). ....	102
Figure 5-3 Time-dependent functionality of four investigated hazard scenarios ( $E_1$ , $E_2$ , $H_1$ , and $H_2$ ). ....	104

Figure 5-4 Long-term resilience for the investigated bridge under earthquake and hurricane hazards using renewal method. ....	105
Figure 5-5 Long-term loss estimation for the investigated bridge under earthquake and hurricane hazards using renewal method (a) for four hazard scenarios (b) for seismic scenarios $E_1$ and $E_2$ .....	106
Figure 5-6 Expected long-term loss affected by (a) financial discount ratio and (b) economic repair loss.....	108
Figure 6-1 Long-term loss model by considering discounting and hazard arrival process. ....	118
Figure 6-2 (a) Expectation and (b) standard deviation of hurricane-induced long-term loss under homogeneous (HPP) and non-homogeneous model (NHPP) by moment generating function (MGF) method and Monte Carlo (MC) simulation. ....	137
Figure 6-3 Standard deviation of hurricane-induced long-term loss under homogeneous (HPP), non-homogeneous (NHPP), and mixed Poisson model by moment generating function (MGF) method and Monte Carlo (MC) simulation. ....	137
Figure 6-4 (a) Expectation and (b) skewness of the long-term loss considering different monetary discount rates.....	138
Figure 6-5 (a) Impact of the variability of loss severity on the long-term loss considering identical expectation $E[L]$ with different standard deviations of loss	

severity $SD[L]$ and (b) the effect of variability of loss severity on the skewness of long-term loss.....	139
Figure 7-1 Schematic diagram of deterioration of system capacity. ....	147
Figure 7-2 Capacity and demand of a system subjected to gradual deterioration and external shock process.....	149
Figure 7-3 Probability of failure considering gradual deterioration, external shock, fatal shock processes, and their interactions. ....	153
Figure 7-4 Effect of dependence among different deterioration processes by considering with dependence ( $\gamma_d = 0.3$ ) and without dependence ( $\gamma_d = 0$ ).....	154
Figure 7-5 Effect of gradual deterioration on the failure probability by considering different expectations of the cumulative gradual deterioration ( $0.1R_0$ , $0.3R_0$ , and $0.5R_0$ ). ....	155
Figure 7-6 Effect of gradual deterioration on the failure probability by considering different COV associated with gradual deterioration.....	155
Figure 7-7 Effect of the external shock deterioration process on the failure probability by considering different mean values of the deterioration amount.....	156
Figure 7-8 Effect of the external shock deterioration process on the failure probability by considering different COV of the deterioration amount.....	157
Figure 7-9 Effect of external shock process on the failure probability by considering different occurrence rates. ....	157

Figure 7-10 Effect of fatal shock process on the failure probability by considering different occurrence rates. ....	158
Figure 8-1 An illustrative diagram of reliability-based preventive maintenance (PM) and essential maintenance (EM) actions. ....	164
Figure 8-2 Assessment of life-cycle maintenance cost using the proposed copula-based multivariate renewal model. ....	170
Figure 8-3 Two maintenance policies with different maintenance interval $W$ and maintenance cost $Z$ . ....	181
Figure 8-4 Scatter plots of the recorded and simulated data of the maintenance interval $W$ and maintenance cost $Z$ of (a) Maintenance Policy 1 and (b) Maintenance Policy 2. ....	182
Figure 8-5 The probability of bridge failing subjected to multiple dependent deterioration processes considering preventive and essential maintenance actions. ....	187
Figure 8-6 (a) Expectation and (b) standard deviation of life-cycle maintenance cost with the FGM copula subjected to Kendall's tau at $-2/9$ , $0$ , and $2/9$ . ....	188
Figure 8-7 Three-dimensional PDFs of different copulas with Kendall's tau = $0.2$ . ....	189
Figure 8-8 Expected life-cycle cost and standard deviation of different dependence scenarios. ....	190

Figure 8-9 The impact of fatal shocks and dependent deterioration processes on the probability of failure and renewal cycle (scenarios are without fatal shocks unless specified)..... 191

## LIST OF TABLES

Table 4-1 Examples of Archimedean copulas and their tail dependence characteristics. .....	66
Table 4-2 Probability of failure of the bridge associated with different copula models under 50-, 75-, 100-, and 500-year hurricane scenarios.....	83
Table 6-1 Statistical moments, i.e., mean, standard deviation (SD), skewness (ske), and kurtosis (kur), of Long-term loss of the bridge under homogeneous, non- homogeneous (NHPP), and mixed Poisson processes. ....	135
Table 8-1 Mean, standard deviation (SD), skewness, and kurtosis of the life-cycle maintenance cost associated with two maintenance policies. ....	183

# CHAPTER 1 INTRODUCTION

## 1.1 Overview and background

During the service life, civil infrastructure is exposed to various hazards (e.g., corrosion, earthquakes, hurricanes, floods). Hazards have either independent or interacting effects with respect to their source, frequency, intensity, and region of impact. According to their interaction relationship, multiple hazards can be divided into three categories: independent, successive, and concurrent. In addition, a single hazard may have a multi-hazard feature. For instance, a hurricane event consists of multiple hazards such as high waves, heavy rain, and strong wind (Gidaris *et al.* 2017; Padgett *et al.* 2008). Neglecting interactions among hazard parameters and the compound effect of multiple hazards may mis-specify hazard characteristics and result in underestimation of severe consequences.

Hazards may devastate the functionality of the system, threaten public safety, and interrupt services, thus leading to devastating consequences. According to the 2021 report card for America's infrastructure (ASCE 2021), there is a total investment need of 5.9 trillion USD for American infrastructure systems to improve the conditions. A similar situation exists in China. By the end of 2019, there are approximately 70,000 number of ageing bridges (accounting for one-twelfth of the total amount) graded as "dangerous" in China (Zhou and Zhang 2019). These ageing bridges require substantial investment in repair and maintenance. In addition to ageing issues, extreme events such as Hurricane Harvey 2017 and Hurricane Irma 2017 bring substantial economic and social losses (Raymond *et al.* 2020). The severe consequence caused by multiple

hazards worldwide intermittently raised the attention of governments and the public to risk assessment and mitigation.

The hazard-induced consequences are commonly measured in terms of financial losses (e.g., repair cost), social losses (e.g., downtime, deaths), and environmental losses (e.g., carbon dioxide emissions). From a long-term perspective, the potential losses can be accumulated and aggravated due to uncertainties throughout the entire life-cycle of civil infrastructure systems (Frangopol and Soliman 2016). The associated uncertainties mainly result from stochastic frequency and magnitude of hazards, structural performance, and consequences (Koduru and Haukaas 2010). Therefore, apart from investigating the performance of a system with respect to a hazard event (e.g., loss and resilience under an earthquake event), it can be more essential to explore the performance in a life-cycle context. Long-term performance indicators incorporating uncertainties are required to assess the structural performance subjected to various hazardous events. These indicators can be significant parameters for decision-makers to propose the optimal design and management strategies.

In addition, various uncertainties associated with the performance indicators, e.g., long-term economic loss, should be captured to provide sufficient information for life-cycle management. In this context, the term ‘long-term loss’ is used to describe the total losses due to the economic cost caused by repair and reconstruction of the damaged structure within the investigated time interval (e.g., service life). In previous studies, analytical assessment of long-term economic loss is typically based on stationary hazards (Wen and Kang 2001). In recent studies, uncertainties and the long-term effects associated with non-stationary characteristics of hazard arrivals have

received increasing attention (Pandey and Van Der Weide 2017; Takahashi *et al.* 2004). For instance, hurricane-induced losses can be significantly influenced by environmental impact and climate change issues (Li *et al.* 2016). In terms of long-term loss, most previous studies focused on the low-order moments (i.e., expectation and variance). Though the minimum expected cost has been widely used as a standard decision criterion, Goda and Hong (2006) indicated the structural design based on the expected life-cycle cost may not be optimal. Therefore, in addition to the mean, it is significant to explore uncertainties associated with extreme losses. The other statistical moments (i.e., standard deviation, skewness, and kurtosis) of the long-term loss should be investigated.

In a life-cycle context, due to the impact of external shocks and environmental exposure, the performance of civil infrastructure degrades with time. Based on the stochastic modeling of hazard occurrence, the associated impact on the system can be described by multiple deterioration processes. Engineering systems typically experience both gradual deterioration (e.g., caused by corrosion, fatigue, and crack growth) and shock deterioration (e.g., caused by occurrence of earthquakes and hurricanes) (Kumar and Gardoni 2014a, 2014b). Assessing the time-dependent structural performance subjected to these deterioration processes plays a fundamental role during the life-cycle analysis. To maintain the performance and functionality of civil infrastructure, maintenance actions are performed, and these intervention actions increase the life-cycle cost accordingly. There is a need to explore the effect of these maintenance actions on the life-cycle performance of the system (Jia and Gardoni 2019; Yang and Frangopol 2019a). A probabilistic life-cycle analysis framework is required to incorporate multiple elements, such as time-dependent reliability, maintenance

policy, maintenance interval, and maintenance cost. Various uncertainties associated with elements should be thoroughly explored to identify their impact on the life-cycle performance of the system.

Given the discussion above, it can be identified that an integrated life-cycle analysis framework should be developed for engineering structures under multiple hazards. A wide range of uncertainties associated with multi-hazard analysis, stochastic hazard arrivals, risk- and resilience-based long-term performance, and life-cycle analysis of engineering structures should be evaluated. The development of these aspects will be described in detail in this thesis.

## **1.2 Objectives and scope**

This thesis aims to develop a risk- and resilience-based life-cycle analysis framework for engineering structures under multiple hazards. The specific objectives are listed as follows:

1. Develop a multivariate analysis approach to assess the structural performance of civil infrastructure under extreme events considering the multi-hazard feature.
2. Propose an analytical approach to assess the long-term performance of civil infrastructure subjected to stationary hazards. Assess the expectation of long-term resilience and loss considering uncertainties associated with hazard frequency and intensity.

3. Perform a higher-order analysis for civil infrastructure to assess the long-term loss under non-stationary hazards. Formulate the associated statistical moments subjected to various stochastic models of hazards.
4. Develop an approach to assess the time-dependent reliability of ageing civil infrastructure considering the effect of multiple hazards. Propose an approach to consider the interaction among different deterioration processes.
5. Propose a life-cycle analysis framework for ageing civil infrastructure to assess the performance subjected to multiple deterioration processes. Develop an approach to assess the dependence between maintenance interval and maintenance cost and investigate the associated impact on the life-cycle maintenance cost.

### **1.3 Thesis organizations**

This thesis consists of nine chapters and the framework is described in Figure 1-1. The following chapters are organized as follows:

Chapter 2 presents the literature review of hazard analysis, vulnerability assessment, risk and resilience assessment, deterioration modeling, and maintenance policies in terms of the life-cycle analysis.

Chapter 3 reviewed and summarized the existed vulnerability approaches, which are demonstrated and validated with illustrative examples of highway bridges. It aims to provide standard formation and methods of vulnerability assessment of bridges subjected to a single hazard, especially earthquake and hurricane.

Chapter 4 develops a multivariate analysis approach to assess the structural vulnerability considering multi-hazard features of hurricanes. The compound effects of dependent hazard parameters on the vulnerability are investigated.

Chapter 5 assesses the long-term resilience and loss of civil infrastructure under stationary hazards using renewal theory.

Chapter 6 performs a higher-order analysis to assess statistical moments of long-term economic loss of civil infrastructure subjected to non-stationary hazards using a moment generating function-based approach.

Chapter 7 assesses the structural performance of civil infrastructure under dependent multiple deterioration processes, considering gradual deterioration, external shock, and fatal shock.

Chapter 8 proposes a life-cycle analysis framework for civil infrastructure. The framework integrates various uncertainties associated with stochastic deterioration, structural reliability, maintenance policy, and life-cycle cost analysis.

Chapter 9 draws conclusions and provides possible future research.

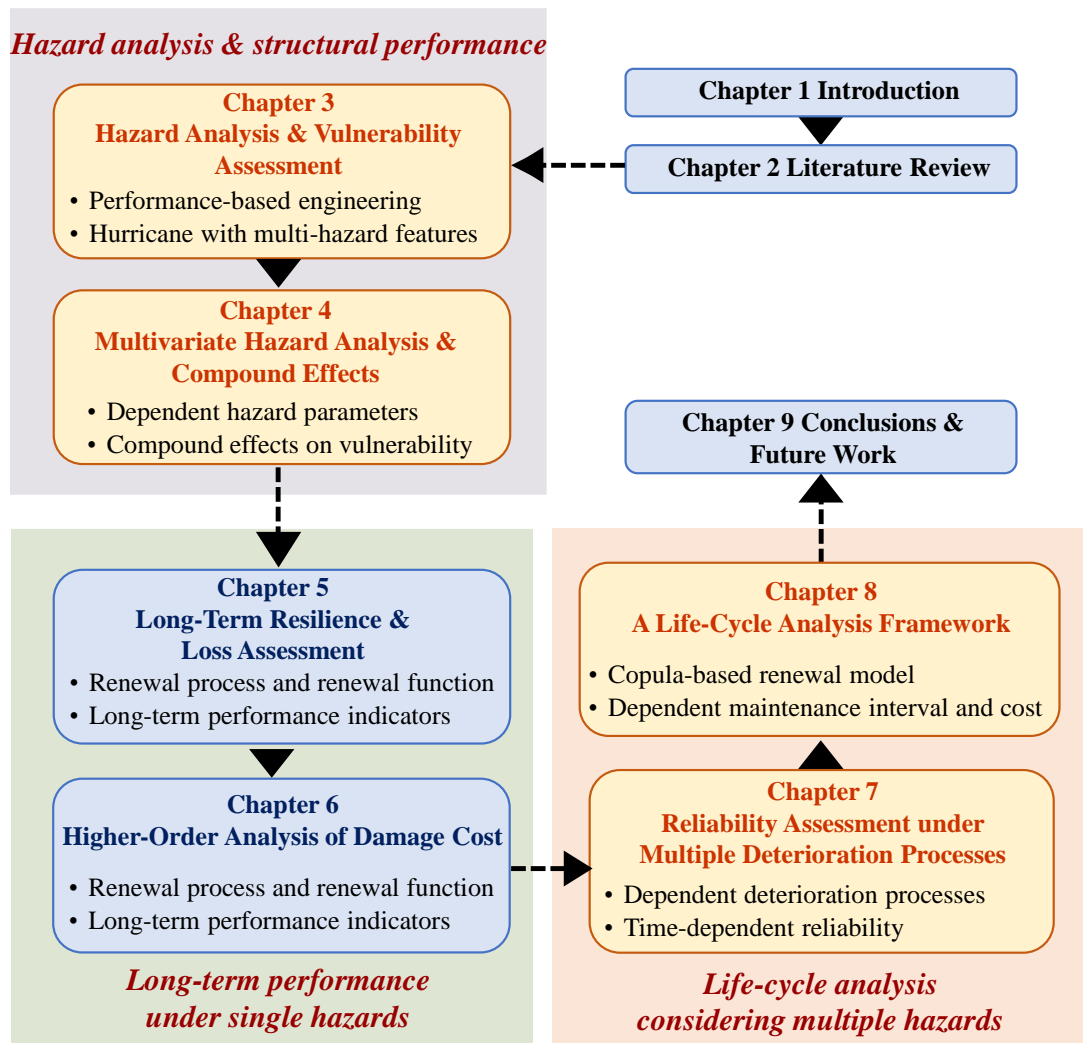


**Figure 1-1** Organization of the thesis and the proposed life-cycle analysis framework.

## 1.4 Contributions

There are four major contributions of this thesis:

1. A multivariate hazard analysis approach is proposed for civil infrastructure to investigate the compound effects of dependent storm parameters on the

structural vulnerability subjected to hurricanes. The copula approach provides superior efficiency in modeling dependency between different hazard parameters (e.g., wave height and peak water level), by separately considering marginal distributions and the joint effects.

2. An analytical approach is developed to assess the long-term resilience and loss of civil infrastructure under hazards based on a renewal process. A stochastic renewal process model is used to compute the expected long-term resilience and loss by considering both time-independent and time-varying occurrence characteristics of hazards.
3. A novel moment generating function method is proposed for the higher-order analysis of long-term loss under both stationary and nonstationary hazards. This method can effectively assess the first four statistical moments of long-term loss under different stochastic models (e.g., homogeneous Poisson process, non-homogeneous Poisson process, mixed Poisson process, and renewal process). Based on the law of total expectation, the developed approach expands the application scope of the moment generating function to nonstationary models and higher-order moments (i.e., skewness and kurtosis). Furthermore, by employing the convolution technique, the proposed approach effectively addresses the difficulty of assessing higher-order moments in a renewal process.
4. A probabilistic life-cycle analysis framework is developed for engineering structures based on a set of performance indicators, e.g., reliability and maintenance cost. The structural reliability under environmental exposure and extreme events is assessed by modeling the stochastic deterioration. Various uncertainties resulting from multiple dependent deterioration processes (e.g.,

gradual deterioration, external shock, and fatal shock), system reliability, intervention actions, and maintenance cost are considered in the proposed framework. In particular, the correlation between the maintenance interval and cost can be modeled by the proposed copula-based multivariate renewal model. This model provides an approach to assess the life-cycle maintenance cost analytically and numerically by incorporating data.

## **CHAPTER 2 LITERATURE REVIEW**

### **2.1 Introduction**

Civil infrastructure systems play a significant role in maintaining the safety and functionality of society. The immediate damage of engineering systems caused by natural hazards can disrupt transportation systems, impede rescue and recovery activities. The disruption may result in tremendous financial and societal losses. In addition to losses, resilience is a paramount performance indicator to evaluate and recover the functionality of structural systems under extreme events. Structural resilience is expected to be enhanced towards the desired level by considering structural functionality before, during, and after an extreme event. Therefore, assessing the vulnerability, recovery capability, potential losses of civil infrastructure under natural hazards becomes a primary concern to decision-makers to facilitate the emergency response and recovery efforts. This chapter aims to present a review associated with the life-cycle performance framework. Essential contributions of previous studies in terms of multi-hazard analysis, risk and resilience assessment under extreme events, and life-cycle management under multiple deterioration processes are reviewed and summarized. Research gaps associated with these aspects are also highlighted.

### **2.2 Multiple hazards and multivariate analysis**

Hazards have either independent or interacting effects with respect to their source, frequency, intensity, and region of impact. Multiple hazards can be divided into three

categories: independent, successive, and concurrent. For instance, independent hazards are discrete and there is no natural interaction. Successive hazards refer to the scenario that a hazard is triggered, broadened, or intensified by another, while concurrent hazards are defined as hazards that overlap or occur simultaneously over time (Akiyama *et al.* 2019; Zaghi *et al.* 2016). A hurricane reflects a multi-hazard feature, due to the joint occurrence of strong wind, high waves, and significant storm surge (Bjarnadottir *et al.* 2014; Gidaris *et al.* 2017).

### **2.2.1 Evaluation of natural hazards for highway bridges**

For civil infrastructure, the multi-hazard consideration has been gaining momentum since early 2010 due to increasing exposure to multiple hazards, especially the highway bridges. Studies of Decò and Frangopol (2011), Kameshwar and Padgett (2014), Wang *et al.* (2014), Liao *et al.* (2018), Akiyama *et al.* (2019) incorporated the effects of multiple natural hazards on highway bridges. When considering the interactive impacts of these extreme events, one key aspect of the multi-hazard analysis is to involve both independent (e.g., an earthquake and environmental-induced corrosion) and interacting (e.g., an earthquake triggering the subsequent tsunami) hazard scenarios into the assessment (Akiyama *et al.* (2019); Gautam and Dong (2018)). In order to assess the structural performance under hazards, an integrated consideration is necessary consisting of the probability of hazard occurrence, the structural vulnerability under hazards, and consequences of structural failure, as indicated in Figure 2-1. A detailed illustration regarding damage of highway bridges associated with earthquakes, hurricanes, and flood hazards is provided in this section.

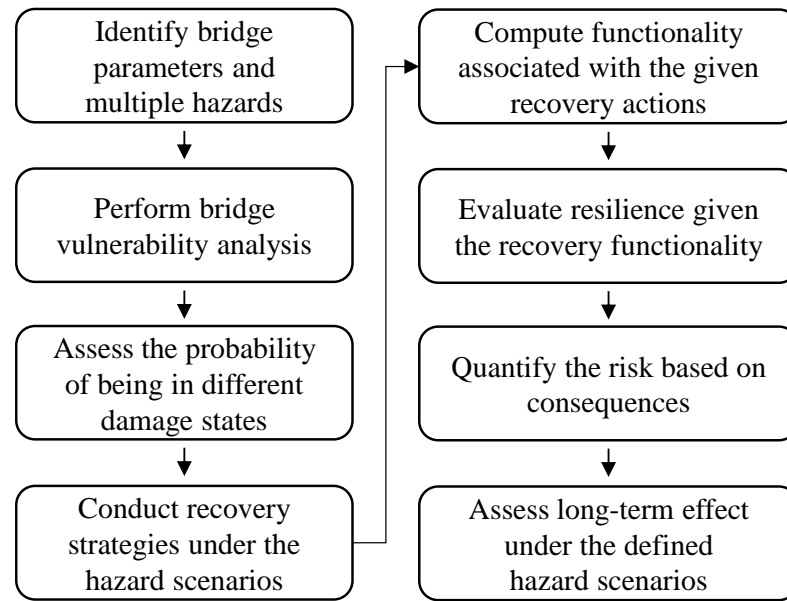


**Figure 2-1** Computational framework integrating resilience and loss assessment.

### 2.2.1.1 Earthquakes

Earthquake is a typical hazard for structural systems. The structural performance under earthquakes can be evaluated by the probabilistic seismic hazard analysis (Baker 2013). The probabilistic seismic hazard analysis framework quantifies various uncertainties from location, size, and intensity of an earthquake, among others to present an explicit distribution of future ground motions. Firstly, the occurrence of earthquakes associated with magnitude can be written as (Gutenberg and Richter 1944)

$$\log_{10} \lambda_m = a - bm \quad (2-1)$$

where  $\lambda_m$  is the rate of earthquakes with magnitudes greater than  $m$ ; and  $a$  and  $b$  are coefficients. Given this relationship, the cumulative distribution function (CDF) of earthquakes considering the range of magnitudes can be derived. Given the

characteristics of earthquakes, the ground motion prediction models (GMPM) can predict the expected levels of ground motion intensity. With the mean and standard deviation from the GMPM model, the exceedance probability of a peak ground acceleration (*PGA*) level can be computed under the given magnitude and site conditions

$$P(IM > x | m, r) = 1 - \Phi\left(\frac{\ln x - \overline{\ln IM}}{\sigma_{\ln IM}}\right) \quad (2-2)$$

where  $\Phi(\cdot)$  is the standard normal CDF;  $\overline{\ln IM}$  is the mean of  $\ln IM$ ; and  $\sigma_{\ln IM}$  is the standard deviation of  $\ln IM$ . The normal distribution parameters are output from the GMPM. Consequently, the annual rate of exceeding a given intensity measure (*IM*) can be derived using the total probability theorem

$$\lambda(IM > x) = \sum_{i=1}^{n_{source}} \lambda(M_i > m_{min}) \int_{m_{min}}^{m_{max}} \int_0^{r_{max}} P(IM > x | m, r) f_{M_i}(m) f_{R_i}(r) dr dm \quad (2-3)$$

where  $\lambda(M_i > m_{min})$  is the rate of occurrence of earthquakes greater than  $m_{min}$  from source  $i$ ;  $\lambda(IM > x)$  is the annual rate of intensity measure greater than  $x$ ;  $n_{source}$  is the number of sources considered;  $f_{M_i}(m)$  is the probability density function (PDF) for magnitude from source  $i$ ; and  $f_{R_i}(r)$  is the PDF of distance for source  $i$ . The inverse of the annual probability of exceedance is known as the return period. The seismic intensity measure values for different return periods can be determined accordingly.

The seismic vulnerability of structural systems could be computed based on structural analysis. The vulnerability of a structural system could be addressed through fragility curves that indicate the probability of reaching or exceeding a particular

damage state under the designated intensity measure level. The fragility curves can be calculated as (Cornell *et al.* 2002)

$$P[DI \geq LS_i | IM] = 1 - \int_0^{LS_i} \frac{1}{\sqrt{2\pi} \cdot \xi_{EDP|IM}} \cdot \exp\left(-\frac{[\ln(edp) - \ln(a \cdot IM^b)]^2}{2(\xi_{EDP|IM})^2}\right) d(edp) \quad (2-4)$$

where  $LS_i$  represents the  $i$ th  $LS$  and  $\xi_{EDP|IM}$  is the standard deviation of the logarithmic distribution. The seismic demand assesses the  $EDP$  as a function of a chosen ground motion intensity and can be quantified using appropriate seismic structural responses, such as deformation or ductility of vulnerable components. For highway bridges, reinforced concrete columns are key components susceptible to seismic damage. Sectional curvature ductility, displacement ductility, and residual displacement are commonly used as the seismic damage indicators for RC columns.

### 2.2.1.2 Floods

Coastal highway bridges can be susceptible to floods. Several historical events have highlighted that floods can be disastrous to bridge structures (Gautam and Dong 2018). For instance, the 2017 central Nepal flash flood washed away a bridge (see Figure 2-2a) due to torrential precipitation of four hours. Although the bridge was built recently (completed in June 2015), the debris with the flash flood in the mountainous terrain was particularly destructive and the bridge disappeared without any signs on the site. According to the records of flooding events, it is found that bridges are extensively damaged due to flash floods. Forensically, it could be inferred that the damage due to

flash floods would surpass the damage due to earthquakes having moderate ground shaking. Flood impact to bridges can be attributed to scour, deterioration of bridge components, water pressure, hydrodynamic forces exposed to the bridge/component, and debris impact and accumulation, among others. Bridge scour, deterioration, and increment of water pressure due to debris accumulation are considered as the major detrimental factors. Increased hydrodynamic forces together with debris and sediments usually cause bridge scouring (see Figure 2-2b), particularly in piers.



**Figure 2-2** (a) Collapsed and washed away bridge due to 2017 flood in Nepal and (b) scouring observed in a bridge in Nepal after the 2017 central Nepal flash flood (photos adapted from (Li *et al.* 2020a)).

Deterioration due to various factors is another notable problem that causes functionality loss or collapse of bridges. In general, environmental conditions, lack of drainage, load fluctuation above the capacity, and lack of periodic maintenance can cause deterioration of bridge components. Occasionally, significant deterioration may lead to serious compromise in the functionality as well. Bridges built in developing countries are more likely to suffer from deterioration aggravation compared to those in developed areas due to a lack of preventive maintenance as well as emergency

maintenance strategies. Additionally, deteriorated bridges are more vulnerable than the non-deteriorated counterparts. For instance, the 1988 and 2015 earthquakes in Nepal highlighted that similar types of bridges close to the epicenter performed better during the 1988 earthquake than the bridges far from the epicenter during the 2015 Gorkha, Nepal earthquake. Compared to the deficient behavior during the 2015 earthquakes, the performance of bridges was satisfactory during the 1988 earthquake. This is most likely attributed to the age of bridges. Ageing can lead to a decrease in structural capacity and an increase in bridge vulnerability (Gautam 2017).

Corrosion of reinforcement usually occurs due to environmental conditions. Thoft-Christensen *et al.* (2011) suggested the reduction in reinforcement area considering a time-dependent model as

$$A(t) = \begin{cases} \frac{\pi D^2}{4} & \text{for } t \leq T \\ \frac{\pi D(t)^2}{4} & \text{for } T < t < T + \frac{D}{r_1} \\ 0 & \text{for } t \geq T + \frac{D}{r_1} \end{cases} \quad (2-5)$$

where  $A(t)$  indicates the effective area of the reinforcement;  $D$  is the diameter of reinforcement;  $T$  is the time when corrosion starts;  $r_1$  is the rate of corrosion; and  $D(t)$  is the effective reinforcement diameter after  $t$  years. Accordingly,  $D(t)$  can be calculated as follows

$$D(t) = D - r_1 \times (t - T) \quad (2-6)$$

Due to the high velocity of water together with the debris and sediments, the increased water pressure also becomes prevalent. AASHTO (2000) suggested estimation of water pressure based on the empirical formula

$$p_w = 5.14 \times 10^{-4} \times C_D \times v^2 \quad (2-7)$$

where  $p_w$  is the water pressure and  $C_D$  is the drag coefficient.

The scour depth for a single pier can be estimated using the empirical formula suggested by (Yanmaz 2001)

$$S = 1.564 \times \chi^{0.405} \times \left( \frac{v}{\sqrt{g \times d}} \right)^{0.413} \quad (2-8)$$

where  $S$  is the scour depth;  $\chi$  refers to the relative approach flow depth;  $v$  is the flow velocity;  $g$  is acceleration due to gravity; and  $d$  indicates the depth of approach flow. Previous studies (e.g., Kim *et al.* (2017)) have highlighted the variation of scour depth per the geometric shape of the pile, location, and arrangement. As suggested by Briaud *et al.* (2007) the deterministic approach of scour depth prediction can be converted into a probabilistic one considering the future flood risk. Zhu and Frangopol (2016) and Liao *et al.* (2018) presented probabilistic approaches to risk assessment of bridges under scouring. Also, a risk-based cost-benefit analysis for the retrofit of bridges exposed to extreme hydrologic events considering multiple failure modes was presented in Mondoro and Frangopol (2018).

Chow (1965) has suggested the procedure to estimate the discharges of 100-year ( $Q_{100}$ ) and 500-year ( $Q_{500}$ ) flood events using linear regression with the help of

historical data. The scour depth due to flood risk can be estimated using the framework suggested by Briaud *et al.* (2007), Guo and Chen (2015), and Guo *et al.* (2016). Given known  $Q_{100}$  and  $Q_{500}$ , the Gaussian parameters (lognormal mean  $\alpha$  and standard deviation  $\beta$ ) can be estimated by solving Eqs. (2-9) and (2-10)

$$P(Q > Q_{100}) = 1 - \frac{1}{\sigma\sqrt{2\pi}} \int_0^{Q_{100}} \frac{1}{Q} \exp\left(-\frac{(\ln Q - \alpha)^2}{2\beta^2}\right) dQ \quad (2-9)$$

$$P(Q > Q_{500}) = 1 - \frac{1}{\sigma\sqrt{2\pi}} \int_0^{Q_{500}} \frac{1}{Q} \exp\left(-\frac{(\ln Q - \alpha)^2}{2\beta^2}\right) dQ \quad (2-10)$$

Subsequently, the expected future stream flow ( $Q_f$ ) can be computed as (Briaud *et al.* 2011)

$$Q_f = \exp(\alpha + x\beta) \quad (2-11)$$

in which  $x$  is the standard normal variable. Thereafter, a relationship between discharge and water velocity as well as the relationship between discharge and water depth is obtained using  $Q_f$ .

### 2.2.1.3 Hurricanes

During hurricanes, coastal infrastructure systems are vulnerable to damage resulting from hurricane-induced storm surge and wave loading. For instance, a total number of forty-four highway bridges along the American Gulf Coast region were damaged during Hurricane Katrina (TCLEE, 2006). Most of these bridges were simply supported and

destroyed due to wave and surge forces, thus resulting in unseating of bridge superstructures (Padgett *et al.* 2008). Such unseating failure occurs when the uplift wave force on the deck exceeds vertical capacity (Ataei and Padgett 2013; Mondoro *et al.* 2017; Zhu and Dong 2020). Subsequently, the impact of hurricanes on coastal infrastructure and bridges is widely investigated, in terms of the vulnerability assessment (Ataei and Padgett 2013; Saeidpour *et al.* 2019). By considering uncertainties in structural and hazard parameters, probabilistic modeling of capacity and demand of bridges can be performed. Based on the modeling, fragility models of bridge considering different intensity measures can be developed and the probability of failure can be assessed (Porter 2003; Qian and Dong 2020). These results are significant information for the subsequent risk assessment with respect to loss estimation and decision-making on the repair and retrofitting (Frangopol *et al.* 2017).

The vulnerability analysis assesses the probability of failure of bridges under the given hurricane scenarios. Failure occurs when the demand surpasses capacity. During hurricane activities, storm surge and the induced inundation can destroy the infrastructures significantly, especially for coastal bridges. The subsequent repairs and replacement of bridges account for a large proportion of the hurricane hazard financial losses. The impacts of hurricanes on bridges mainly result from the strong surge and wave-induced loading. Deck unseating is recognized as the predominant failure mode for simply-supported bridges during hurricanes (Kulicki 2010).

The vertical loading on the bridge superstructure contributes to deck unseating failure. According to AASHTO (2008), the maximum quasi-static vertical force is defined as

$$F_{V-\max} = \gamma_w \bar{W} \beta \left( -1.3 \frac{H_{\max}}{d_s} + 1.8 \right) [1.35 + 0.35 \tanh(1.2(T_p) - 8.5)]$$

$$(b_0 + b_1 x + \frac{b_2}{y} + b_3 x^2 + \frac{b_4}{y^2} + \frac{b_5 x}{y} + b_6 x^3)(TAF)$$
(2-12)

where  $\gamma_w$  is the unit weight of water,  $H_{max}$  refers to the maximum wave height,  $d_s$  is the water depth at or near the bridge, and  $T_p$  is the wave period.  $\bar{W}$  is the defined wetted deck width,  $\beta$  is a coefficient associated with the wave crest and bridge deck,  $x$  and  $y$  are defined as the ratio of maximum wave height over wave length and the ratio of wetted deck width over wave length respectively,  $b_0$  to  $b_6$  are coefficients relevant with bridge deck spans and  $TAF$  is the trapped air factor considering the effect of trapped air. The vertical slamming force is

$$F_s = A \gamma_w H_{\max}^2 \left( \frac{H_{\max}}{\lambda} \right)^B$$
(2-13)

in which  $A$  and  $B$  are variables relevant with maximum wave height and the distance between storm water to the girder.  $\lambda$  is the wave length and typically not provided in the hurricane records, and it is suggested as

$$\lambda = \frac{g T_p^2}{2\pi} \sqrt{\tanh\left(\frac{4\pi^2 d_s}{T_p^2 g}\right)}$$
(2-14)

where  $g$  is the gravitational acceleration. The maximum uplift force on the bridge deck is the summation of the above two force elements

$$F_v = F_{V-\max} + F_s$$
(2-15)

The significant wave height is defined as

$$H_s = 0.283 \tanh\left[0.53\left(\frac{gd}{U^{*2}}\right)^{3/4}\right] \tanh\left\{\frac{0.00565\left(\frac{gF}{U^{*2}}\right)^{1/2}}{\tanh\left[0.53\left(\frac{gd}{U^{*2}}\right)^{3/4}\right]}\right\} \left(\frac{U^{*2}}{g}\right) \quad (2-16)$$

in which the maximum wave height  $H_{\max}$  is typically defined as  $H_{\max} = 1.80H_s$ . The wave period is given as

$$T_p = 7.54 \tanh\left[0.833\left(\frac{gd}{U^{*2}}\right)^{3/8}\right] \tanh\left\{\frac{0.0379\left(\frac{gF}{U^{*2}}\right)^{1/3}}{\tanh\left[0.833\left(\frac{gd}{U^{*2}}\right)^{3/8}\right]}\right\} \left(\frac{U^*}{g}\right) \quad (2-17)$$

in which  $F$  is the fetch length,  $d$  is the average water depth and  $U^*$  is the wind stress factor. The maximum quasi-static horizontal force

$$F_{H-\max} = F_{H-\max}^* \exp\left[-3.18 + 3.76 \exp\left(\frac{\omega}{\lambda}\right) - 0.95 \left[\ln\left(\frac{\eta_{\max} - Z_c}{d_b + r}\right)\right]^2\right] \quad (2-18)$$

with

$$F_{H-\max}^* = \gamma_w \pi (d_b + r) \left(\omega + \frac{1}{2} H_{\max}\right) \left(\frac{H_{\max}}{\lambda}\right) \quad (2-19)$$

where  $d_b$  equals the girder height plus slab thickness for girder bridges while it equals slab thickness plus deck thickness for slab bridges.  $\lambda$  is the wave length.  $H_{\max}$  is the distance from the storm water level to the design wave crest.  $r$  is the rail height.  $\omega$  is dependent on bridge width (refer to (AASHTO 2008)).  $\gamma_w$  is the unit weight water taken as 0.064 kip/ft<sup>3</sup>.  $Z_c$  is the vertical distance from the bottom of the cross-section to the storm water level, positive if the storm water level is below the bottom of the cross-section. Unit illustrated are in ft in this analytical method.

Computational approaches are widely used in recent investigations. For instance, the computational fluid dynamics (CFD) modelling establishes numerical simulations, which can be applied to analyze the wave structure interactions such as computing the wave-induced forces on the bridge deck. Jin and Meng (2011) conducted a study using CFD software Flow-3D to investigate wave forces on the superstructure of coastal bridges but stated that this CFD method was relatively time-consuming. A two-dimensional potential flow modelling was proposed alternatively in their research. Seiffert *et al.* (2014) later suggested a CFD program OpenFOAM calculating solitary wave forces on bridge decks based on the theory of Euler equations. The outcomes of the hazard analysis and vulnerability are the inputs of the proposed stochastic loss model.

### **2.2.2 Multivariate analysis and copula model**

For the multivariate analysis under extreme events, it is commonly necessary to evaluate the interaction of hydrodynamic variables, as the sea state condition primarily relies on these parameters simultaneously (DNV, 2014). For instance, during hurricanes, elevated sea level and extreme waves can be caused by atmospheric pressure change and extreme wind (Mousavi *et al.* 2011). Masina *et al.* (2015) demonstrated that there is a non-negligible positive correlation among variables such as significant wave height and peak water level under storm events. Chebana and Ouarda (2011) showed that the univariate variables cannot provide a comprehensive representation of the multivariate nature of hydrological events. Due to the interaction between parameters, the compounding impact of non-severe environmental activities may result in significant

consequences. For instance, Serafin *et al.* (2019) investigated the impact of multiple loads on along-river water levels, and indicated that there was a portion of peak storm surge observed during low-wave events along the coastal river. In their study, a surrogate model was applied to simulate the joint relationship between river discharge and wave height based on hydraulic modeling. Hence, analyses based on exclusively univariate distributions may mis-specify the coastal conditions, thus resulting in inaccurate estimation of the associated damage or consequences, e.g., Corbella and Stretch (2012). Therefore, the joint impact of storm variables should be accounted for in the vulnerability assessment and risk management of coastal infrastructure.

In previous studies, the multivariate impact was commonly taken into account by assuming the joint probability distribution based on empirical models. For instance, Ataei and Padgett (2013) conducted a fragility analysis of coastal bridges subjected to hurricanes considering intensity measures with respect to relative surge elevation and wave height. A joint probabilistic density function was used to describe the dependence between wave height and wave period. Lucas and Soares (2015) proposed the bivariate distributions of the mean wave period and significant wave height based on a conditional modeling method. Nevertheless, the dependency structure between variables using the joint probability distributions is limited to simple relationships with constant correlation coefficients. Consequently, advanced mathematical techniques such as copulas should be employed to address such limitations.

The copula approach can be employed to model the dependence of storm variables for the probabilistic vulnerability assessment of infrastructure subjected to hurricanes. A copula function couples the multivariate distribution function to their

marginal distribution functions (Nelsen 2006). Compared with the conventional joint model, the copula approach provides significant flexibility, as it specifies the dependence structure and the univariate distributions separately. Due to its merits, the copula tool has been widely applied to coastal hazard analysis to model dependency among hazard parameters. For instance, De Michele and Salvadori (2003) proposed a 2-Copula to describe the dependence between the average rainfall intensity and storm duration during storm rainfall, in which both variables have heavy tail distributions. Bushra *et al.* (2019) employed the Gumbel copula to model the dependence of storm surge on the cyclone wind speed along the coastline of the Bay of Bengal. Another study performed by Trepanier *et al.* (2017) assessed the risk of more than twenty coastal cities in the United States Gulf of Mexico under the combined effects of extreme cyclone winds and storm surge. The dependence structure between the two storm parameters was modeled by the extreme value Archimedean copula. Moftakhari *et al.* (2017) assessed the increase in flooding probability caused by sea level rise in a warming climate. The proposed bivariate copula model provides an effective approach for computing the combined effects of fluvial flooding and sea level rise.

Copula models are also increasingly applied to investigate the dependence between wave height and water levels. As stated by Gouldby *et al.* (2014), extreme sea condition parameters (e.g., significant wave height and sea level) are essential parameters for coastal structural design and flood risk analysis. In their study, a multivariate extreme value method was applied to estimate the joint probability distribution of sea condition variables, e.g., significant wave height, sea level, and mean wave period. McCullough *et al.* (2011) indicated that copulas show considerable potential to evaluate extreme event statistics (e.g., associated with hurricane

parameters), as copulas allow simulation with limited information of variables. Another study conducted by Wahl *et al.* (2016) evaluated the flooding and erosion risk in the northern Gulf of Mexico based on a large number of observations of wave and water level from 1980 to 2013. Dependency analysis between six hydrodynamic parameters affecting the total water level was performed based on the goodness-of-fit test of the data. The Student's *t*-copula was suggested to model the dependence structure between variables. Additionally, a copula-based approach was applied to evaluate the probability of flooding at a coastal site under storm events (Masina *et al.* 2015). In their study, the positive correlation of significant wave height and peak water level was modeled by a copula function, and the tail behavior of storm variables was quantified in the copula modeling using the tail dependence coefficients.

## **2.3 Risk and resilience assessment under hazards**

### **2.3.1 Risk assessment**

Catastrophic damage caused by recent natural hazards such as Hurricane Katrina and Hurricane Michael and other natural disasters worldwide raised awareness of the public to the importance of risk mitigation and assessment on engineering systems (Kilanitis and Sextos 2019; Yang and Frangopol 2019b; Zhang *et al.* 2018a; Zhang *et al.* 2017). Risk is one of the most commonly used performance indicators in the life-cycle analysis. Evaluation of risk plays a significant role for engineering structures, as it accounts for consequences of potential damage and failure under hazards. There are various uncertainties associated with risk assessment. Therefore, in recent studies,

quantification of uncertainties within the risk assessment is of great importance in order to achieve a higher confidence level.

For the given hazard, risk refers to the product of the possibility and the consequences. The instantaneous total risk of a structural system is defined as (Vrouwenvelder *et al.* 2001)

$$Risk = \int \cdots \int \delta(x_1, x_2, \dots, x_n) f_{X_1, X_2, \dots, X_n}(x_1, x_2, \dots, x_n) dx_1 dx_2 \dots dx_n \quad (2-20)$$

in which  $\delta$  refers to consequences, and  $f_X(x) = f_{X_1, X_2, \dots, X_n}(x_1, x_2, \dots, x_n)$  is the joint PDF of a set of random variables  $\{X_1, X_2, \dots, X_n\}$ .

In literature, the risk can be described in three metrics: financial losses (e.g., repair cost), social losses (e.g., downtime, deaths), and environmental losses (e.g., carbon dioxide emissions) (Frangopol *et al.* 2017). Ellingwood (2001) simplified Eq. (2-20) using the assumption that hazards are mutually exclusive and collectively exhaustive, and defined the risk as

$$Risk = \sum_{i=1}^n C_c \times P[F|H_i] \times P[H_i] \quad (2-21)$$

in which  $P[H_i]$  is the likelihood of hazard occurrence  $H_i$ ,  $P[F/H_i]$  is the conditional failure probability of the system under hazard,  $C_c$  is the cost due to repairs or replacement associated with the failure, and  $n$  is the total number of hazards. The failure probabilities are typically associated with structural vulnerability analysis. The cost in terms of consequences due to damage and failure of engineering structures can be extremely high. In addition to the rebuilding cost, the loss of functionality may also

result in significant environmental and financial losses as the surrounding areas can be significantly affected, thus yielding a much higher cost.

During the life-cycle analysis, the total loss can be computed by summing up the loss of all hazard events. However, the present and future values about the monetary losses can be different, and such differences must be taken into account when assessing the risk. For instance, future losses should be discounted into the present value (Deco 2013; Yeo and Cornell 2009)

$$PL = FL(t)D(t) \quad (2-22)$$

where  $PL$  is the present monetary loss,  $FL(t)$  is the future monetary loss at time  $t$ , and  $D(t)$  is the discount factor. The discount factors in continuous and discrete time domains can be described as Eqs. (2-23) and (2-24), respectively (Hepburn 2007)

$$D(t) = \exp(-rt) \quad (2-23)$$

$$D(t) = \frac{1}{(1+r)^t} \quad (2-24)$$

in which  $r$  is a constant monetary discount rate.

For engineering structures, the analytical formulation of long-term loss is essential. Although numerical modeling is accessible, simulations are usually computationally expensive and time-consuming. Quantification of uncertainties associated with hazard occurrence and intensity can be one of the most significant parts of the analytical risk assessment. Stochastic models, such as Poisson processes, are widely employed to quantify these uncertainties. As the long-term loss is a random

variable, its mean and variance (i.e., low-order moments) are commonly computed as the two major statistical parameters in previous studies (Dong and Frangopol 2016; Yeo and Cornell 2009). Based on the homogeneous Poisson process, an analytical formulation of the expected life-cycle cost of buildings under single and multiple hazards was presented by Wen and Kang (2001). Recently, several studies assessed the long-term loss (e.g., mean and variance) of civil infrastructure under nonstationary stochastic processes. For instance, Yeo and Cornell (2005) proposed analytical expressions for the expected loss caused by earthquakes using homogeneous and non-homogeneous Poisson models. Wang *et al.* (2017a) computed the mean and variance of hurricane-induced damage loss using the non-homogeneous Poisson process. Lin and Shullman (2017) assessed the risk of New York City being damaged by hurricanes and surge flooding in a nonstationary environment. To simplify the computational process, the nonstationary Poisson model was converted into a stationary one in these studies. Within these studies, the long-term loss is generally limited to Poisson models and the first two moments.

In addition to Poisson model, recent studies proposed new approaches for the loss assessment. For instance, Pandey and Van Der Weide (2017) used a stochastic renewal process to formulate the expectation and variance of the discounted damage cost of a structure under earthquakes. The derivations were based on the renewal decomposition properties of renewal processes. The renewal model was also used to evaluate the lifetime resilience and cost of structural systems considering progressive deterioration (Yang and Frangopol 2019a). Although the renewal approach provides an alternative option to assess the loss under nonstationary hazards, it cannot be applied to other stochastic models, such as the non-homogeneous Poisson process. Meanwhile,

uncertainties associated with higher-order moments (i.e., skewness and kurtosis) are not taken into account in previous studies.

### **2.3.2 Resilience assessment**

To mitigate the impacts of extreme hazards, structural resilience is expected to be enhanced towards the desired level by considering structural functionality before, during, and after an extreme event. Resilience, related to the functionality of structural systems under extreme events and recovery patterns, is becoming a paramount performance indicator within the hazard management process (Bruneau *et al.* 2003; Bocchini and Frangopol 2011; Frangopol 2011; Frangopol and Soliman 2016; Frangopol *et al.* 2017; Zheng and Dong 2019). It highlights the evaluation of the capability of civil infrastructure systems to maintain prescribed safety, flexibility, and to recover from extreme events. Highway bridges are essential infrastructure components to ensure the safety and functionality of society. Though the reliability assessment with respect to external disasters has been emphasized in previous studies (Akiyama *et al.* 2011; Thanapol *et al.* 2016), the ability of recovering functionality to acceptable levels under multiple extreme events has not been explored extensively and more studies are required on resilience quantification. Therefore, it is necessary to provide a comprehensive resilience and probabilistic loss assessment of highway bridges under natural hazards to aid the preparation of emergency response and recovery decisions.

Resilience, as an important structural performance indicator, is defined as the ability of a civil infrastructure system to maintain its functionality and return to

normality after an extreme event. A resilience assessment establishes a connection between structural performance, post-hazard functionality, and recovery. Typically, this assessment comprises identification of multi-hazard risks, resilience analysis, and evaluation of resilience as shown in Figure 2-3 (ISO 2009). Risk assessment plays an important role as risk is related to both the consequences caused by structural failure or loss of functionality associated and the probability of structural failure. The outputs of communication are used to assess the risk and resilience effectively by establishing the context. Subsequently, cumulative risk and resilience of the given infrastructure system could be obtained under multiple natural hazards. Once resilience assessment is conducted, evaluation in terms of resilience parameters and their acceptability and viability should be performed. It is worth noting that performance parameters and countermeasures may vary in time and space at a local scale due to the interaction between resilience and risk. The proposed framework allows decision-makers and practitioners to assess and enhance the resilience of structures and to propose rational actions associated with planning, maintenance, and rehabilitation against natural hazards. These actions generally consist of social measures (e.g., awareness), physical measures (e.g., infrastructural preparedness), and corrective measures (e.g., life-cycle assessment of retrofitting decisions). In addition to analysis, continuous monitoring and periodic review are essential. An adaptable process of resilience assessment is required to encapsulate changes in contexts and record continuous evolution of resilience, as indicated in Figure 2-3.

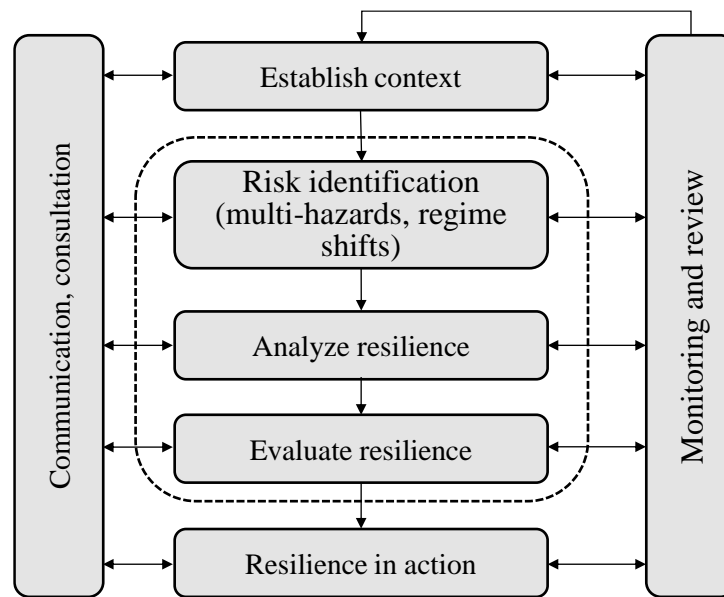


**Figure 2-3** Resilience assessment framework (adapted from ISO (2009)).

Resilience, related to the functionality of structural systems under extreme events and recovery patterns, is becoming a paramount performance indicator within the hazard management process (Bruneau *et al.* 2003; Bocchini and Frangopol 2011; Frangopol 2011; Frangopol and Soliman 2016; Frangopol *et al.* 2017; Zheng and Dong 2019). It highlights the evaluation of the capability to maintain prescribed safety, flexibility, and to recover from extreme events. Several definitions of resilience were proposed in the literature. One of the most widely used definitions was provided by Bruneau *et al.* (2003): “Resilience is defined as the ability of social units (e.g., organizations, communities) to mitigate hazards, contain the effects of disasters when they occur, and carry out recovery activities in ways that minimize social disruption and mitigate the effects of future earthquakes”. Resilience has four properties: robustness, rapidity, redundancy, and resourcefulness. Robustness is the strength or the ability of units to withstand a certain level of stress without suffering degradation or loss of function; Redundancy is the ability to satisfy functional requirements when

disruption, degradation, or loss of functionality occurs; Resourcefulness is the ability to apply material and human resources to achieve established priorities, resources mobilization and other goals; Rapidity is the capacity to achieve priorities and other goals in a timely manner to reduce the losses and avoid future disruption (Bruneau *et al.* 2003). Resilience has been increasingly implemented to performance-based seismic design of bridges as a vital performance indicator (Frangopol *et al.* 2017; Zheng and Dong 2018; Broccardo *et al.* 2015). Embedding resilience within the performance-based design could incorporate more decision variables (e.g., repair cost, time) within the structural design process.

A probabilistic model that can be used in the performance-based bridge design under multiple hazards is (Moehle and Deierlein 2004)

$$\begin{aligned}
 & P(D > dv | IM = im) \\
 & = \int_{dm} \int_{edp} \int_{im} G_{DV|DM}(dv | dm) \cdot dG_{DM|EDP}(dm | edp) \cdot dG_{EDP|IM}(edp | im) \cdot dG_{IM}(im)
 \end{aligned} \tag{2-25}$$

where P indicates the aggregate probability of a structure reaching or exceeding the limit state; DM indicates the damage measure; EDP indicates the engineering demand parameter; IM indicates the intensity measure; and DV indicates the decision variables. Eq. (2-25) is a significant part of the PEER framework (PEER 2013) from the Pacific Earthquake Engineering Research Center (PEER). Broccardo *et al.* (2015) validated the effectiveness of using the PEER framework to assess the probabilistic resilience of civil systems. Incorporating resilience as a decision variable, the PEER framework satisfied the optimal target under the investigated hazard through accomplishing resilience management strategies. Additionally, different decision variables can be implemented based on this framework.

A recent case study of reinforced concrete buildings presented a systematic analysis integrating resilience, sustainability, and loss into the PEER framework (Hashemi *et al.* 2019). Apart from seismic hazard, the integrated framework has been applied to other different hazard types, such as coastal bridges against extreme wave-induced loads. Qeshta *et al.* (2019) provided a review of resilience assessment on coastal bridges against extreme wave-induced loading, in which studies were comprehensively concluded in terms of wave forces, bridge response, vulnerability analysis, and resilience assessment incorporating with the PEER framework. Different from earthquakes, the hurricane-induced impact upon bridges is a typical example of a concurrent multi-hazard event, as bridges are affected by wind, storm surge, and waves simultaneously. Therefore, instead of focusing on the single intensity measure, (e.g., peak ground acceleration of seismic hazard), the integrated assessment framework under hurricanes requires multiple independent or correlated intensity measures, such as wave height, wave period, clearance, and inundation depth.

Zhang and Alam (2019) indicated that damage to bridges can be additionally considered at transportation levels besides the commonly defined structural levels. The structural level damage comprises the losses arising from bridge repair. Similarly, transportation level damage accounts for the serviceability of bridges leading to indirect loss such as traffic delays and detours (Yang and Frangopol 2018). Meanwhile, due to continuous exposure to the traffic, it is likely that the indirect loss caused by transportation damage would fairly surpass the direct loss resulted from structural damage. These examples have provided effective approaches for multi-hazard considerations. Overall, various metrics can be selected for the performance-based studies of structures and civil infrastructure systems in the multi-hazard analysis.

The resilience model provided by Bruneau *et al.* (2003) gives

$$R_{\text{Resi}} = \frac{1}{\Delta t_r} \int_{t_0}^{t_0 + \Delta t_r} Q(t) dt \quad (2-26)$$

where  $Q(t)$  is the functionality of a bridge defined by the recovery function at time  $t$  (e.g., days);  $t_0$  is the initial investigated time; and  $\Delta t_r$  is the investigated time interval. The functionality is significant during the resilience quantification as restoration of structure highly depends on how the repair and recovery work. Functionality levels can be defined to classify the emergency response and recovery post-earthquake period. For example, for the planning of emergency response, the functionality can be considered as the capability of a bridge located on a link transferring resources to the affected areas. With respect to the recovery at the post-earthquake phase, the functionality can be considered in different stages as open, limited use, and closed. The expected functionality is evaluated from that associated with the investigated damage states. There are several models available for functionality quantification. Decò *et al.* (2013) proposed an effective probabilistic model to compute the time-dependent functionality of bridges after a seismic event based on six probabilistic parameters including uncertainties. However, implementation of this comprehensive approach can be challenging when there is limited information available. Cimellaro *et al.* (2010) indicated that the functionality computational process could be classified based on the community preparation levels, while quantification of these levels might be difficult during the multiple-hazard analysis. These community preparation levels were classified as a prepared community, not well-prepared community, and well-prepared community, respectively. Another efficient recovery model was proposed by ATC

(1999) to assess the functionality restoration process of bridges based on lognormal cumulative distribution function. This method allows quantification of functionality under the given recovery pattern and requests the least inputs compared to the other approaches.

The recovery models for earthquakes are widely investigated, whereas there is limited research on the recovery models of coastal bridges under hurricanes. The majority of recovery models applied to hurricane-induced damage are based on seismic restoration methodologies and tsunami-based approaches (Gidaris *et al.* 2017). For instance, Bocchini and Frangopol (2012) proposed the functionality recovery model considering various restoration scenarios using a sinusoidal process. Though different performance stages are evaluated, it is difficult to calibrate the parameters used in this recovery model, as there is large uncertainty in the damage collection. When considering the hurricane-induced waves and surge, a HAZUS tsunami approach (FEMA 2013) can be utilized, which presents a framework based on expert opinion survey to evaluate the loss being in different damage states. However, the HAZUS approach is a simplified model as the bridge is assumed to be restored to full performance rather than different levels. Qeshta *et al.* (2019) indicated that some seismic restoration models can be applied to other types of natural hazards (e.g., damaged bridges by hurricanes).

Another resilience model introduced by Minaie and Moon (2017) focused on the practical implementation of resilience assessment and proposed a simplified resilience quantification framework of bridges under extreme events. The bridge resilience is illustrated as the capability of a bridge to maintain a robustness level and

to recover to a target performance level within the shortest time. Robustness refers to the residual performance after a natural hazard, which can be computed by integrating hazard, vulnerability, and uncertainties (Minaie and Moon (2017))

$$P_R = 100\% - \max(9.259 \times H \times V \times UF) \times I \quad (2-27)$$

in which  $I$  represents the importance factor of the investigated bridge;  $H$  is related to the hazard severity;  $V$  refers to the vulnerability, the product  $H \times V$  depends on each extreme event and vulnerability category; and  $UF$  is the uncertainty factor. Through this equation, the robustness could represent the worst potential scenario affecting bridge functionality. A simplified model of recovery is provided considering the recovery time as a function of adjustment factors and restoration, in which the recovery time is adjusted based on the management practices from the agency, historical records of extreme events in the past year, and bridge types. Accordingly, for a control time within one year (i.e., 365 days), the bridge resilience can be evaluated as the ratio of the area of the post-event performance to the area under the desired performance level (e.g., 100% for full recovery)

$$R = \frac{\int_{t_0}^{t_0+365\text{days}} P(t) dt}{\int_{t_0}^{t_0+365\text{days}} P(100\%) dt} \quad (2-28)$$

where  $P(t)$  refers to the structural performance and  $P(100\%)$  is the optimized performance. This engineering-based resilience quantification method efficiently assesses the resilience capturing key parts of bridge operation, knowledge of experts, and lessons learnt from past disruptive events. In addition to the two methods presented

in Eqs. (2-26) and (2-28), there are several other effective models available for the resilience assessment in the literature (e.g., Franchin *et al.* (2015)).

The previous studies on resilience were mainly focused on the assessment of bridges associated with single-hazard analysis. Decò *et al.* (2013) and Dong and Frangopol (2015) assessed the resilience of highway bridges under seismic hazards. The resilience of bridges under flood effects with different return periods was investigated by Dong and Frangopol (2016). There were a limited number of resilience studies of bridges dealing with multiple hazard effects (Decò and Frangopol (2011); Pescaroli *et al.* (2018); Akiyama *et al.* (2019)). Multiple hazards could bring considerably more disastrous consequences to the society than a single hazard (Padgett *et al.* (2009); Jalayer *et al.* (2011); Dong and Frangopol (2017); Zheng *et al.* (2018). Gidaris *et al.* (2017) underlined that structural vulnerability, loss evaluation, recovery, and restoration models were key elements for accurate quantification of the resilience of highway bridges in the multi-hazard analysis. Bruneau *et al.* (2017) reviewed the state of the art of structural performance under multiple hazards by considering the resilience and hazard interaction effects were highlighted for different structural systems. This work indicated that further efforts should be implemented to explore the multi-hazard performance in a life-cycle context for a variety of hazards and structural portfolios.

In the long-term performance evaluation of highway bridges, uncertainties associated with vulnerability, loss, and resilience can be accumulated due to different occurrence probabilities of different hazardous events. Under the multi-hazard consideration, different indicators may show various performance characteristics of a

range of hazardous events. Thus, it is essential to incorporate consideration of multiple hazards into performance studies of structures and civil infrastructure systems to identify the most dominant and costliest hazard scenario to help decision-makers propose the optimal design and management strategies.

## **2.4. Deterioration modeling and maintenance policy**

### **2.4.1 Interaction among deterioration processes**

Civil infrastructure systems are generally designed with a certain service life according to the design codes and standards. In recent decades, major engineering systems are expected to serve longer than their design life due to sustainability requirements, and researchers have made various efforts to this aspect (Bocchini *et al.* 2014; Dong *et al.* 2013; Gardoni *et al.* 2016). On the other hand, the service life of systems can be adversely affected by multiple deterioration processes. Therefore, life-cycle analysis of engineering systems has drawn increasing attention to achieve sustainable planning and management (Biondini and Frangopol 2016; Dong *et al.* 2014; Gardoni 2017; van Noortwijk and Frangopol 2004).

During the lifetime, the system performance degrades due to different deterioration processes, in which system performance can be measured as reliability, capacity, or functionality. Engineering systems typically experience both gradual and shock deterioration (Kumar and Gardoni 2014a, 2014b). The gradual or progressive deterioration is commonly caused by corrosion (Frangopol *et al.* 1997), fatigue (Bastidas-Arteaga *et al.* 2009), crack growth (Zhong *et al.* 2010), and Alkali-Silica

reaction (Huang *et al.* 2014); and the shock or sudden deterioration results from external extreme events such as hurricanes (Li *et al.* 2020c), earthquakes (Dong *et al.* 2015), blasts (Akiyama *et al.* 2011). When the system performance degrades below a certain threshold, intervention actions such as replacement or repairs are required to restore the system. Therefore, in a complete life-cycle analysis, stochastic deterioration, recovery processes, and various uncertainties are essential components (Cheng *et al.* 2012; Jia and Gardoni 2019).

In previous research, studies mainly focus on one deterioration process, either gradual (Ghosh and Padgett 2010) or shock deterioration (Li *et al.* 2020b). Few recent studies investigate both two deterioration processes. For instance, Kumar *et al.* (2015) developed a stochastic framework to model deterioration processes combining both shock and gradual deterioration. Guo *et al.* (2020) proposed a two-step translation method to assess structural reliability under continuous deterioration and sudden events. In these studies, interactions among different processes are neglected and the potential adverse impact is not considered. However, deterioration processes are commonly dependent and interact with each other (Bastidas-Arteaga *et al.* 2009; Wang and Pham 2011). For example, the deterioration caused by corrosion (e.g., environmental exposure) and the deterioration caused by fatigue (e.g., subjected to cyclic loading) have interactive effects. The localized corrosion with pitting can be a potential area for fatigue initiation and accelerate the fatigue process (Bastidas-Arteaga *et al.* 2009).

Additionally, the interaction between deterioration processes cannot be neglected. For example, the corrosion caused by gradual deterioration interacts with the shock deterioration due to seismic damage. The initiation of corrosion and the corrosion

rate of rebars in reinforced concrete can be accelerated by the cracks due to previous earthquakes (Jia *et al.* 2017). Otieno *et al.* (2010) showed that even small cracks can affect the corrosion process significantly. Therefore, ignoring the interactive impact among deterioration processes may result in underestimation of the deterioration and mis-specify the performance state in a life-cycle analysis. There is a need to incorporate dependence into deterioration processes.

#### **2.4.2 Condition-based maintenance**

There are various critical maintenance measures to avoid unexpected failure due to deterioration processes. Condition-based maintenance is a commonly used maintenance policy to manage the reliability of deteriorating systems (Cheng *et al.* 2012). This policy suggests maintenance actions based on information of the system gathered during condition monitoring processes (Ahmad and Kamaruddin 2012). In life-cycle analysis, decision-makers aim to find an optimal maintenance plan for the system to manage major repair schedules and/or performance threshold for replacement (Yang and Frangopol 2019a). The condition-based maintenance policy mainly relies on the renewal theorem in previous studies (Caballé *et al.* 2015). The optimization is conditioned on the cost rate and the renewal theorem provides an effective analytical approach for the computation. The cost rate is defined as the ratio of expected maintenance cost and the expected maintenance interval within one renewal cycle. For instance, Yang *et al.* (2017) proposed a condition-based maintenance policy considering failure caused by degradation and shock. The total cost associated with the given policy is quantified by using the renewal theorem. Cheng *et al.* (2012) assessed

the maintenance cost of the system subjected to degradation based on a gamma process. The renewal theorem is used to provide closed-form expressions of the total maintenance cost.

## **2.5 Research Gaps**

This chapter has provided a review with respect to hazard analysis, vulnerability assessment, risk and resilience assessment, deterioration modeling, and maintenance policies in life-cycle analysis. The review has revealed a series of research gaps and challenges in terms of the probabilistic life-cycle analysis framework for civil infrastructure:

1. The multivariate analysis associated with correlated hazard parameters and the effect of compound extreme events on structural vulnerability have not been discussed.
2. The long-term effects of hazards on civil infrastructure systems in terms of resilience and loss have not been explored. Additionally, the existing models to assess the long-term effects are mainly based on the stationary Poisson process, while the impact of nonstationary characteristics has not been investigated.
3. Though the expected damage cost has been applied as a standard decision criterion in life-cycle cost analysis, uncertainties springing from standard deviation and higher-order moments have been neglected. There is a need to explore the information indicated by statistical moments of the cost.

4. Furthermore, a comprehensive life-cycle analysis framework has not been developed for engineering systems to consider multiple hazards (e.g., extreme events and gradual deterioration), intervention actions, life-cycle cost analysis, and various uncertainties.

The following chapters will discuss these issues and provide solutions to fill these gaps.

# **CHAPTER 3 PROBABILISTIC HAZARD ANALYSIS AND STRUCTURAL PERFORMANCE UNDER SINGLE HAZARD**

## **3.1 Introduction**

Performance-based engineering concepts have been widely applied as a general approach for the life-cycle management and design of civil infrastructure systems in recent decades. For instance, the performance-based earthquake engineering framework has been developed and implemented to various structures by the Pacific Earthquake Engineering Research Center (Ellingwood 2001; Porter 2003). Based on the risk assessment of seismic hazards, the performance-based framework has shown sufficient efficiency in facilitating construction, maintenance, retrofit, and design of structural systems. Owing to the effectiveness in dealing with seismic hazards, the framework has been extended to other fields, such as performance-based tsunami engineering and hurricane engineering. Hazard analysis and vulnerability assessment are two essential components in the performance-based framework.

This chapter aims to present standard methodologies for the probabilistic hazard analysis and vulnerability assessment of highway bridges under single hazard. Methods are reviewed and applied to assess the failure probability of highway bridges subjected to earthquakes and hurricanes. Validations of the methods are also provided by conducting experimental studies. The computational results are inputs for the loss and resilience assessment in the following sections. Compared with the seismic hazard,

hurricanes reflect multi-hazard features, due to the multiple hazard sources such as high waves, heavy rain, and strong wind. In particular, the vulnerability of highway bridges subjected to deck unseating failure under hurricanes is discussed.

## **3.2 Structural performance under earthquakes**

Probabilistic seismic hazard analysis and structural vulnerability assessment are the two essential steps of the performance-based earthquake engineering framework. This section presents detailed procedures to obtain seismic hazard curves and fragility curves for the investigated highway bridge.

### **3.2.1 Probabilistic seismic hazard analysis**

The recurrence relationship between earthquake frequency and magnitude provides the annual rate of earthquakes larger than magnitude  $m$  as follows (Gutenberg and Richter 1944)

$$\log_{10} \lambda_m = a - bm \quad (3-1)$$

in which  $\lambda_m$  is the annual rate of earthquakes greater than magnitude  $m$  in the given region and  $a$  and  $b$  are coefficients based on analysis of historical records. Though this recurrence relationship defines the magnitude without an upper bound, the regional magnitude generally has an upper limit because of finite faults. Therefore, the CDF of earthquake magnitude considering the minimum and maximum magnitudes can be described as (Baker 2013)

$$F_M(m) = \frac{1 - 10^{-b(m - m_{\min})}}{1 - 10^{-b(m_{\max} - m_{\min})}}, \quad m_{\min} < m < m_{\max} \quad (3-2)$$

where  $F_M(m)$  is the CDF at  $m$ ;  $m_{\max}$  represents the maximum earthquake of the given source; and  $m_{\min}$  demonstrates the minimum magnitude. The probability of occurrence of discrete magnitudes can be determined from this CDF and gives

$$P(M = m_j) = F_M(m_{j+1}) - F_M(m_j) \quad (3-3)$$

where  $m_j$  defines a set of discrete magnitudes with  $m_j < m_{j+1}$ . Discrete magnitudes can replace continuous magnitudes during the analysis when closed space is set between the two discrete magnitudes  $m_j$  and  $m_{j+1}$ .

Depending on the characteristics of earthquakes, the ground motion prediction models can predict the expected levels of ground motion intensity. The mean and standard deviation of the natural logarithm of the  $IM$  are the main outputs of a GMPM. The  $IM$  is specified as  $PGA$ . The ground motion prediction equation is given as (Boore *et al.* 2014)

$$\begin{aligned} \ln Y = & F_E(M, mech) + F_P(H_{JB}, M, region) \\ & + F_S(V_{S30}, H_{JB}, M, z_1) + \varepsilon_n \sigma(M, H_{JB}, V_{S30}) \end{aligned} \quad (3-4)$$

where  $\ln Y$  is the natural logarithm of  $IM$  representing  $\ln PGA$  in this circumstance;  $F_E$ ,  $F_P$ , and  $F_S$  are functions for event source, path, and site parameters, respectively;  $M$  is magnitude;  $mech$  is the mechanism of the seismic event;  $H_{JB}$  is the distance representing the shortest distance to the surface projection of the fault surface from a site;  $region$  represents the investigated region;  $V_{S30}$  is the shear wave velocity averaged over top 30 m;  $z_1$  is the basin depth;  $\varepsilon_n$  is the fractional number of standard deviations of a single

predicted value of  $\ln Y$  away from the mean; and  $\sigma$  is the total standard deviation of the model. The total standard deviation is obtained from the combination of between-event and within-event variability, given by

$$\sigma(M, H_{JB}, V_{S30}) = \sqrt{\phi^2(M, H_{JB}, V_{S30}) + \tau^2(M)} \quad (3-5)$$

where  $\tau$  is the between-event standard deviation dependent on  $M$ ; and  $\phi$  is the within-event standard deviation dependent on  $M$ ,  $H_{JB}$ , and  $V_{S30}$ .

With the mean and standard deviation from this GMPM model, the exceedance probability of a  $PGA$  level can be computed under the given magnitude and site conditions

$$P(PGA > x | m, h) = 1 - \Theta\left(\frac{\ln x - \overline{\ln PGA}}{\sigma_{\ln PGA}}\right) \quad (3-6)$$

where  $\Theta(\cdot)$  is the standard normal CDF;  $h$  refers to the distance;  $\overline{\ln PGA}$  is the mean of the natural logarithm of  $PGA$ ; and  $\sigma_{\ln PGA}$  is the standard deviation of the natural logarithm of  $PGA$ . This equation follows the same assumption of (Baker 2013), which suggests the natural logarithm of  $PGA$  following a normal distribution.

Combining uncertainties of the seismic source, distance, and intensity, a probability distribution of the  $IM$  can be calculated based on the total probability theorem. Given the investigated earthquake, the probability of exceeding a  $PGA$  level  $x$  is computed

$$P(PGA > x) = \int_{m_{\min}}^{m_{\max}} \int_0^{h_{\max}} P(PGA > x | m, h) f_M(m) f_H(h) dh dm \quad (3-7)$$

in which  $P(PGA > x | m, h)$  is from the ground motion details of Eq. (3-6) and  $f_M(m)$  and  $f_H(h)$  represent the PDFs for the seismic magnitude and distance, respectively. This relationship is alternatively known as the hazard curve. Herein, a minimum magnitude is considered as 5.5 excluding non-damaging earthquakes with small magnitudes. The maximum magnitude is assumed as 8.5 for the investigated region. The corresponding coefficients  $a$  and  $b$  from the recursive relationship Eq. (3-1) are assigned as 3.94 and 0.89, respectively (USGS 2003).

Accordingly, the annual rate of earthquakes with magnitudes greater than 5.5 is computed as 0.1109. The fault type in the investigated region is determined as a strike-slip fault. It is assumed that the earthquakes have an identical probability of occurrence along the fault. The distance is assumed to be 5 km. The shear wave velocity averaged over top 30 m is assumed to be 480 m/s at the site. Given these inputs, the exceedance probability of different  $PGA$  levels is obtained by calculating the median and standard deviation from GMPM. The hazard curve can be provided based on these analyses, as indicated in Figure 3-1.

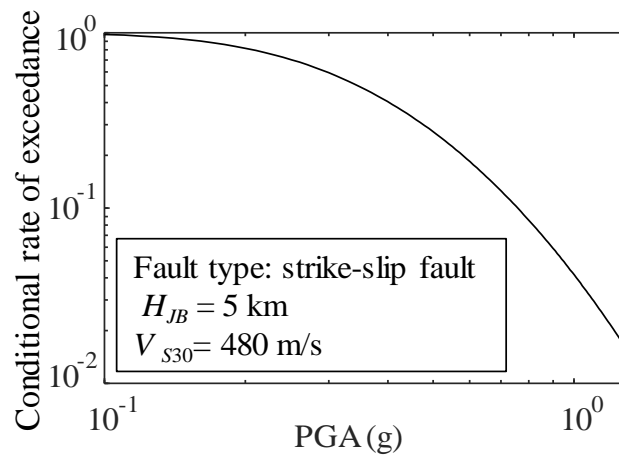


**Figure 3-1** Seismic hazard curve under the investigated seismic scenario.

### 3.2.2 Structural vulnerability assessment of highway bridge

A finite element model of a typical two-span continuous reinforced concrete bridge is established using the software OpenSees (McKenna *et al.* 2009) to assess the structural performance, as shown in Figure 3-2. This 58-m bridge has a box girder with a height of 1.2 m and a width of 10 m and two circular 10-m high columns with a diameter of 1.6 m. The compressive strength of the concrete is 26 MPa and the yield strength of the reinforcement is 470 MPa. The longitudinal reinforcement ratio for the concrete columns is 1.01%.

The fragility curves provide the probability of the demand ( $D$ ) exceeding capacity ( $C$ ) at a specified damage state under a given  $IM$ . For instance, Kim and Shinozuka (2004) provided the fragility curves of bridges under different damage states by considering peak ductility demand of the columns. Herein, the displacement ductility is also used for the fragility curve, which is the ratio of the maximum

displacement at the top of the column to the displacement of the identical position when yielding occurs.

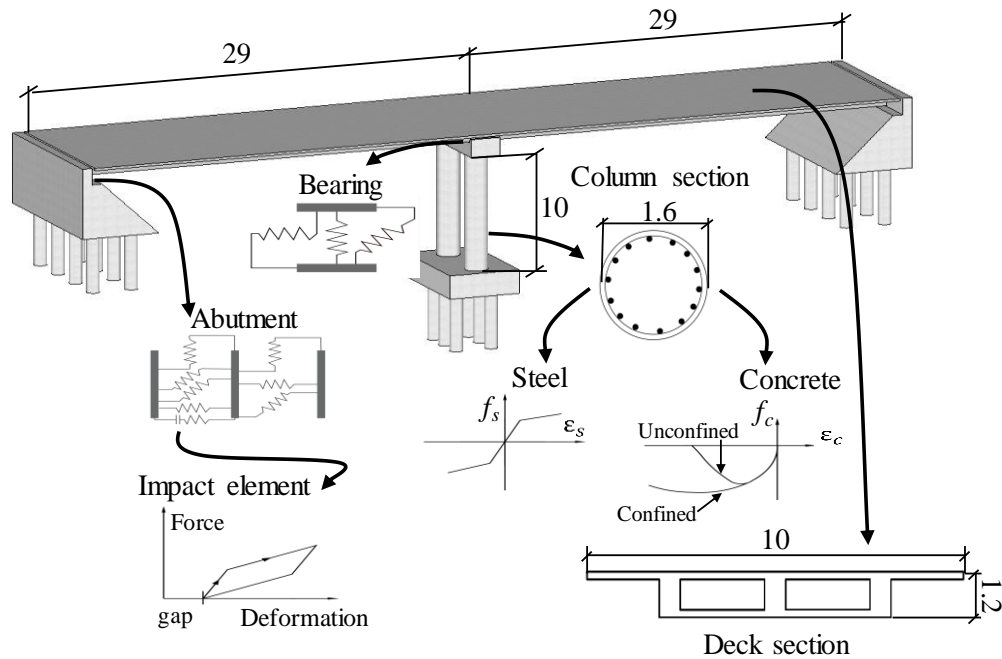


**Figure 3-2** The three-dimensional bridge model with dimensions (unit: meter).

Five damage states of the bridge are specified as no damage, slight, moderate, major, and complete, according to HAZUS (1999). The seismic demand is the curvature ductility of the bridge column obtained from the finite element model. For each damage state, the limit of curvature ductility  $\mu$  has been classified as  $\mu < 1.29$ ,  $1.29 \leq \mu < 2.10$ ,  $2.10 \leq \mu < 3.52$ ,  $3.52 \leq \mu < 5.24$ , and  $\mu \geq 5.24$ , respectively (Nielson 2005). The required curvature ductility can be attained through a nonlinear time history analysis. A total of 80 ground motion records are used for the regression analysis to assess the response of the bridge (Baker *et al.* 2011; Qian and Dong 2020). Based on these records, the probability seismic demand model can be firstly established, and the associated parameters can be determined by the regression analysis. The fragility curve provides

the probability of the seismic demand  $D$  exceeding capacity  $C$ . The fragility function can be expressed as

$$P[D \geq C | PGA] = \Phi \left[ \frac{\ln(S_D/S_C)}{\sqrt{\beta_D^2 + \beta_C^2}} \right] = \Phi \left[ \frac{\ln(PGA) - [\ln(S_C) - \ln(A)]/B}{\sqrt{\beta_D^2 + \beta_C^2}/B} \right] \quad (3-8)$$

where  $S_D$  and  $S_C$  represent the median of seismic demand and capacity, respectively.  $\beta_D$  and  $\beta_C$  refer to the standard deviation of the demand and capacity, respectively. Herein, it should be noted that the column damage has been taken as the proxy for the system damage. The impact of multi-component response is not considered in this example. The regression relationship gives the value of  $A$  as 2.8869 and  $B$  as 1.0702. Accordingly, the seismic fragility curves of four different damage states considering displacement ductility are obtained, shown in Figure 3-3. The standard deviation for demand is calculated as 0.7422 and the standard deviation for capacity is assumed as 0.25.

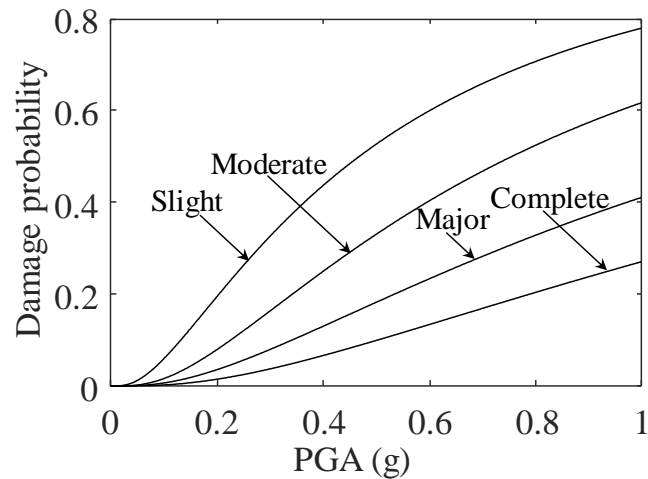


**Figure 3-3** Fragility curves associated with four damage states.

### 3.3 Structural performance under hurricanes

The impact of hurricanes upon highway bridges shows a typical example of interacting multi-hazard effects. For instance, the bridge is threatened by concurrent hazards during a hurricane event including strong wind, high waves, and storm surge. The effects of hurricanes on highway bridges mainly stem from storm surge and wave-induced loading. The resulting uplift forces in vertical and horizontal directions produce large displacements at supports. When the displacements surpass the limitation at supports, the deck unseating may occur (Mondoro *et al.* 2017). It is commonly recognized that deck unseating failure is the most primary damage for simply supported bridges (Kulicki 2010). Some bridge spans even with fixed connections using dowelling undergo complete connectivity failure during the Hurricanes Katrina (Padgett *et al.* 2008). Wang *et al.* (2017a) recommended a method to assess hurricane-induced structural damage loss from the perspective of insurers and performed a hurricane vulnerability analysis considering model uncertainty.

In this section, vulnerability assessment of highway bridges subjected to hurricanes is performed by considering deck unseating failure mode. A two-dimensional computational fluid dynamic model of bridge superstructure is constructed to obtain the uplift forces caused by waves during hurricanes. A pilot experiment is performed to validate the maximum uplift force obtained from numerical modeling. The wave height and surge elevation are adopted as the intensity measures for the vulnerability analysis. Structural vulnerability is assessed by computing the demand and capacity under hurricanes. A flowchart is presented in Figure 3-4 to show the key steps to assess the structural performance of highway bridges under hurricane hazard.

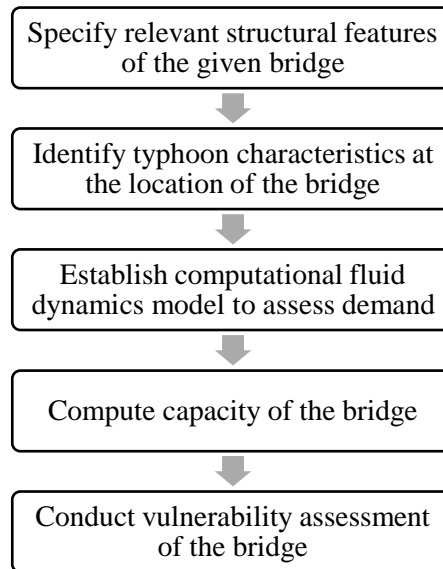


**Figure 3-4** A process diagram to assess the structural performance of highway bridges subjected to hurricanes.

### 3.3.1 Hazard parameters

During hurricanes, the wave- and surge-induced loads on the bridge are conditioned on multiple parameters, such as wind speed, storm surge, bathymetry, local geography, and geometry of bridge superstructure. In previous studies, hurricane hazard is commonly characterized by a single parameter, e.g., wind speed. For instance, Li and Ellingwood (2006) and Wang *et al.* (2017a) suggested using Weibull distribution to describe hurricane wind speed during hurricane risk assessment. The CDF and PDF of the hurricane wind speed can be described by (Wang *et al.* 2017)

$$F_v(v, t) = \Pr(V < v) = 1 - \exp\left[-\left(\frac{v}{u(t)}\right)^{\alpha(t)}\right] \quad (3-9)$$

$$f_v(v, t) = \frac{\partial F_v(v, t)}{\partial v} = \exp \left[ - \left( \frac{v}{u(t)} \right)^{\alpha(t)} \right] \frac{\alpha(t)}{u(t)} \left( \frac{v}{u(t)} \right)^{\alpha(t)-1} \quad (3-10)$$

in which  $u(t)$  and  $\alpha(t)$  are time-variant parameters associated with the Weibull distribution. In recent research, studies indicate that multiple parameters are needed to describe complicated interaction effects among hurricane parameters. For instance, Phan *et al.* (2007) indicated the joint distribution of wind speeds and annual surge heights can be applied to distribute hurricane risk. Ataei and Padgett (2013) adopted maximum wave height and relative surge elevation as intensity measures to assess the fragility of highway bridges subjected to hurricanes.

### 3.3.2 Structural vulnerability assessment under hurricanes

For the vulnerability assessment under hurricanes, the probability of failure of the bridge under the unseating failure mode can be determined by assessing the structural capacity and demand incorporating uncertainties. The failure probability of bridge  $P_f$  is the likelihood that the demand  $D$  exceeds structural capacity  $C$  (Li and Ellingwood 2006)

$$P_f = P[(C - D) < 0] \quad (3-11)$$

The demand of the bridge is the total uplift force acting upon the bridge caused by surge and waves, determined by numerical modeling. For illustrative purposes, a simply supported two-span reinforced concrete bridge is investigated herein. The selected girder bridge has a total length of 40 m. The superstructure has a width of 10.45

m, consisting of a deck and six girders. The girder is 1.05 m high and the deck is 0.3 m thick. The cross-section of the superstructure of this bridge is described in Figure 3-5(a). All the six girders are simplified as rectangles, each of which has a width of 0.3 m and is evenly distributed along the deck. The still water depth is 8m and vertical clearance is set as 4.5 m. A 2D computational fluid dynamics model of bridge superstructure under the impact of a hurricane-induced solitary wave can be established by CFD software *ANSYS Fluent 17.2 Package* (ANSYS 2016). Figure 3-5(b) shows the numerical diagram of the computation domain.

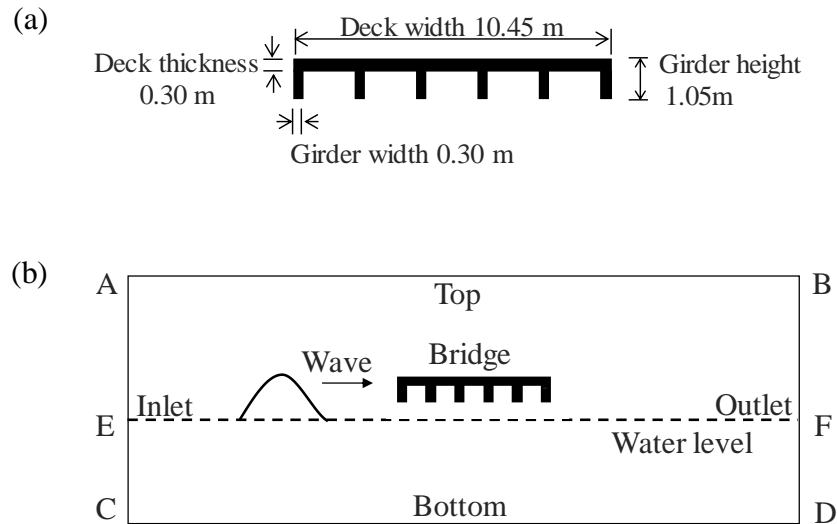


**Figure 3-5** (a) Geometry of bridge superstructure and (b) numerical diagram of computation domain of the FEM model.

From the CFD model, the hurricane-induced uplift force can be evaluated. Figure 3-6 illustrates the interactive effects among air, wave, and deck at four different moments: wave arrives the deck, the water surface rises (e.g., Figure 3-6(a)) and leaves (e.g., Figure 3-6(d)). During the dynamic fluid interaction, the movement of fluid in the

physical domain depends on various properties. Changes in these characteristics are commonly examined by the Navier-Stokes equations based on laws of conservation. In the 2D domain, the Navier-Stokes equations can be defined as (Temam 2001)

$$\rho \left( \frac{\partial u_x}{\partial t} + u_x \frac{\partial u_x}{\partial x} + u_y \frac{\partial u_x}{\partial y} \right) = -\frac{\partial p}{\partial x} + \mu \left( \frac{\partial^2 u_x}{\partial x^2} + \frac{\partial^2 u_x}{\partial y^2} \right) + \rho g_x \quad (3-12)$$

$$\rho \left( \frac{\partial u_y}{\partial t} + u_x \frac{\partial u_y}{\partial x} + u_y \frac{\partial u_y}{\partial y} \right) = -\frac{\partial p}{\partial y} + \mu \left( \frac{\partial^2 u_y}{\partial x^2} + \frac{\partial^2 u_y}{\partial y^2} \right) + \rho g_y \quad (3-13)$$

where  $\rho$  represents the mass density of water;  $u_x$  and  $u_y$  are velocity components in  $x$  and  $y$  direction;  $p$  is pressure; and  $\mu$  refers to dynamic viscosity. These two equations can be combined as one in vector form (Temam 2001)

$$\rho \frac{D\mathbf{V}}{Dt} = \rho \mathbf{g} - \nabla p + \mu \nabla^2 \mathbf{V} \quad (3-14)$$

in which  $V$  is flow velocity and  $\nabla$  represents divergence. In order to process these complex computations, the CFD model is required for numerical analysis. In terms of the structural simulation, the total force along a designated force vector equals the sum of the dot product of the viscous forces and pressure horizontally and vertically. This relationship is demonstrated by (Kohnke 1994)

$$F_a = \vec{a} \cdot \vec{F}_p + \vec{a} \cdot \vec{F}_v \quad (3-15)$$

where  $\vec{a}$  is the designated force vector;  $\vec{F}_p$  is the pressure force vector, and  $\vec{F}_v$  is the viscous force vector.

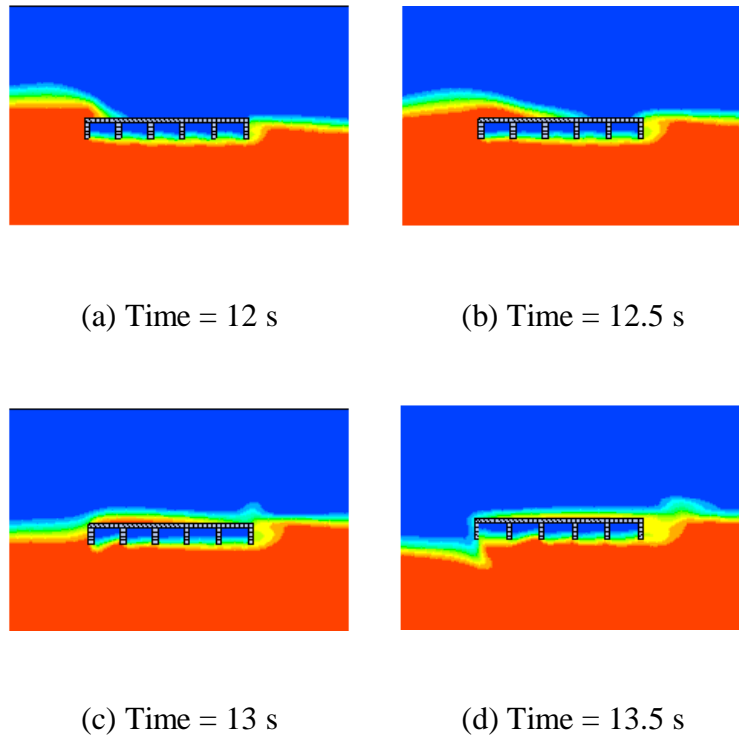


**Figure 3-6** An illustrated 2D CFD model showing wave behavior acting upon a bridge superstructure changing with time (unit: second).

To verify the numerical results from the ANSYS software, an experimental study at scale 1:30 was conducted at the Hydraulics Laboratory of Hong Kong Polytechnic University, aiming at measuring hurricane loading acting upon the bridge superstructure. This experiment was conducted in an open channel of 27 *m* in length, 1.5 *m* in width, and 1.5 *m* in depth. Waves were generated by a piston-type wavemaker located at one end of the channel. The water elevation was captured by using capacitive wave height gauges. The bridge model was suspended at a certain level according to the surge elevation. The wave forces on the bridge model were measured by a multi-axis load cell. To compare the results to the numerical model, experimental measurements were computed based on the Froude scale model. At a certain surge

elevation, the uplift force increases along with the growing wave height. Generally, the numerical results were validated by the experiments with acceptable differences. A series of the maximum total uplift forces on bridge superstructure changing over different wave heights were selected to compare them with the numerical results at the surge elevation of 2.2 m. The comparison between the numerical results and the experimental results is shown in Figure 3-7.

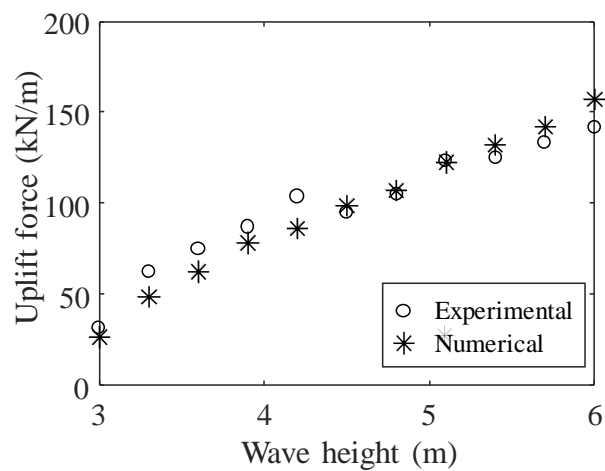


**Figure 3-7** Comparison between numerical and experimental results of the maximum total uplift force acting on the bridge superstructure.

The capacity of the bridge under hurricane-induced wave force refers to the vertical resistance, consisting of the self-weight of the bridge deck and connection strength between deck and substructure (Ataei and Padgett 2013; Mondoro *et al.* 2017). The weight of superstructure  $W_s$  can be computed as

$$W_s = (d_b W_0 + A_g n_g) \gamma l \quad (3-16)$$

in which  $d_b$  and  $W_0$  are thickness and width of the deck, respectively;  $A_g$  is the cross-sectional area of girders;  $n_g$  is the number of girders;  $\gamma$  is the unit weight of the material; and  $l$  is the length of span. For simply supported bridges, the vertical connectivity provided by the anchor bolts can be estimated by the concrete breakout strength. The total breakout strength  $F_c$  can be computed as the product of the total number of bolts and the connection strength of a single bolt, as shown in Eq. (3-17) (ACI, 2005)

$$F_C = n_{cb} \times \frac{A_N}{A_{N_0}} \psi_2 \psi_3 N_b \quad (3-17)$$

in which  $n_{cb}$  is the number of bolts;  $A_N$  is the projected area of the failure for the anchor;  $A_{N_0}$  is the projected area of the failure surface of a single anchor remote from edges;  $N_b$  is the basic concrete breakout strength of a single anchor; and  $\psi_2$  and  $\psi_3$  are modification factors. A normal distribution is adopted for concrete strength with a COV of 0.11 (Ellingwood and Hwang 1985).

The above functions illustrate the computation process of deterministic demand and capacity. Subsequently, the vulnerability of the bridge can be assessed by the probabilistic demand and capacity considering various uncertainties in hazard and structural parameters based on Monte Carlo simulation (Tu *et al.* 2017). Uncertainties associated with loading and capacity parameters, modeling, and biased errors are considered. The probability distributions of the associated parameters are mainly consistent with the error modeling provided in Ataei and Padgett (2013) unless specified. Such uncertainties could have a large impact on the vulnerability assessment. For instance, Ataei and Padgett (2015) identified the effect of various errors on fragility models for coastal bridges subjected to hurricane hazards. Therefore, uncertainty

should be carefully examined during the analysis. Uncertainties associated with the structural capacity mainly result from construction materials, construction error, and workmanship error, etc. The densities of concrete and steel are assumed to be normally distributed (JCSS, 2001). The expected density of reinforced concrete is  $2,400 \text{ kg/m}^3$ , with a coefficient of variation (COV) of 0.04. The mean density for steel is  $7,850 \text{ kg/m}^3$  and the COV is 0.01. The deck thickness follows a uniform distribution with the mean ranging from 95% to 105% considering construction and workmanship errors. Additionally, a model error is used to account for the uncertainty in concrete strength, with a mean of one and the COV of 0.23 (Eligehausen *et al.* 2006).

According to the above structural analyses, the total uplift force and vertical resistance are obtained. Subsequently, the probability of deck unseating can be computed by assessing the probability of demand exceeding capacity through Monte Carlo simulation. For a hurricane scenario with a return period of 100 years, the expected storm surge can be obtained as 1.74 m using the surge models of ADCIRC and SLOSH simulations and the wave height can be 4.06 m (Lin *et al.* 2010). The expected storm tide is usually estimated as 0.3 m to 0.5 m higher than the surge level (Lin *et al.* 2012). Herein, the total surge elevation can be evaluated as 2.05 m. Given these inputs, the probability of deck unseating failure of the hurricane with a return period of 100 years can be calculated as 0.1982.

### **3.4 Summary**

This chapter reviews and presents the application of the standard methodologies to assess the structural performance of civil infrastructure under single hazards. The procedures of probabilistic hazard analysis and structural vulnerability assessment under seismic and hurricane hazards are provided. Different from earthquakes, hurricanes show multi-hazard features and require multiple hazard parameters during the analysis. Various uncertainties associated with stochastic characteristics in hazard parameters (e.g., hazard frequency and intensity), demand, and capacity are considered during the analysis. The failure probability of the bridge can be calculated given specific hazard scenarios (such as defining return periods). The failure probability results can be significant inputs for risk and resilience assessment of the civil infrastructure in the following chapters.

# **CHAPTER 4 MULTIVARIATE ANALYSIS AND VULNERABILITY ASSESSMENT UNDER COMPOUND EXTREME EVENTS**

## **4.1 Introduction**

Recently, substantial financial and social losses caused by hurricane events, such as Hurricane Harvey 2017 and Hurricane Irma 2017, raised awareness of the government and the public to risk assessment and management. For instance, as stated by the U.S. Federal Emergency Agency (FEMA), commodities and essential resources including water and meals were exhausted during the emergency responses to Hurricanes Harvey and Irma (Raymond *et al.* 2020). Though efforts were made to minimize damage and losses, hurricanes remain one of the most hazardous and costly natural hazards (NCEI, 2020). In hurricane-prone areas, coastal civil infrastructure systems, such as highway bridges, are exposed to hurricane hazards throughout their lifetime. The repair and replacement of these systems may cause significant social disruption and economic consequences to the community. In order to manage such risks and enhance the resilience of coastal communities, it is crucial to assess the vulnerability of civil infrastructure under hurricane hazards. A hurricane indicates the multi-hazard feature, as it consists of concurrent hazards such as large waves, high storm surge, and strong wind. The compounding effects of hurricanes on civil infrastructure have not been fully investigated. The correlated relationship among hurricane parameters and the associated impact on the structural vulnerability should be studied.

This chapter aims to propose a copula-based probabilistic framework for coastal infrastructure to assess vulnerability subjected to hurricanes. The copula function is applied to model the dependence between storm parameters when modeling the probabilistic demand of highway bridges. An illustrative example is provided to calculate the probability with respect to deck unseating failure of a typical simply supported highway bridge. A three-dimensional model of the bridge is established to compute the surge and wave loads acting on the bridge deck. Dependence between peak water level and maximum wave height is modeled based on data records. The peak water level refers to the fluctuation peaks of sea level, consisting of the impact of storm surge and tide in this context. The dependence between peak water level and maximum wave height is considered only for hurricane events. Due to the flexibility of the copula approach, the proposed framework is not limited to illustrate the interrelationship of hurricane parameters, which can be implemented to dependence analyses under various hazards. The vulnerability assessment utilizes the approach introduced in CHAPTER 3 by considering various uncertainties springing from parameters associated with demand and capacity. Consequently, a copula-based framework for vulnerability analysis is developed to aid risk assessment and management of civil infrastructure by considering dependent hazard parameters.

## **4.2 Multivariate dependence model**

In this context, dependence (or correlation) refers to the statistical association between random variables (Joe 2014). The tail dependence implies the correlation between variables at the tail of the distribution. For instance, the lower tail dependence indicates

correlation in the lower-left quadrant and the upper tail dependence is associated with the upper-right quadrant (Joe 2014; Nelsen 2006). Such tail phenomena are commonly observed in data associated with extreme events (Salvadori *et al.* 2007), particularly among storm (Wahl *et al.* 2015) and marine variables (Zhang *et al.* 2018b). Different copula functions are capable to represent different degrees of tail dependence.

A copula couples the marginal distributions to the multivariate distribution function, in which the marginal distribution for each variable is uniform over the unit interval (Nelsen 2006). Let a series of random variables  $X_1, X_2, \dots, X_d$  have marginal distribution functions  $F_i(x_i), i = 1, \dots, d$ . The joint distribution function of these random variables is defined as  $J$ . According to Sklar's theorem (Sklar 1959), there exists a copula  $C: [0, 1]^d \rightarrow [0, 1]$  such that

$$J(x_1, \dots, x_d) = C(F_1(x_1), \dots, F_d(x_d)) \quad (4-1)$$

As shown in Eq. (4-1), the joint effect described by the copula function and the marginal distributions of random variables are separately considered. Such a dependence structure provides sufficient flexibility during the simulation and analysis. Based on this advantage, complicated dependence structures can be effectively modeled by changing the copula model without affecting the marginals. If the marginals  $F_i(x_i)$  are all continuous, the  $d$ -dimensional copula  $C$  is unique

$$C(u_1, \dots, u_d) = J(F_1^{-1}(u_1), \dots, F_d^{-1}(u_d)) \quad (4-2)$$

The probabilistic density function of copula  $C$  can be denoted as  $c(u)$

$$c(u) = \frac{\partial^d C(u_1, \dots, u_d)}{\partial u_1 \dots \partial u_d} \quad (4-3)$$

Accordingly, the joint density  $f_X(x_1, x_2, \dots, x_d)$  of random variables can be expressed as

$$f_X(x_1, \dots, x_d) = c\{F_1(x_1), \dots, F_d(x_d)\} \prod_{i=1}^d f_i(x_i) \quad (4-4)$$

As shown in Eq. (4-4), the copula function establishes the dependency structure separately from the marginals. In other words, the dependence between random variables is governed by a copula regardless of the selection of univariate distributions. Compared to directly dealing with the complex joint probability  $J$ , the theorem of copula offers significant flexibility during applications (Jane *et al.* 2018; Zhang *et al.* 2018b).

Herein, the bivariate relationships are considered. The three most commonly used copula families are introduced: elliptical copulas, Archimedean copulas, and Extreme Value copulas. The elliptical family is based on elliptical distribution functions and consists of the Gaussian copula and the Student's  $t$ -copula. The Gaussian copula is the most popular one in practice. It is given by

$$C(x_1, x_2) = \Phi_{\zeta}(\Phi^{-1}(x_1), \Phi^{-1}(x_2)) \quad (4-5)$$

in which  $\Phi(\cdot)$  is the CDF of a multivariate normal distribution;  $\zeta$  is the correlation matrix; and  $\Phi^{-1}(\cdot)$  is the inverse CDF of the standard normal distribution. The Gaussian copula does not have tail dependence, i.e., lower and upper tail dependence are zero.

The Student's  $t$ -copula is a generalization of the Gaussian copula. Compared with the Gaussian copula having one dependence parameter, the student's  $t$ -copula is associated with two parameters, resulting in more probability density at the tails. The function of the student's  $t$ -copula can be written as

$$C(x_1, x_2) = t_{v, \zeta}(t_v^{-1}(x_1), t_v^{-1}(x_2)) \quad (4-6)$$

where  $t_v(\cdot)$  is the CDF of a multivariate standardized student's  $t$  distribution;  $v$  is the parameter indicating the degree of freedom;  $\zeta$  is the correlation matrix; and  $t_v^{-1}(\cdot)$  is the inverse of the CDF of the standard student's  $t$  variable. The Student's  $t$ -copula has identical lower and upper tail dependence, which can be computed as

$$\lambda_l = \lambda_u = 2t_{v+1}\left(-\sqrt{\frac{(v+1)(1-\rho)}{1+\rho}}\right) \quad (4-7)$$

Instead of relying on probabilistic distribution functions, the Archimedean copulas are constructed incorporating monotonic characteristics. Commonly used Archimedean copulas include Clayton, Gumbel, and Frank copulas, in which the Gumbel copula is also an Extreme Value copula (Genest and Rivest 1989). The three copulas have only one dependence parameter and exhibit different tail dependence conditions. For instance, the Clayton copula has lower tail dependence but has no upper tail dependence. In contrast, the Gumbel copula interprets upper tail dependence with no lower tail dependence. The Frank copula has no tail dependence. Table 4-1 gives the copula functions and tail dependence characteristics of the Clayton, Gumbel, and Frank copulas using the dependence parameter  $\theta$ .

**Table 4-1** Examples of Archimedean copulas and their tail dependence characteristics.

Name	Copula function $C(x_1, x_2)$	Tail dependence (lower, upper)
Clayton	$(x_1^{-\theta} + x_2^{-\theta} - 1)^{-1/\theta}, \theta > 0$	$(2^{-1/\theta}, 0)$
Gumbel	$\exp\left[-((-\ln x_1)^\theta + (-\ln x_2)^\theta)^{1/\theta}\right], \theta \geq 1$	$(0, 2 - 2^{1/\theta})$
Frank	$-\frac{1}{\theta} \ln\left(1 + \frac{(\exp(-\theta x_1) - 1)(\exp(-\theta x_2) - 1)}{\exp(-\theta) - 1}\right), \theta \in \mathbb{R}$	$(0, 0)$

In addition to elliptical and Archimedean copulas, the Extreme Value family plays an important role in the dependence analysis. As the Extreme Value copulas arise naturally from the extreme value theory, they can model the tail dependence associated with extreme events (Gudendorf and Segers 2010). The Extreme Value copulas are generated from the Extreme Value theory to describe the limit characteristics of values associated with extreme events, such as natural hazards (Gudendorf and Segers 2010; Joe 1997). The Hüsler-Reiss copula, as a special case of Extreme Value copulas, is introduced herein. It is given by (Hüsler and Reiss 1989)

$$C(x_1, x_2) = \exp\left\{-\tilde{x}_1 \Phi\left[\frac{1}{\theta} + \frac{1}{2} \theta \ln\left(\frac{\tilde{x}_1}{\tilde{x}_2}\right)\right] - \tilde{x}_2 \Phi\left[\frac{1}{\theta} + \frac{1}{2} \theta \ln\left(\frac{\tilde{x}_2}{\tilde{x}_1}\right)\right]\right\} \quad (4-8)$$

in which the dependence parameter  $\theta$  is larger than or equal to zero;  $\tilde{x}_1 = -\ln x_1$ ; and  $\tilde{x}_2 = -\ln x_2$ . For the Extreme Value copulas, the parametric submodel can be determined by using the Pickands dependence function (Gudendorf and Segers 2010). For instance, Pickands dependence function of Hüsler-Reiss copula can be written as

$$A(y) = y\Phi\left[\frac{1}{\theta} + \frac{1}{2}\theta\ln\left(\frac{y}{1-y}\right)\right] + (1-y)\Phi\left[\frac{1}{\theta} - \frac{1}{2}\theta\ln\left(\frac{y}{1-y}\right)\right] \quad (4-9)$$

By using Eq. (4-9), the upper tail dependence  $\lambda_u$  as shown in Eq. (4-10) associated with the Hüsler-Reiss copula can be computed using

$$\lambda_u = 2(1 - A(1/2)) \quad (4-10)$$

The lower tail dependence of Extreme Value copulas is zero, except for the case with perfect dependence  $A(1/2) = 1/2$ . In other words, lower tails of Extreme Value copulas are asymptotically independent.

Copula models can be applied to describe various dependence relationships. Statistical inference of the dependence structure relies on the measure of association. Previously, the degree of dependence among variables is widely assessed by Pearson's correlation coefficient due to its simplicity and convenience. Pearson's coefficient measures the linear correlation between variables (Joe 2014). For instance, Vishnu *et al.* (2021) modeled the correlation impact associated with resilience and sustainability metrics by using the Pearson's rank correlation. Due to its limited application range, other measures such as Kendall's tau and Spearman's rho are developed to evaluate the association. Herein, Kendall's tau is employed. This correlation coefficient computes

the variation between probabilities of discordance and concordance (Joe 2014). For two independently and identically distributed random vectors  $(X_1, Y_1)$  and  $(X_2, Y_2)$  with the identical joint probability distribution, Kendall's tau is given by

$$\tau = P[(X_1 - X_2)(Y_1 - Y_2) > 0] - P[(X_1 - X_2)(Y_1 - Y_2) < 0] \quad (4-11)$$

Let  $C(u, v)$  refers to the copula function of  $X$  and  $Y$ , Kendall's tau can be written as

$$\tau = 4 \iint_{[0,1]^2} C(u, v) dC(u, v) - 1 \quad (4-12)$$

For the random vector  $(X, Y)$  with a sample size of  $n$ , Kendall's tau can be presented as

$$\tau_n = \frac{(N_c - N_d)}{N_c + N_d} \quad (4-13)$$

where  $N_c$  and  $N_d$  are the number of concordant pairs and the number of discordant pairs, respectively.

### 4.3 Multivariate hazard analysis under hurricanes

The vulnerability analysis evaluates the performance and the probability of failure of civil infrastructure subjected to hazards. The hurricane-induced wave and surge forces may lead to deck unseating damage of coastal simply supported bridges. The vulnerability assessment considering probabilistic modeling of demand and capacity incorporating dependent storm parameters is presented in this section.

A conventional approach to assess vulnerability subjected to hurricane hazards is based on a single parameter, e.g., the wave height. The main limitation of such univariate assessment is that the prediction of failure probability of infrastructure is highly dependent on the selected parameter. In consequence, the impact of model parameter variation on infrastructure performance has to be assessed by costly re-analysis of different sets of parameter combinations (Ghosh *et al.* 2013). To address such limitations, multivariate fragility analysis has been increasingly applied in hazard risk assessment. For instance, Jane *et al.* (2018) presented a fragility representation for shingle beaches based on multiple variables, including wave height, period, and water level. The dependence between geometric parameters was modeled by a Gaussian copula. By incorporating the inundation hazard assessment model, Vorogushyn *et al.* (2010) conducted a comprehensive flood hazard assessment to compute the probability of failure of dike breaches. Multiple intensity indicators were involved in their work, such as flow velocity, inundation depth, and inundation duration. Charvet *et al.* (2015) proposed the representation of multivariate fragility functions for the city of Kesenuma subjected to tsunami damage, by considering different tsunami intensity measures (e.g., the surveyed flow depth, simulated flow velocity, and the debris impact). Segura *et al.* (2020) presented a multivariate fragility assessment framework to generate seismic fragility surfaces of concrete gravity dams incorporating machine learning techniques. Balomenos *et al.* (2020) proposed parameterized fragility models for regional-level risk assessment of bridges by considering different bridge classes, where the joint impact of surge and wave loads is investigated by using the joint probability method.

As described in CHAPTER 3, evaluating the failure probability under hurricanes is conditioned on the intensity measure. Due to the complex interaction between storm parameters, it is inappropriate to concentrate on a single wave or surge parameter to quantify the demand or failure probability. Thus, there should be at least two intensity measure parameters employed to maintain the efficiency and accuracy of the probabilistic vulnerability analysis. There are several parameters associated with the hurricane hazard, such as wave height, wave period, and relative surge elevation. Ataei and Padgett (2013) selected the maximum wave height and relative surge height as the intensity measures to conduct fragility analysis for coastal highway bridges, as these two parameters are essential inputs for the equations of wave and surge loads (AASHTO, 2008).

Herein, owing to the dependency analysis in Wahl *et al.* (2016) and Masina *et al.* (2015) and the inputs for the proposed probabilistic demand model, the dependence between the peak water level and maximum wave height is considered. Such dependence is considered only for hurricane events. These two parameters are utilized to compute the probabilistic demand. The peak water level refers to the relative elevation of storm surge and tide, above mean sea level. The mean value of storm surge can be computed from the maximum wind speed. For instance, Liang and Julius (2017) proposed a linear relationship between the storm surge and maximum wind speed, based on 58 wind-surge events that occurred near Chesapeake Bay, Virginia, from 1995 to 2015. The surge height is assumed to be uniformly distributed ranging from 80% to 120% of the mean (Saeidpour *et al.* 2019). The initial water depth is assumed to be deterministic. The average tide level is set as zero. The probabilistic distribution of annual tidal is determined by using the density histogram of the hydrodynamic model

presented in (McInnes *et al.* 2013). Subsequently, the marginal distribution of the peak water level can be fitted based on the surge and tide. Wahl *et al.* (2016) indicated that the water level can be fitted by the generalized extreme value (GEV) distribution using historical observations. The PDF of the GEV distributed peak water level  $W$  is

$$f_w(w) = \frac{1}{\sigma} Q(w)^{\xi+1} \exp(-Q(w)), \text{ and}$$

$$Q(w) = \begin{cases} (1 + \xi(\frac{w-\varepsilon}{\sigma}))^{-1/\xi}, & \xi \neq 0 \\ \exp(-\frac{w-\varepsilon}{\sigma}), & \xi = 0 \end{cases} \quad (4-14)$$

where  $\xi$  is the shape parameter;  $\varepsilon$  is the location parameter; and  $\sigma$  is the scale parameter. It should be noted that the wind speed informs the parameters of the surge distribution, thus the wind speed also affects the marginal parameters of the GEV distributed peak water level. When different return period scenarios of hurricanes are considered, the marginal parameters of the peak water level should be assessed by using the hurricane-induced wind speed for each return period. The maximum wave height  $H$  can be computed by a classical Rayleigh model (Longuet -Higgins 1980)

$$f_H(h) = \frac{4h}{H_s^2} \exp\left(-\frac{2h^2}{H_s^2}\right) \quad (4-15)$$

where  $f_H(h)$  is the PDF of the maximum wave height and  $H_s$  is the significant wave height, defined as the mean height of the highest third of waves.

Given the marginal density functions associated with storm parameters, the CDFs of both the peak water level  $W$  and maximum wave height  $H$  can be determined,

and they are denoted as  $F_W(w)$  and  $F_H(h)$ , respectively. Subsequently, the copula function of the random vector  $(W, H)$  is given by

$$J(w, h) = C(F_W(w), F_H(h)) \quad (4-16)$$

As the relevant parameters (e.g., water level) are sensitive to regional/local factors, e.g., bathymetry and the shape of the coast, different copulas could be selected for different investigated regions. When there are data available, the copula model can be determined by using goodness-of-fit tests (Jane *et al.* 2018; Zhang *et al.* 2018b). The process of finding the optimal copula model typically requires two stages. The first stage is to determine appropriate distributions for the univariate variables. Candidate distributions can be chosen from empirical models for the investigated storm variable (Trepanier *et al.* 2017). Graphical approaches such as the L-moments method (Hosking and Wallis 1997) can be applied. L-moments refer to linear combinations of order statistics (similar to the statistical moments), which can be used to describe information about the shape, location, and dispersion of a probability distribution (Hosking and Wallis 1997). By plotting the L-moment ratio diagram, the candidate distribution that has the closest L-skewness and L-kurtosis values to data should be adopted for the following copula analysis (Um *et al.* 2017). Subsequently, the probability plot correlation coefficient (PPCC) test (Heo *et al.* 2008; Vogel and Kroll 1989) can be used to perform the goodness-of-fit test for the univariate distribution. The second stage is to find the optimal copula model. Candidate copulas can be selected from different copula families, as introduced in the previous section. Dependence parameters with respect to each copula function can be determined by the maximum likelihood method. For instance, by incorporating the corrected Akaike and/or Bayesian information

criterion (Burnham and Anderson 2004), the candidate copula with the smallest information criterion is recommended (Masina *et al.* 2015). For validation, the goodness-of-fit assessment for this stage can be checked by using the approach delivered by Genest *et al.* (2006), by checking the Cramér-von Mises statistics  $S_n$ . A smaller value of  $S_n$  indicates a better copula model among the candidates. The bootstrap method presented by Genest *et al.* (2009) can be applied to compute the  $p$ -value associated with the statistics  $S_n$ , and a larger  $p$ -value implies a better fit.

#### **4.4 Illustrative example**

The proposed copula-based vulnerability assessment framework is applied to compute the vulnerability of a highway bridge under hurricanes. The investigated bridge is an I-10 bridge over Escambia Bay, Florida, and it was severely damaged by Hurricane Ivan in 2004 (Douglass *et al.* 2004). The bridge is simply supported, which is susceptible to deck unseating during hurricanes, as described in CHAPTER 3. The study area graphic and tracks of historical tropical cyclones (the track of Hurricane Ivan is highlighted) are shown in Figure 4-1. The bridge has a span of 15.85  $m$  and a width of 9.14  $m$ . Dimensions of the bridge superstructure are illustrated in Figure 4-2(a). The distance from the initial water level to the bottom of the girder is assumed to be 6.3  $m$ . Four scenarios of hurricane hazard are considered, with return periods of 50 years, 75 years, 100 years, and 500 years, respectively. Dependent storm parameters are modeled using copula functions. The Clayton, Gaussian, and Hüsler-Reiss copulas are employed to explore the effect of different copula families and tail dependence characteristics on structural vulnerability.

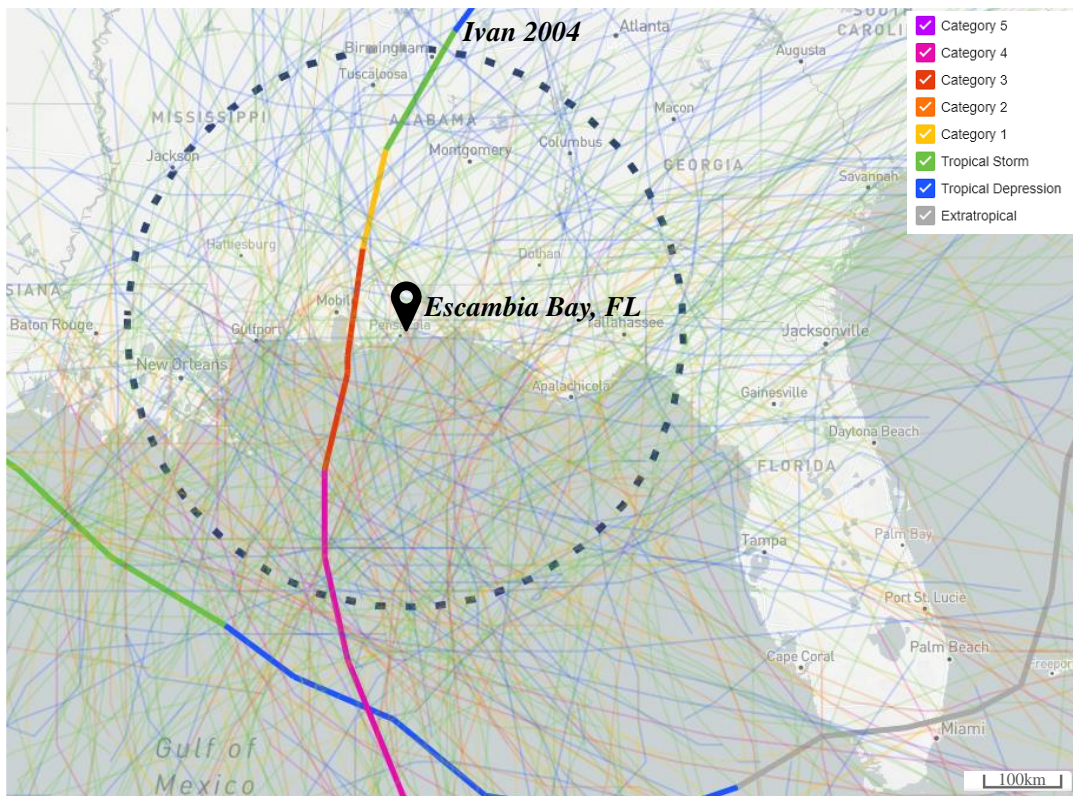


**Figure 4-1** The bridge in Escambia Bay, Florida, and tracks of historical tropical cyclones, including Hurricane Ivan (adapted from NOAA 2020).

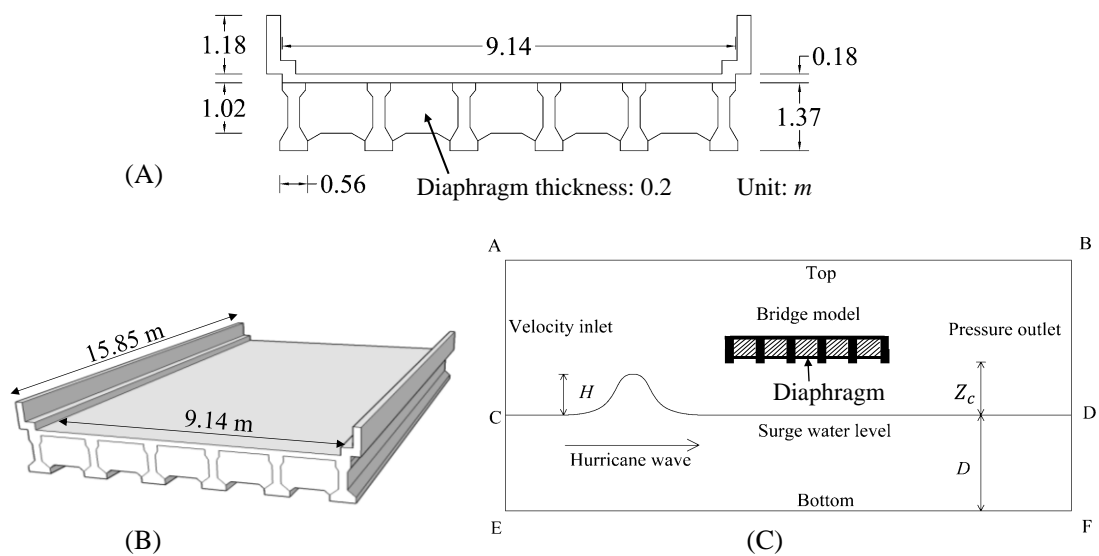


**Figure 4-2** (a) Geometry of the bridge deck; (b) The three-dimensional model of the bridge deck; and (c) Diagram of the computational domain of the numerical model.

The demand, i.e., the maximum vertical wave loads acting upon the deck, can be assessed by modeling based on the CFD analysis. Two-dimensional CFD models are commonly adopted in fragility analysis (Li *et al.* 2020a; Zhu and Dong 2020), as described in Section 3.3.2. Although the two-dimensional numerical model reduces the computation cost, the analysis of the fluid-structure interaction is limited to the longitudinal axis, thus providing less accurate results. The simulation results attained by the two-dimensional model can be relatively different from the analytical outcomes (Jin and Meng 2011). Xu *et al.* (2016) indicated that the wave-bridge interaction based on the two-dimensional model may not completely capture the wave components. Moreover, inappropriate simplification by the two-dimensional model may result in errors in the wave results (Bozorgnia and Lee 2012). Therefore, a three-dimensional CFD model is established to study the fluid-structure interaction and evaluate the external wave loads on the bridge model. The correlated maximum wave height and peak water level are inputs for the analysis. The wave loads acting upon the bridge deck can be assessed accordingly.

A three-dimensional numerical model of the bridge superstructure is established by using the software *ANSYS Fluent* (V.17.2). The I-shaped girders are modeled with rectangular sections to reduce the computational expense. The numerical model of the bridge is shown in Figure 4-2(b) and the diagram of the computation domain of the model is demonstrated in Figure 4-2(c). The plane CD is the water level, which indicates the interface between air and water. Planes AE and BF refer to the velocity

inlet and pressure outlet, respectively. The top plane AB is set as the constant atmospheric pressure and the bottom EF is defined as the no-slip stationary wall condition. The total force component is computed as the sum of the dot product of the pressure and viscous forces on each face with the specified force vector (ANSYS 2009). Based on the CFD model, the wave-air-structure interaction can be evaluated. The three-dimensional model shows insights into the interactive effects. For instance, the wave-air-deck interaction with a relative clearance ( $Z_c$ ) at 1.5  $m$  and a maximum wave height ( $H$ ) of 3  $m$  is shown in Figure 4-3. The wave-air-deck interaction effects are shown on the left column (i.e., Figure 4-3(a), (c), and (e)), and the associated wave profiles are shown on the right column (i.e., Figure 4-3(b), (d), and (f)). The solitary wave starts from the origin and flows along the x-axis. The water volume fraction is represented by different colors according to the volume of fluid method. For instance, the water volume fraction of the water phase is one, while the value of the air phase is zero. In Figure 4-3, three chronological stages of the wave acting upon the deck are presented. Initially, there is a constant water level. When there is a wave generated, the water surface starts to rise. Subsequently, the wave arrives, and overtopping occurs, thus resulting in loading acting on the bridge deck.

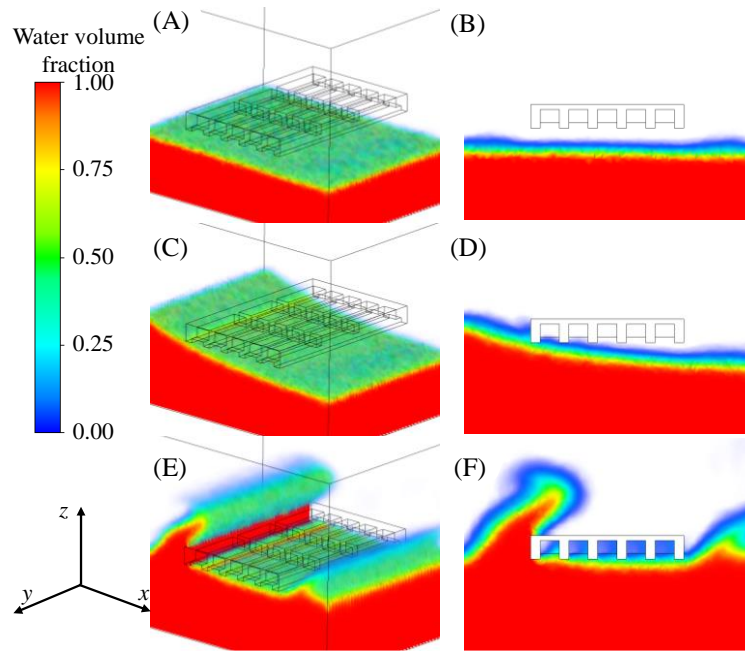


**Figure 4-3** An illustrative diagram of the wave-air-structure interaction effects in the three-dimensional CFD model.

Given the return period, the relevant hurricane-induced wind speed can be computed using the model developed by Vickery *et al.* (2000). Li and Ellingwood (2006) and Mondoro *et al.* (2017) indicated that the Weibull distribution can be adopted to describe the wind speed  $V$ . For instance, the log transform of the CDF of the Weibull distributed wind speed  $F_V(v)$  can be written as

$$\ln[-\ln(1 - F_V(v))] = \alpha_v \ln(v) - \alpha_v \ln(\mu_v) \quad (4-17)$$

in which  $\mu_v$  and  $\alpha_v$  are scale and shape parameters. The CDF of wind speed  $F_V(v)$  can be expressed by the return period  $T$  (Vickery *et al.* 2000)

$$F_V(v) = P[V \leq v] = 1 - \frac{1}{T} \quad (4-18)$$

Accordingly, scale and shape parameters for Eq. (4-17) can be determined from the design wind speed maps (i.e., maps of hurricane-induced wind speeds) associated with different storm return levels (Vickery *et al.* 2000). Subsequently, the wind speed of the four investigated hurricane scenarios with return periods of 50, 75, 100, and 500 years can be computed as 47 m/s, 57 m/s, 63 m/s, and 72 m/s, respectively. Other models of the estimated return levels can also be applied, e.g., Malmstadt *et al.* (2010). Herein, the analytical approach developed by Vickery *et al.* (2000) is adopted. Based on the Saffir–Simpson Hurricane wind scale (Schott *et al.* 2019), the hurricane scenario with a 50-year return period can be considered as a non-major hurricane, while the other three scenarios can be classified as major hurricanes. The wind speed informs the mean value of storm surge following the model of Liang and Julius (2017) as introduced in the previous section. Probabilistic surge and tide are computed based on the aforementioned empirical models. Subsequently, the marginal distribution of the peak water level is fitted to a GEV distribution. Herein, the estimation of tide and surge is based on empirical models, and the interaction between them is not considered. Tide and surge are independently modeled using their univariate probabilistic distribution. Based on Wahl *et al.* (2016), there can be some dependence between these two parameters, which could affect the peak water level. Further studies are needed to assess the interaction and pairing of tides and surges. The significant wave height  $H_s$  can be assessed from the wind speed based on the Shore Protection Manual (CERC, 1984)

$$H_s = 5.112 \times 10^{-4} U_A F^{0.5} \quad (4-19)$$

in which  $U_A = 0.71 V^{1.23}$  is the adjusted wind velocity based on the wind velocity  $V$ ; and  $F$  is the fetch length and assumed to be 1000 m. The maximum wave height  $H$  is taken

as 1.8 times of the significant wave height  $H_s$  (e.g.,  $H = 1.8 H_s$ ) (AASHTO, 2008). Consequently, different parameters of the marginal distributions associated with the peak water level and maximum wave height are related to the wind speeds at different return periods. Based on these marginal parameters, the two storm parameters (i.e.,  $W$  and  $H$ ) can be simulated from the copula function and transformed back to the original scale.

The copula function associated with the maximum wave height and peak water level can be determined using goodness-of-fit tests based on observed data. Wahl *et al.* (2016) assessed the flooding and erosion risk in the northern Gulf of Mexico by modeling six hydrodynamic variables (i.e., astronomical tide, storm surge, significant wave height, peak wave period, wave direction, and sea-storm event duration) affecting the total water level. In their study, 67 groups of annual average significant wave height and the averaged peak water level for sea-storm events were extracted from observation records at a tide gauge on Dauphin Island from 1980 to 2013. According to Wahl *et al.* (2016), sea-storm events are identified when the hourly total water level exceeding a critical threshold, i.e., 1.2 m above the North American Vertical Datum of 1988. Additionally, average significant wave heights associated with the events are selected when the heights exceed 1.6 m and 1.4 m for winter and summer, respectively. The detailed processing procedure of the data can be found in Wahl *et al.* (2016).

Based on their 67 groups of data, the copula function of the correlated maximum wave height and peak water level is assessed by using goodness-of-fit tests. Herein, the impact of seasonal cycles on the dependence structure between variables is neglected, but it can be considered in future studies. For the marginal distribution, it is identified

that there are many distribution options to fit the marginal distribution, due to the limited data record. Herein, marginal distributions of the significant wave height and peak water level are fitted using the Rayleigh and GEV distributions, respectively. For dependence modeling, Kendall's tau correlation coefficient is 0.41. Different copula candidates are employed for the goodness-of-fit tests, including Gaussian, Student's  $t$ , Clayton, Gumbel, Frank, and Hüsler-Reiss copulas. Subsequently, based on the Akaike information criterion (AIC), the Clayton copula is adopted among the copula candidates, with the smallest  $S_n$  ( $= 0.0191$ ) and largest  $p$ -value ( $= 0.6176$ ). In comparison, the elliptical and Extreme Value families show deficient performance in fitting the dataset. For instance, the  $S_n$  and  $p$ -value for the Gaussian copula are 0.0350 and 0.0490, respectively, while values for the Hüsler-Reiss copula are 0.0652 and 0.0098, respectively. Figure 4-4 shows the scatter plot of observed and simulated values at the site in the Gulf of Mexico, in which there are 500 samples simulated from the Clayton copula.

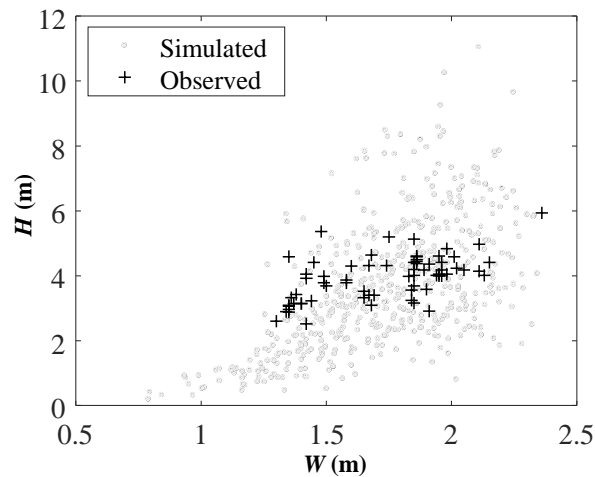


**Figure 4-4** Scatter plot of observed and simulated maximum wave height and peak water level based on the selected Clayton copula.

In this illustrative example, as the data record extracted from Wahl *et al.* (2016) are close to the investigated region, the fitted Clayton copula can be an appropriate option to model the positive correlation between the maximum wave height and peak water level. In the field of risk assessment, when there is a lack of data, dependence models may be constructed based on the correlation coefficient (Hong *et al.* 2014; Wang *et al.* 2020). In order to investigate the effect of copula family and tail dependence behavior between hazard parameters on the structural vulnerability, the Gaussian and Hüsler-Reiss copulas are also employed herein. The Clayton copula allows for lower tail dependence, while the Hüsler-Reiss interprets upper tail dependence. The Gaussian copula indicates no tail dependence. Different values of Kendall's tau (equal to 0.1, 0.5, and 0.9) are considered to identify the impact of the degree of dependence between storm parameters on the bridge vulnerability. An illustrated diagram of correlated maximum wave height  $H$  and peak water level  $W$  in the copula domain with 1000 samples is shown in Figure 4-5. It can be identified that

the correlation between variables increases with Kendall's tau. The tail dependence behavior can also be observed. For instance, the correlation resulting from the Hüsler-Reiss copula is more pronounced in the upper tail area, while the correlation caused by Clayton copula is more prominent in the lower tail region.

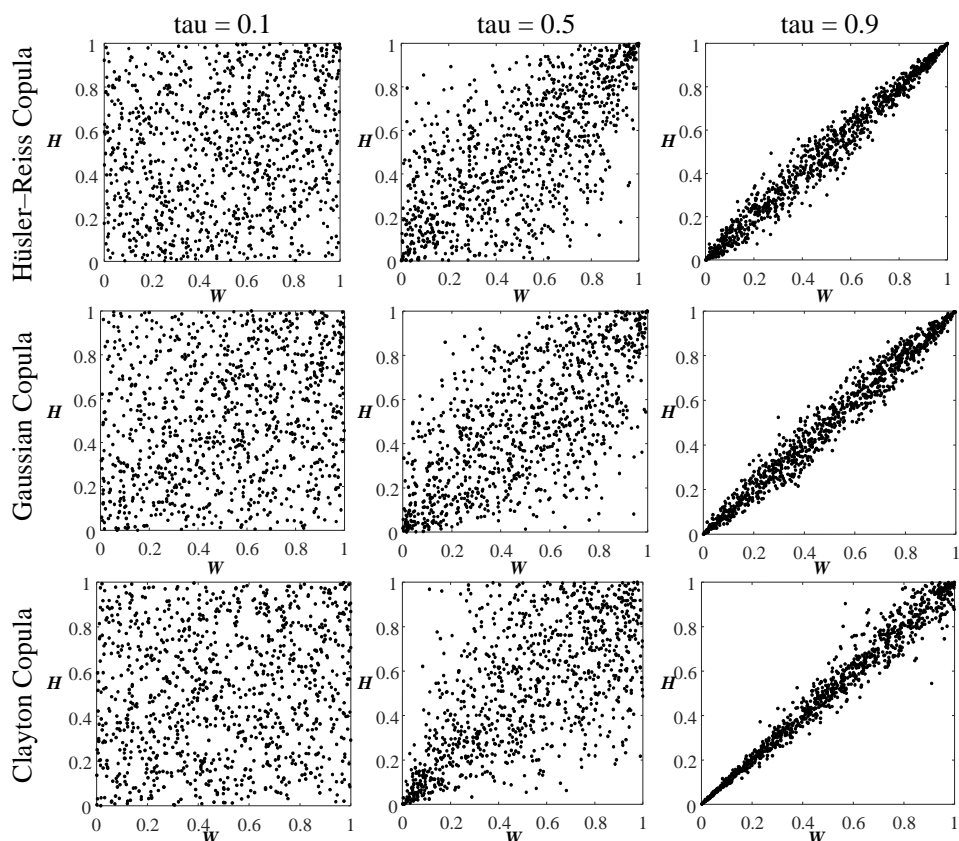


**Figure 4-5** Samples of correlated  $H$  and  $W$  in the copula domain using Hüsler-Reiss, Gaussian, and Clayton copula functions considering Kendall's tau equal to 0.1, 0.5, and 0.9.

The vulnerability of the bridge associated with the four hazard scenarios (50-, 75-, 100-, and 500-year return periods) is calculated by performing Monte Carlo simulations, as shown in Table 4-2. For a given return period and Kendall's tau value,

a range of storm and structural parameters are generated with a sample size of 500,000. When the maximum wave height and peak water level are independent, the structural vulnerability can be computed by setting Kendall's tau as zero. At the 50-year return period, the probability of the bridge failing under the case with dependent storm parameters increases significantly compared with the independent case. For example, the failure probability associated with the Clayton copula model is nearly tripled compared to the independent result. For the scenario with a 75-year return period, copulas have a moderate impact on the probability of failure (i.e., a modest increase in the failure probability), compared with the 50-year return period scenario. Under the same degree of correlation (e.g., with the same Kendall's tau), the vulnerability of the bridge differs with respect to each copula model, due to different tail dependence characteristics in copula models. For instance, for the 50-year scenario, when there is a medium correlation (Kendall's tau equal to 0.5), the probability of failure is 0.0445 with the Clayton copula and is 0.0605 with the Hüsler-Reiss copula.

**Table 4-2** Probability of failure of the bridge associated with different copula models under 50-, 75-, 100-, and 500-year hurricane scenarios.

Return period	50 years			
	Kendall's tau = 0	Kendall's tau = 0.1	Kendall's tau = 0.5	Kendall's tau = 0.9
Clayton copula	0.0251	0.0282	0.0445	0.0699
Gaussian copula	0.0251	0.0318	0.0563	0.0686
Hüsler-Reiss copula	0.0251	0.0348	0.0605	0.0689

Return period	75 years			
Kendall's tau	0	0.1	0.5	0.9
Clayton copula	0.1687	0.1778	0.2090	0.2163
Gaussian copula	0.1687	0.1779	0.2012	0.2117
Hüsler-Reiss copula	0.1687	0.1748	0.1984	0.2101

Return period	100 years			
Kendall's tau	0	0.1	0.5	0.9
Clayton copula	0.2980	0.3064	0.3278	0.3166
Gaussian copula	0.2980	0.3032	0.3111	0.3131
Hüsler-Reiss copula	0.2980	0.2989	0.3032	0.3107

Return period	500 years			
Kendall's tau	0	0.1	0.5	0.9
Clayton copula	0.7897	0.7826	0.7648	0.7776
Gaussian copula	0.7897	0.7865	0.7869	0.7821
Hüsler-Reiss copula	0.7897	0.7926	0.7956	0.7824

For hurricane scenarios with return periods of 100 and 500 years, the vulnerability of the bridge is not significantly affected by the dependent hazard parameters. The failure probability computed using different copula functions may experience a slight increase (e.g., at the 100-year return period) or fluctuate around the result of the independent case (e.g., at the 500-year return period). Probably, under such

intense hurricanes, uncertainties caused by probabilistic modeling of demand and capacity have a greater influence on the vulnerability of bridges, compared to uncertainties resulting from the copula modeling. For instance, there may exist a larger dispersion (i.e., standard deviation) in terms of the storm surge for the 500-year return period scenario than the 50-year return period scenario. In this example, the storm surge is uniformly distributed ranging from 80% to 120% of the mean. When there are strong hurricanes, both the mean and the standard deviation of surge are escalated with the hurricane intensity. Subsequently, uncertainties associated with probabilistic demand may be amplified. Additionally, under the investigated scenarios, for a given Kendall's tau, the Hüsler-Reiss copula gives consistently greater failure probability estimates than the other copulas at the 500-year return period. Further studies should be conducted to investigate the effect of the upper tail dependence on the extremes of storm variables by considering different Extreme Value copulas and different intensity measures.

There are several limitations of the proposed approach. Due to the limited data record, the Clayton copula is fitted based on the annual average significant wave height and water level. The dependence structure between storm parameters is not based on hurricane events. Under the circumstance, the goodness-of-fit result associated with the Clayton copula may not be optimal for the investigated area. The fitting of marginal distribution functions can also be enhanced given more data. As sea condition parameters can be influenced by seasonal cycles, further studies may investigate the impact of seasonal change on the dependence structure between storm parameters. The interaction between tide and surge needs to be considered in future studies, as their pairing may have an impact on the peak water levels.

## 4.5 Summary

This chapter develops a copula-based vulnerability assessment framework for civil infrastructure subjected to hurricane hazards. A mathematical tool using the copula function is introduced to model the dependent hazard parameters for the vulnerability assessment. The proposed framework is applied to a typical coastal bridge. The Clayton, Gaussian, and Hüsler-Reiss copulas are used to model the dependence structure between the maximum wave height and peak water level. These copula models are employed to identify the impact of different tail dependence characteristics on the vulnerability of the bridge. Given the deck unseating failure, probabilistic modeling of demand, referring to hurricane-induced surge and wave loading acting on the bridge deck, is calculated by establishing a three-dimensional model. The mathematical copula tool delivers desired performance in modeling dependent hazard parameters, as the marginal distribution and the correlated effects are considered separately.

The probability of failure with respect to the investigated bridge can be affected by incorporating dependent storm parameters. In the illustrative example, such effects may be more pronounced for non-major hurricanes, compared with the results for major hurricanes. Different degrees of correlation between the maximum wave height and peak water level are considered. For the investigated scenarios with return periods of 50 and 75 years, the probability of the bridge failing increases with the correlation coefficient. For scenarios with return periods of 100 and 500 years, the vulnerability incorporating the fitted Clayton copula is close to the result of the independent case, which is insensitive to the change in the correlation coefficient. Three copula models,

including Clayton, Gaussian, and Hüsler-Reiss copulas, are employed to identify the impact of tail dependence between storm parameters on the structural vulnerability. Under the identical degree of correlation, the vulnerability of the bridge differs with the tail dependence behavior. Therefore, the tail dependence between hazard parameters should be carefully considered and evaluated during the assessment. The proposed framework can be implied to the risk management of civil infrastructure.

# **CHAPTER 5 LONG-TERM RESILIENCE AND LOSS UNDER STATIONARY HAZARDS USING RENEWAL APPROACH**

## **5.1 Introduction**

During their service life, civil infrastructure systems are exposed to various hazards such as earthquakes, floods, and hurricanes. The resulting structural damage can cause significant disruption to transportation systems and substantial economic loss to society. From a long-term perspective, the potential risk and loss can be accumulated and aggravated due to uncertainties throughout the entire life-cycle of civil infrastructure systems. Therefore, risk mitigation of engineering structures has received increasing awareness from researchers, policy-makers, and insurers in terms of assessing the performance, recovery capability, and long-term loss of engineering systems under natural hazards. Risk and resilience, as paramount performance indicators, play a significant role during life-cycle analysis.

In previous studies, the effect of stochastic occurrence and intensity of hazards on resilience and risk has not been investigated in most previous research. Despite the concept of long-term resilience was introduced by Yang and Frangopol (2019a), specific physical-informed damage models were not taken into account and the closed-form of expected long-term resilience has not developed. A general approach to formulate analytical expressions of long-term resilience and loss is required.

This chapter aims to present a renewal approach to quantify the long-term resilience and loss of civil infrastructure under a single hazard. Stationary hazard models, i.e., the homogeneous Poisson process, are focused. Monte Carlo simulation is conducted to validate results from the proposed renewal-based approach. An illustrative example is provided to assess the long-term resilience and loss of a typical highway bridge under representative hazard scenarios of earthquakes and hurricanes. The damage loss and resilience of a single hazard event require inputs from vulnerability assessment, which can be obtained by using the approach described in CHAPTER 2 and CHAPTER 3. The significance of considering long-term resilience is highlighted.

## **5.2 Stationary hazard model: homogeneous Poisson process**

As one of the most classical stationary models, the homogeneous Poisson process is adopted for stationary hazard arrivals and illustrated by using two different models: the homogenous Poisson process and the renewal process.

A homogeneous Poisson process is an arrival process with stationary increments. It has a constant occurrence rate  $\lambda$ . The occurrence rate is defined as the number of hazard events within the time unit (e.g., per year), which is also known as the intensity function. A homogeneous Poisson process can be denoted by the number of occurrence  $\{N(t_{\text{int}}), t_{\text{int}} > 0\}$  with the time interval  $(0, t_{\text{int}}]$ . The expected number of hazard arrivals can be expressed as  $E[N(t_{\text{int}})] = \lambda t_{\text{int}}$  with  $N(0) = 0$ . The probability of having  $n$  number of arrivals within the time interval  $t_{\text{int}}$  is

$$P[N(t_{\text{int}}) = n] = \frac{(\lambda t_{\text{int}})^n \exp(-\lambda t_{\text{int}})}{n!}, n = 0, 1, 2, \dots \quad (5-1)$$

The homogeneous Poisson process can be alternatively described as a renewal process. A renewal process is a counting process, in which the inter-arrival times are independently identically distributed. For instance, over the period  $(0, t_{\text{int}}]$ , arriving times of hazards are a series of non-negative random variables  $\{T_1, T_2, \dots, T_k\}$ . Inter-arrival times can be denoted as  $\{W_1, W_2, \dots, W_k\}$ . By the definition, the arriving time is the summation of inter-arrival times,  $T_k = W_1 + W_2 + \dots + W_k$ . When the inter-arrival time follows an exponential distribution, a renewal process becomes a homogeneous Poisson process, also known as a Poisson renewal process. The probability density function of the inter-arrival time  $W$  gives

$$f_w(x) = \lambda \exp(-\lambda x) \quad (5-2)$$

### 5.3 Long-term assessment under stationary hazards

This section aims to provide a long-term assessment framework of engineering structures with respect to resilience and structural damage loss under natural hazards. During the life-cycle analysis, the large uncertainty related to the frequency and intensity of natural hazards in the life-cycle analysis can be quantified by the stochastic occurrence model. The stochastic renewal process has been widely applied to model the occurrence of hazards.

Given the investigated time period  $(0, t_{\text{int}}]$ , each hazard event (e.g., earthquake) occurring within this period is described using index  $k$ .  $T_k$  denotes the arrival time of

hazard,  $L_k$  is the economic loss due to repair, and  $R_k$  refers to the resilience under the investigated hazard. Interarrival time is defined by  $W_k$ , where arrival time equals the sum of interarrival times  $T_k = W_1 + W_2 + \dots + W_k$ . An illustrative diagram illustrating the long-term resilience and loss framework is shown in Figure 5-1. The hazard occurrence is modeled by the renewal process, where the interarrival time  $W_k$  is independently identically distributed (IID). The time period  $t_{\text{int}}$  can be taken as the lifespan of infrastructure and the total number of hazard occurrence is  $N(t_{\text{int}})$ , with  $T_k \leq t_{\text{int}}$ . Based on the established stochastic model, the long-term resilience  $LTR(t_{\text{int}})$  within investigated period  $t_{\text{int}}$  can be written as

$$LTR(t_{\text{int}}) = \sum_{k=1}^{N(t_{\text{int}})} R_k \quad (5-3)$$

in which  $R_k$  is the resilience associated with a single hazard and  $N(t_{\text{int}})$  is the total number of hazard occurrences within investigated service life. Long-term resilience is the sum of the resilience of all the hazard events. In addition to the resilience, the long-term loss can also be evaluated based on the renewal process. The cumulative long-term loss  $LTL(t_{\text{int}})$  can be formulated as

$$LTL(t_{\text{int}}) = \sum_{k=1}^{N(t_{\text{int}})} L_k e^{-rT_k} \quad (5-4)$$

where  $L_k$  is the loss severity, which is the damage cost associated with each hazard event;  $T_k$  is the arrival time of the  $k$ th hazard; and the monetary discount rate  $r$  is used to transform future loss into the present within the investigated time horizon. Long-term loss is discounted to the present value using a constant discount rate  $r$ .

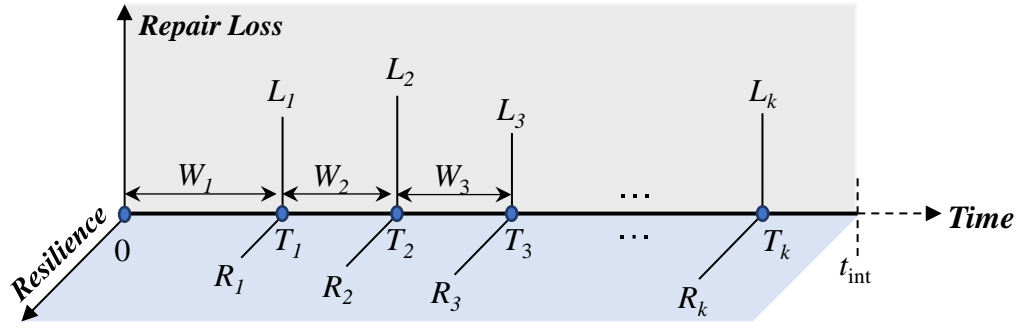


**Figure 5-1** The long-term resilience and loss framework based on the stochastic renewal process.

## 5.4 Renewal approach for long-term loss and resilience

### 5.4.1 Renewal function

The long-term resilience and loss can be quantified by using analytical computation and numerical Monte Carlo (MC) simulations, but the simulation approach can be expensive. Analytically, the expected long-term resilience and loss can be quantified analytically using the properties of renewal theory (Ross 2014). The key to solve Eqs. (5-3) and (5-4) is to identify the number of hazard events, which can be expressed as

$$E[N(t_{int})] = \sum_{k=1}^{\infty} F_W^{(k)}(t_{int}) = Y(t_{int}) \quad (5-5)$$

in which  $F_W^{(k)}(t_{int})$  is a  $k$ -fold convolution of interarrival time  $W_k$  and  $Y(\cdot)$  is known as the renewal function in the renewal process.

The renewal function satisfies an integral equation conditioning on the first arrival time  $y$ . The CDF of interarrival time  $F_W(t)$  is assumed to be continuous. Hence,

the expected number of events denoted by a density function yielding at the first renewal  $dF_W(y)$  can be written as

$$\Upsilon(t_{\text{int}}) = E[N(t_{\text{int}})] = \int_0^{\infty} E[N(t_{\text{int}}) | W_1 = y] dF_W(y) \quad (5-6)$$

When the first arrival time is larger than  $t_{\text{int}}$ , there is no event within the investigated period, with  $E[N(t_{\text{int}})] = 0$ . When  $y \leq t_{\text{int}}$ , the renewal process enables the renewals to have the same distribution. Hence,

$$E[N(t_{\text{int}}) | W_1 = y \leq t_{\text{int}}] = 1 + E[N(t_{\text{int}} - y)] = 1 + \Upsilon(t_{\text{int}} - y) \quad (5-7)$$

Substituting Eq. (5-7) into Eq. (5-6), the expected number of arrivals can be written as

$$\Upsilon(t_{\text{int}}) = F_W(t_{\text{int}}) + \int_0^{t_{\text{int}}} \Phi(t_{\text{int}} - y) dF_W(y) \quad (5-8)$$

Using the renewal function, the expected long-term resilience can be determined by the properties of the compound stochastic process (Ross 2014), which equals the sum of the number of arrivals times the expected resilience

$$E[LTR(t_{\text{int}})] = E[R_k] E[N(t_{\text{int}})] = E[R_k] \Upsilon(t_{\text{int}}) \quad (5-9)$$

For the discounted long-term loss, the expectation can be written into two parts by conditioning on the first renewal time  $y$

$$\begin{aligned}
E[LTL(t_{\text{int}})] &= E\left[E[e^{-ry}L_1 + e^{-ry}LTL(t_{\text{int}} - y) | W_1 = y]\right] \\
&= E[L] \int_0^{t_{\text{int}}} e^{-ry} dF_W(y) + E[L] \int_0^{t_{\text{int}}} e^{-ry} E\left[\sum_{k=1}^{(t_{\text{int}}-y)} e^{-rT_k}\right] dF_W(y) \quad (5-10)
\end{aligned}$$

in which the CDF of interarrival time  $F_W$  in a finite time domain is a defective distribution for interarrival time, denoted as  $\psi(t_{\text{int}})$  (Léveillé and Garrido 2001; Rolski *et al.* 2009).

$$\psi(t_{\text{int}}) = \int_0^{t_{\text{int}}} e^{-rs} f_W(s) ds = \int_0^{t_{\text{int}}} e^{-rs} dF_W(s) \quad (5-11)$$

In an infinite time horizon, the defective distribution is the Laplace transform of  $F_W$ , denoted as  $\psi_r(\infty)$ . For the investigated finite time domain, the expected long-term loss is expressed as

$$E[LTL(t_{\text{int}})] = E[L]\psi(t_{\text{int}}) + E[L]E\left[\sum_{k=1}^{N(\cdot)} e^{-rT_k}\right] * \psi(t_{\text{int}}) = E[L] \sum_{k=1}^{\infty} \psi^{(k)}(t_{\text{int}}) \quad (5-12)$$

To connect Eq. (5-12) with the expected number of arrivals of hazards in the renewal process, the convolution power of  $\psi(t_{\text{int}})$  is computed

$$\begin{aligned}
\psi^{(k+1)}(t_{\text{int}}) &= \int_0^{t_{\text{int}}} e^{-rs} \psi^{(k)}(t_{\text{int}} - s) dF_W(s) = \int_0^{t_{\text{int}}} \int_0^{t_{\text{int}}-s} e^{-r(s+v)} dF_W^{(k)}(v) dF_W(s) \\
&= \int_0^{\infty} e^{-rs} I_{\{0, t_{\text{int}}\}}(s) dF_W^{(k+1)}(s) = \int_0^{t_{\text{int}}} e^{-rs} dF_W^{(k+1)}(s) \quad (5-13)
\end{aligned}$$

where  $I_A(\cdot)$  represents the indicator function of a set  $A$ . It equals to one only if  $A$  is true but equals to zero otherwise: e.g.,  $I_{\{0, t_{\text{int}}\}}(s)$  equals to one if  $0 \leq s \leq t_{\text{int}}$ . Since the renewal function is the  $k$ -fold convolution of the PDF of interarrival time, Eq. (5-13) is rearranged as follows

$$\sum_{k=1}^{\infty} \psi^{(k)}(t_{\text{int}}) = \int_0^{t_{\text{int}}} e^{-rs} d \sum_{k=1}^{\infty} F_W^{(k)}(s) = \int_0^{t_{\text{int}}} e^{-rs} dY(s) \quad (5-14)$$

Substituting Eq. (5-14) into Eq. (5-12), the expected long-term loss is

$$E[LTL(t_{\text{int}})] = E[L] \int_0^{t_{\text{int}}} e^{-rs} dY(s) \quad (5-15)$$

In summary, the expected long-term resilience and loss can be formulated as follows

$$E[LTR(t_{\text{int}})] = E[R]Y(t_{\text{int}}) \quad (5-16)$$

$$E[LTL(t_{\text{int}})] = E[L] \int_0^{t_{\text{int}}} e^{-rt} dY(t) \quad (5-17)$$

in which  $E[N(t_{\text{int}})]$  is the expectation of the number of hazard events within the service life. It is assumed that the damaged structure is repaired to the pre-damage state before the next hazard event.

Given  $E[N(t_{\text{int}})] = \lambda t_{\text{int}}$  based on the Poisson-based renewal process, the expected long-term resilience and loss associated with the Poisson process can be formulated as

$$E[LTR(t_{\text{int}})] = R\lambda t_{\text{int}} \quad (5-18)$$

$$E[LTL(t_{\text{int}})] = \frac{L\lambda}{r} (1 - e^{-rt_{\text{int}}}) \quad (5-19)$$

in which the expected resilience of each hazard event and economic repair loss are defined as  $E[R] = R$  and  $E[L] = L$ , respectively.

### 5.4.2 Other applications of renewal approach

Apart from the expected long-term loss, the proposed renewal approach can be applied to derive the variance. The variance can be an essential indicator to show the variability of the expected damage cost. Following similar procedures of expectation, the second moment of long-term loss can be derived as follows conditioning on the first renewal time

$$\begin{aligned}
E[LTL^2(t_{\text{int}})] &= E \left\{ E \left[ \left( \sum_{k=1}^{N(t_{\text{int}})} L_k e^{-rT_k} \right)^2 \mid N(t_{\text{int}}) \right] \right\} \\
&= E \left\{ E \left[ \sum_{k=1}^{N(t_{\text{int}})} L_k^2 e^{-2rT_k} + \sum_{i=1}^{N(t_{\text{int}})} \sum_{j=1, j \neq i}^{N(t_{\text{int}})} L_i L_j e^{-r(T_i+T_j)} \mid N(t_{\text{int}}) \right] \right\} \quad (5-20) \\
&= E[L^2] E \left[ \sum_{k=1}^{N(t_{\text{int}})} e^{-2rT_k} \right] + E^2[L] E \left[ \sum_{i=1}^{N(t_{\text{int}})} \sum_{j=1, j \neq i}^{N(t_{\text{int}})} e^{-r(T_i+T_j)} \right]
\end{aligned}$$

in which

$$\begin{aligned}
&E \left[ \sum_{i=1}^{N(t_{\text{int}})} \sum_{j=1, j \neq i}^{N(t_{\text{int}})} e^{-r(T_i+T_j)} \right] \\
&= 2 \int_0^{t_{\text{int}}} e^{-2r\xi} E \left[ \sum_{j=1}^{N(t_{\text{int}}-\xi)} e^{-rT_j} \right] dF_W(\xi) \\
&+ \int_0^{t_{\text{int}}} e^{-2r\xi} E \left[ \sum_{i=1}^{N(t_{\text{int}}-\xi)} \sum_{j=1, j \neq i}^{N(t_{\text{int}}-\xi)} e^{-r(T_i+T_j)} \right] dF_W(\xi) \quad (5-21) \\
&= 2 \sum_{k=1}^{\infty} \sum_{m=1}^{\infty} \psi^{(k)} * \psi_{2r}^{(m)}(t_{\text{int}}) = 2 \int_0^{t_{\text{int}}} \int_0^{t_{\text{int}}-s} e^{-r(2s+v)} dm(v) dm(s)
\end{aligned}$$

where  $\psi_{2r}^{(k)}(t_{\text{int}})$  refers to the Esscher transform of  $k$ -fold convolution of  $F_W$  at  $2r$  for a finite time interval  $t_{\text{int}}$ . Therefore, the second moment can be calculated as

$$\begin{aligned}
E[LTL^2(t_{\text{int}})] &= E[L^2] \int_0^{t_{\text{int}}} e^{-2rs} dm(s) \\
&+ 2E[L]^2 \int_0^{t_{\text{int}}} \int_0^{t_{\text{int}}-s} e^{-r(2s+v)} dm(v) dm(s)
\end{aligned} \tag{5-22}$$

Therefore, the variance can be obtained from the first and the second moment

$$\begin{aligned}
\text{Var}[LTL(t_{\text{int}})] &= E[LTL^2(t_{\text{int}})] - E[LTL(t_{\text{int}})]^2 \\
&= E[L^2] \int_0^{t_{\text{int}}} e^{-2rs} dm(s) \\
&+ 2E^2[L] \int_0^{t_{\text{int}}} \int_0^{t_{\text{int}}-s} e^{-r(2s+v)} dm(v) dm(s) \\
&- E[L]^2 \left[ \int_0^{t_{\text{int}}} e^{-rs} dm(s) \right]^2
\end{aligned} \tag{5-23}$$

In addition to the homogeneous Poisson process, the proposed renewal approach can be applied to renewal processes with different inter-arrival time models. For instance, in earthquake engineering, there are several other nonstationary renewal processes adopted with time-varying interarrival time models except exponential models. For instance, the renewal process with a Brownian model is usually adopted in the long-term seismic analysis and forecasting for severe earthquakes (Matthews et al. 2002). The interarrival time follows Brownian passage-time (BPT) distribution with a PDF

$$f_w(t) = \left( \frac{\mu}{2\pi\alpha^2 t^3} \right)^{1/2} \exp \left\{ -\frac{(t-\mu)^2}{2\mu\alpha^2 t} \right\} \tag{5-24}$$

where  $\mu$  is the mean and  $\alpha$  is the coefficient of variation. The long-term resilience and loss based on the renewal BPT model can be computed using Eqs. (10) to (12), where the expected number of hazards is computed by the integration. The CDF of BPT distribution is provided in Matthews *et al.* (2002). Based on the proposed renewal

approach, a variety of time-varying interarrival time models can be applied to assess long-term resilience and loss, such as Gamma (Hainzl *et al.* 2006) and lognormal (Michael 2005) distributions.

### 5.4.3 Validation by using Monte Carlo simulation

The analytical renewal approach is validated by using the Monte Carlo simulation method. The simulation method can simulate the stochastic process and yield long-term resilience and loss by generating a large number of random samples. The Monte Carlo method is particularly powerful to address statistical distribution problems and risk metrics. The key to attaining the long-term loss is to generate the stochastic process. A homogeneous Poisson process has an arrival rate  $\lambda$ . It specifies the renewal process with exponentially distributed inter-arrival times. Each arrival epoch of an earthquake  $T_k$  is added by the inter-arrival times  $W_k$ . Given the defined time interval, a stochastic renewal process is generated by the simulation. For the loss severity, the mean and second moment can be either generated from samples or simulated by probabilistic distribution fitting. Resilience is a deterministic constant. The algorithm to assess the expected long-term loss and resilience based on a homogeneous Poisson process is provided:

*Simulation algorithm:*

- (1) Initialize  $i = 0$ ,  $X_i \sim Uni(0, 1)$  and  $t = -\ln(X_0)/\lambda$ ;
- (2) While  $t < t_{\text{int}}$ ,  $i = i+1$ ,  $T_i = t$ , and  $t = t - (1/\lambda)\ln(X_i)$ , end;

- (3) Deliver  $\{T_1, T_2, \dots, T_i\}$  in  $(0, t_{int})$ ;
- (4) Compute  $LTL$  and  $LTR$  using  $\{T_1, T_2, \dots, T_i\}$ ;
- (5) Repeat Step(1) to (5) for  $N_{MC}$  times using Monte Carlo simulation;
- (6) Deliver expectations  $E[LTL]$  and  $E[LTR]$ .

However, the simulation of the homogeneous Poisson process is not applicable to general renewal processes. The simulation of nonstationary renewal processes can be more complicated. The thinning method and inversion method are required (Gerhardt and Nelson 2009). The key concept is to transform the nonstationary renewal process into a stationary one. Once the arrival times are attained, the long-term resilience and loss can be calculated. During the validation, it shows that the Monte Carlo simulation is inefficient and time-consuming, as it may take up to two hours to gain convergence for a defined lifetime. In comparison, the analytical renewal method provides accurate solutions immediately in seconds.

## 5.5 Illustrative example

This section aims to provide an example to evaluate the life-cycle performance of civil infrastructure by considering performance indicators in terms of long-term resilience and loss. Herein, the simply supported highway bridge introduced in Section 3.3.2 is selected as an illustrative application. The bridge has a total length of 40 m and the geometry of the bridge deck has been described in Figure 3-5(a). For illustration purposes, it is assumed that the bridge is located at a location exposed to earthquakes

and hurricanes. The bridge is subjected to multiple independent seismic and hurricane hazards during its service life. Four hazard scenarios are considered: two hurricane scenarios with return periods of 100 years (Hurricane scenario one denoted as  $\mathbf{H}_1$ ) and 200 years (Hurricane scenario two denoted as  $\mathbf{H}_2$ ) and two earthquake scenarios with return periods of 75 years (Earthquake scenario one denoted as  $\mathbf{E}_1$ ) and 120 years (Earthquake scenario two denoted as  $\mathbf{E}_2$ ). The occurrence model of hurricanes is a homogeneous Poisson process (Ellingwood and Lee 2016) and the earthquake arrivals is a renewal process with a BPT distribution (Takahashi *et al.* 2004).

Following the methods of probabilistic hazard analysis and vulnerability assessment introduced in CHAPTER 3, the probability of failure associated with the four hazard scenarios can be determined. Parameters remain unchanged unless specified in this example. For the two hurricane scenarios (with return periods of 100 years  $\mathbf{H}_1$  and 200 years  $\mathbf{H}_2$ ), the associated storm surge can be 1.74 m and 2.18 m, respectively, according to the surge models of ADCIRC and SLOSH simulations (Lin *et al.* 2010). The possible storm tide is considered, which is approximately 0.3 to 0.5 m higher than the storm surge level (Lin *et al.* 2012). Hence, the total surge elevation is evaluated as 2.05 m for  $\mathbf{H}_1$  and 2.45 m for  $\mathbf{H}_2$ , respectively. The wave height for  $\mathbf{H}_1$  is 4.60 m and that for  $\mathbf{H}_2$  equals 5.35 m using the model demonstrated by Lin *et al.* (2010). Given these inputs, the probability of deck unseating failure under the investigated two hurricane scenarios  $\mathbf{H}_1$  and  $\mathbf{H}_2$  are 0.1982 and 0.9013, respectively.

Two seismic scenarios with the return period of 75-year (Earthquake scenario one denoted as  $\mathbf{E}_1$ ) and 120-year (Earthquake scenario two denoted as  $\mathbf{E}_2$ ) are considered for the investigated bridge. The associated return period of the hazard

scenario is the mean of the BPT distribution in the long-term seismic analysis, as shown in Eq. (5-24). The COV of the BPT distribution is set to 1 (Matthews *et al.* 2002). Given the return periods of earthquakes, the PGA values for  $E_1$  and  $E_2$  are determined as 0.1605g and 0.2152g, respectively. The fragility curves can be generated by identifying the seismic demand and capacity selected for the bridge. In this example, a fragility curve for the multi-span simply supported concrete bridges conducted by Nielson and DesRoches (2007) is adopted to assess the system-level vulnerability of the bridge. The system fragility is obtained through evaluating the correlated joint probability distribution based on the individual components, consisting of the concrete columns, elastomeric bearing, and abutments in both transverse and longitudinal directions. Using the damage states provided by Nielson and DesRoches (2007), the fragility curves for slight, moderate, major, and complete damage states of the bridge are shown in Figure 5-2. Thus, the probability of failure of the bridge for scenario  $E_1$  under slight, moderate, major, and complete damage states is 0.3675, 0.0256, 0.0057, and 0.0011, respectively. For scenario  $E_2$ , the probability of failure under slight, moderate, major, and complete damage states is 0.5449, 0.0670, 0.0189, and 0.0046, respectively.

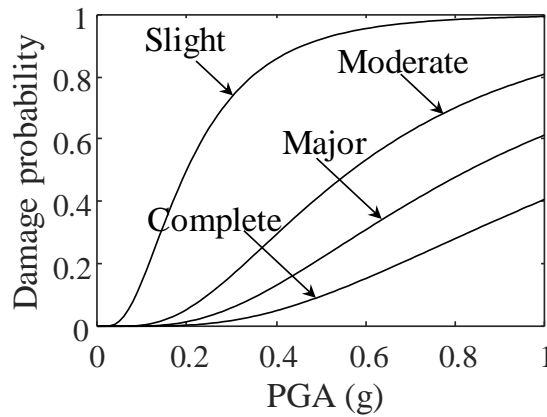


**Figure 5-2** System-level fragility curves for the bridge at different damage stages (adapted from Nielson and DesRoches (2007)).

Given the defined hazard scenarios and fragility inputs, the long-term resilience and loss of the bridge under earthquakes and hurricanes are assessed in this section. The arrivals of earthquakes are modeled by the renewal process with BPT distribution, while a classical Poisson process is used to model the hurricane arrivals. The occurrence rate is taken as the inverse of the return period (e.g., the occurrence rate of a 100-year hurricane is 0.01). Two significant inputs for Eqs. (5-16) and (5-17) are the resilience and economic repair loss (i.e., loss severity).

In this example, the resilience is assessed by Eq. (2-26) and the recovery model is based on the model developed by ATC (1999), as described in CHAPTER 2, while any other approaches could also be incorporated during the computational process. By providing recovery actions, the bridge functionality is recovered to a satisfactory level. A similar repair scheme is utilized for the bridge under hurricane-induced damage but only the collapse damage is included. The same recovery time from earthquake analysis is utilized for hurricane analysis. Herein, the quantification of resilience is based on the

ATC function for illustrative purposes. Future studies are needed to incorporate more detailed investigations associated the restoration modeling, resource availability, constraints, how damage can be mapped to functionality, and restoration actions. The functionality related to the four hazard scenarios is shown in Figure 5-3. Under the same type of hazard, the bridge under a higher level of hazard intensity has a smaller residual functionality, which means the structure requires additional efforts for recovery. Given the investigated time interval  $\Delta t_r = 400$  days, the resilience can be calculated. The bridge resilience under two earthquake hazards  $\mathbf{E}_1$  and  $\mathbf{E}_2$  are 0.9958 and 0.9918, respectively. With the same investigated time interval, the bridge resilience under the hurricane scenarios  $\mathbf{H}_1$  and  $\mathbf{H}_2$  is computed as 0.9204 and 0.6467, respectively. These four resilience values are considered as the mean resilience inputs for the long-term assessment. Consequently, the expected long-term resilience for earthquakes and hurricanes are computed, associated with the stochastic BPT renewal process and Poisson process, respectively. In a 100-year service life, the expected long-term resilience for the hazard scenarios  $\mathbf{E}_1$ ,  $\mathbf{E}_2$ ,  $\mathbf{H}_1$ , and  $\mathbf{H}_2$  is 1.2835, 0.7536, 0.9204, and 0.3233, respectively. Figure 5-4 shows the expected long-term resilience under the four scenarios changing over the investigated service life. It is found that the long-term resilience of bridge of scenarios  $\mathbf{E}_2$  is the lowest in the first 30 years, while the lowest scenario turns to  $\mathbf{H}_2$  in the remaining service life. As a result, decision-makers are required to make appropriate management strategies for the bridge according to the changes of total resilience at different ages.

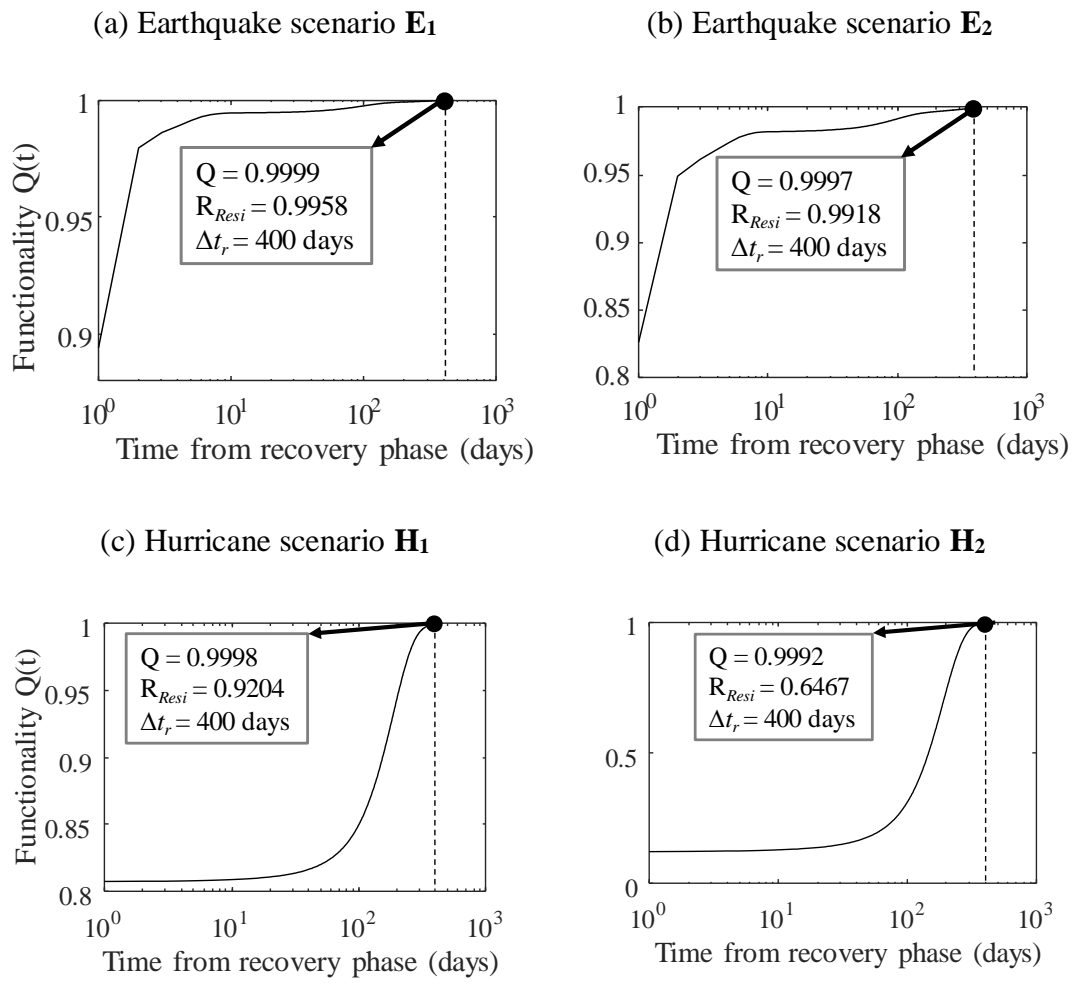


**Figure 5-3** Time-dependent functionality of four investigated hazard scenarios ( $\mathbf{E}_1$ ,  $\mathbf{E}_2$ ,  $\mathbf{H}_1$ , and  $\mathbf{H}_2$ ).

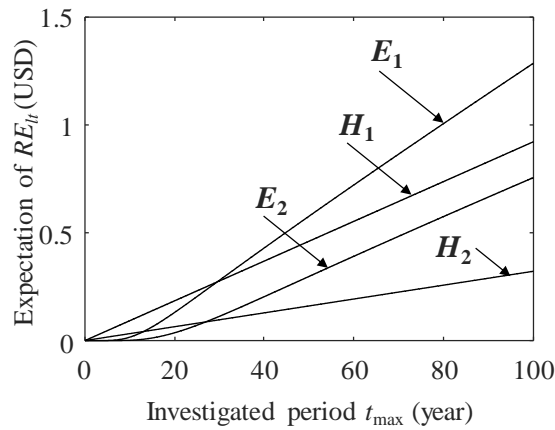


**Figure 5-4** Long-term resilience for the investigated bridge under earthquake and hurricane hazards using renewal method.

The economic repair loss caused by natural hazards can be computed as the product of rebuilding cost and the probability of failure under the investigated scenario. In this example, the rebuilding cost of the bridge is computed as USD 963,908, based on the consequence evaluation parameters provided by Zheng *et al.* (2018). For bridges damaged by deck unseating during hurricanes, the rebuilding cost is mainly due to the repair of the superstructure, taken as 40% of the rebuilding cost (Mondoro *et al.* 2017). The expectation of long-term loss of the bridge under earthquake and hurricane is computed, including inputs of the occurrence rate of investigated hazard, service life, hazard intensity, and financial discount rate. The economic repair loss for the hazard scenarios  $E_1$ ,  $E_2$ ,  $H_1$ , and  $H_2$  is USD  $0.1909 \times 10^5$ ,  $0.4019 \times 10^5$ ,  $7.6419 \times 10^5$ , and  $3.4751 \times 10^5$ , respectively. The service life remains 100 years and a financial discount rate of 3% is used. Based on the renewal model, the expected long-term loss under the hazard scenarios  $E_1$ ,  $E_2$ ,  $H_1$ , and  $H_2$  is USD  $0.629 \times 10^4$ ,  $0.679 \times 10^4$ ,  $2.420 \times 10^4$ , and  $5.503 \times 10^4$ , respectively. Figure 5-5 shows the expected long-term loss changing over the investigated period under the four scenarios.

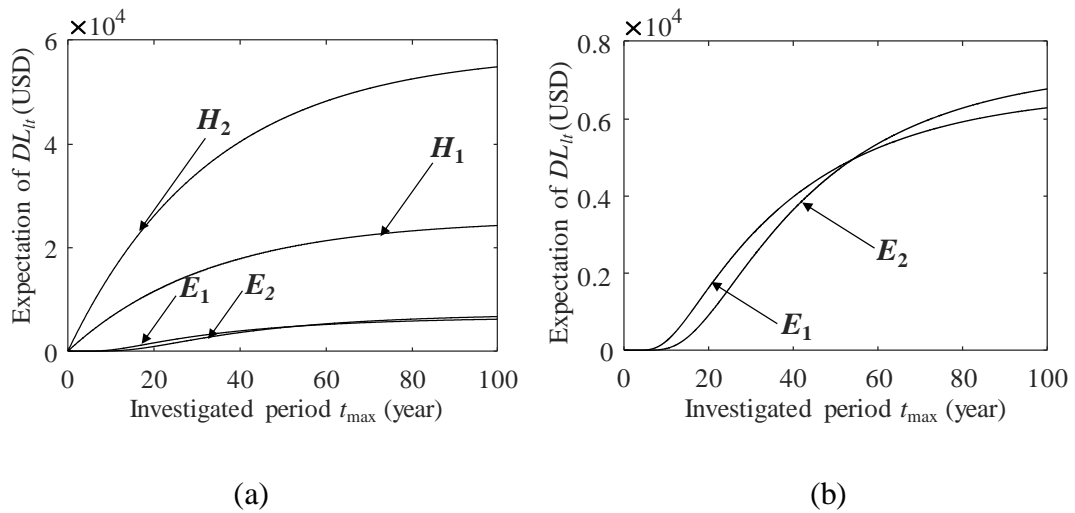


**Figure 5-5** Long-term loss estimation for the investigated bridge under earthquake and hurricane hazards using renewal method (a) for four hazard scenarios (b) for seismic scenarios  $E_1$  and  $E_2$ .

It is identified from the long-term loss that the bridge is exposed to dominated hurricane hazard scenario  $H_2$ , which leads to the highest expected long-term loss throughout the investigated period. This outcome is reasonable since the bridge has the largest probability of failure and a relatively high repair cost under the hazard scenario  $H_2$ . On the contrary, the hazard scenario  $E_1$  and  $E_2$  can cause the lowest long-term loss of the bridge. Due to the stochastic time-independent HPP model, the expected long-term loss of hurricane scenario  $H_2$  is consistently higher than that of scenario  $H_1$ , as shown in Figure 5-5(a). However, the changing pattern of long-term loss under two earthquake scenarios is different, as shown in Figure 5-5(b), due to the time-varying occurrence rate in the BPT renewal process. When the service life is smaller than 55 years, the total loss of scenario  $E_1$  is larger than  $E_2$  but the situation is opposite in the remaining 45 years. Therefore, the decision-makers should consider both the long-term resilience and loss, as only focusing on the long-term loss may lead to inappropriate

decisions. For instance, though the long-term loss of scenario **H<sub>2</sub>** is the highest throughout the investigated period, the long-term resilience of **E<sub>2</sub>** is the lowest when the bridge service life is smaller than 30 years.

The above results obtained through the analytical renewal-based approach are validated by the MC simulations. The stochastic renewal process is constructed by modeling the interarrival times according to the given probability distribution. The interarrival times having BPT distribution are modeled using inverse transform sampling. Consequently, the expected long-term loss and resilience are computed using the Eqs. (5-3) and (5-4). Through the MC approach, the expected long-term resilience for the hazard scenarios **E<sub>1</sub>**, **E<sub>2</sub>**, **H<sub>1</sub>**, and **H<sub>2</sub>** is 1.2819, 0.7531, 0.9208, and 0.3233, respectively, for the 100-year service life. The associated expected long-term loss under the hazard scenarios **E<sub>1</sub>**, **E<sub>2</sub>**, **H<sub>1</sub>**, and **H<sub>2</sub>** is USD  $0.637 \times 10^4$ ,  $0.699 \times 10^4$ ,  $2.461 \times 10^4$ , and  $5.595 \times 10^4$ , respectively. Overall, these numerical results have an acceptable agreement on the analytical outcomes.

For the dominant scenario **H<sub>2</sub>**, the expected long-term loss is sensitive to the change of financial discount rate and the economic repair loss as shown in Figure 5-6(a) and Figure 5-6(b), respectively. The long-term loss with a discount rate of 1% is nearly three times larger than that with a discount rate of 4%. Therefore, identifying the appropriate value for the discount rate is essential for the long-term loss evaluation. In addition, the long-term loss can be significantly enlarged by the increase of economic repair loss. By defining the original economic repair loss for scenario **H<sub>2</sub>** as  $L_0$ , the expectation of long-term loss affected by triple, double, a half, and a third of  $L_0$  is shown in Figure 5-6(b). Since the economic repair loss highly depends on the vulnerability

analysis in terms of the probability of failure, it indicates the large uncertainty related to fragility curves during the long-term loss estimation. Based on the outcomes, decision-makers can further decide the risk mitigation strategies associated with this dominated scenario.

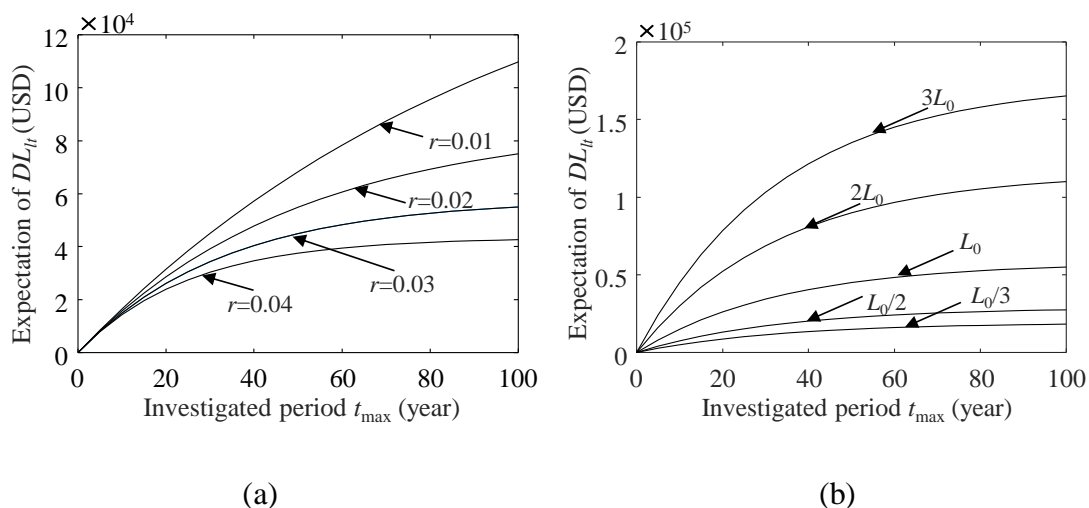


**Figure 5-6** Expected long-term loss affected by (a) financial discount ratio and (b) economic repair loss.

## 5.6 Summary

This chapter provides a renewal approach for the long-term resilience and loss assessment of highway bridges under stationary hazards. The renewal process is used to characterize the stochastic frequency and intensity of hazards. By using the renewal function, the expected long-term resilience and loss can be effectively derived analytically. In addition to the stationary homogeneous Poisson process, the proposed renewal approach can be applied to renewal processes with time-varying occurrence models, e.g., with a BPT distribution. The variance of long-term loss can also be

estimated based on the renewal function. The proposed approach is illustrated on a typical highway bridge to highlight the importance of considering long-term resilience during life-cycle analysis. The highway bridge is subjected to multiple independent hazards, considering four hazard scenarios: seismic hazards with return periods of 75 years and 120 years and hurricane hazards with return periods of 100 years and 200 years. Uncertainties arising from hazards, structural vulnerability, functionality, and consequences are considered during the assessment. The time-dependent functionalities under recovery patterns for four different hazard scenarios are calculated. The bridge resilience under each hazard scenario is evaluated.

In the illustrative example, the results reveal that the hurricane with a 200-year return period is the costliest hazard for the bridge. Though the long-term loss caused by the 200-year hurricane is the highest throughout the investigated 100-year service life, the long-term resilience of the earthquake with a 120-year return period is the lowest in the first 30 years. Thus, decision-makers are expected to consider both long-term resilience and loss. The long-term loss significantly depends on the occurrence and intensity of hazards, remaining service life, and financial discount rate. Careful evaluations of the financial discount rate and the structural fragility analysis are important. Based on the results presented, decision-makers can decide the risk mitigation strategies associated with various hazard scenarios. The approach presented can benefit insurers and policy-makers to manage bridges against the impacts of multiple hazards in a life-cycle context. Further studies are expected to consider the interdependencies and interactions of hazardous events. The life-cycle management can be further incorporated into the proposed framework by considering the intervention

actions (e.g., inspection, maintenance, and repair) to deliver the optimal solution for decision-makers.

# CHAPTER 6 HIGHER-ORDER ANALYSIS UNDER NONSTATIONARY HAZARDS IN A LIFE-CYCLE CONTEXT

## 6.1 Introduction

During the life-cycle of civil infrastructure, various hazards (e.g., earthquakes, hurricanes, and progressive deterioration) may impair structural functionality, thus resulting in severe consequences. The hazard-induced consequences are commonly measured in terms of financial losses (e.g., repair cost), social losses (e.g., downtime, deaths), and environmental losses (e.g., carbon dioxide emissions). Uncertainty quantification plays a vital role in life-cycle analysis. In terms of long-term economic loss, most previous studies focused on the low-order moments (i.e., expectation and variance). Though the minimum expected cost has been widely used as a standard decision criterion, it is only suitable for risk-neutral decision-makers. This criterion cannot cope with different attitudes (Levy 2015). Goda and Hong (2006) indicated the structural design based on the expected life-cycle cost may not be optimal, and stated the need for statistical moments (e.g., variance, skewness, and kurtosis) of the cost. Some studies discussed the probability distribution associated with seismic loss modeling. For instance, Pandey and van der Weide (2018) modeled the probability distribution of seismic loss considering the life-cycle of engineering structures. De Risi *et al.* (2020) provided a component-level methodology to assess the seismic damage cost due to repair, in which the uncertainty associated with the standard deviation of the cost is considered. However, few studies have investigated the higher-order

moments of hurricane-induced losses. Furthermore, the mean-variance criterion is sufficient only when the utility function within the decision-making process is quadratic or the investment return (e.g., the loss represents a negative return) follows a normal distribution (Markowitz and Todd 2000). Therefore, there is a need to investigate the higher-order moments of the cost in a life-cycle context.

Higher-order moments, i.e., skewness and kurtosis, measure asymmetry and tail conditions of the distribution with respect to the long-term loss. In risk management, large skewness and kurtosis of loss imply heavy tail risks. Such undesired risks are associated with low-probability events with disastrous consequences, e.g., credit risk crisis (Kelly and Jiang 2014) and COVID-19 pandemic (Beck 2020). Higher-order moments are required when risk preferences of decision-makers are considered, e.g., in the stochastic dominance criteria (Aksaraylı and Pala 2018; Levy 2015). For instance, a decision-maker with the absolute risk-averse attitude prefers positive skewness and small kurtosis of the investment return, as highly skewed data with large kurtosis indicate an increased likelihood of extreme losses (Maringer and Parpas 2009). Different decision results may be obtained due to the exclusion of these moments. Therefore, the assessment of higher-order moments of long-term loss is necessary. These moments can be used to aid the decision-making and optimal structural design of civil infrastructure by considering different attitudes.

This chapter proposes a novel framework for the higher-order analysis of long-term loss under both stationary and nonstationary hazards. An analytical approach based on the moment generating function is developed to assess the first four statistical moments of long-term loss under different stochastic models (e.g., homogeneous

Poisson process, non-homogeneous Poisson process, renewal process). Based on the law of total expectation, the developed approach expands the application scope of the moment generating function to nonstationary models and higher-order moments (i.e., skewness and kurtosis). Compared with the method using the renewal function described in CHAPTER 5, the proposed approach effectively addresses the difficulty of assessing higher-order moments in a renewal process. Besides the loss analysis, the mixed Poisson process, a relatively new stochastic model, is introduced to consider uncertainty springing from the stochastic occurrence rate. An illustrative example is presented to demonstrate practical implementations of the developed approach. The example shows the impact of different nonstationary characteristics on the long-term loss assessment. The advantages and limitations of using the renewal model described in CHAPTER 5 and the proposed moment generating function approach in this chapter are also discussed. The proposed framework can aid decision-makers to select the optimal option by incorporating higher-order moments of long-term loss within the decision-making process.

## **6.2 Nonstationary arrival models**

In previous studies, stationary models (e.g., homogeneous Poisson process) have been widely used for loss estimation. However, the approach based on the stationary model is not applicable for nonstationary hazard arrivals. Studies show that various hazards show nonstationary behavior in terms of stochastic occurrence (Lee and Ellingwood 2017). For instance, the long-term earthquake forecast is simulated by a renewal process, in order to incorporate the time-varying energy accumulation of the fault

(Ellsworth *et al.* 1999; Field *et al.* 2015). The time-dependent trends are also identified in other hazards, such as more frequent hurricane landfalls under climate change (Bender *et al.* 2010), increased wind speeds (Jagger and Elsner 2006), extreme precipitation (Tramblay *et al.* 2013), and sea-level rise (Obeysekera and Park 2013). In addition to natural hazards, the progressive deterioration of structural systems is also stochastic and time-variant (Yang and Frangopol 2019a). Given the time-dependent characteristics of hazards, a general framework is needed to evaluate the long-term loss of civil infrastructure under both stationary and nonstationary hazards. Therefore, the stationary occurrence rate is an idealized assumption and a realistic rate can be time-dependent and stochastic. Herein, three typical examples of nonstationary processes are provided: the non-Poisson renewal process, non-homogeneous Poisson process, and mixed Poisson process. In this context, a process is considered as ‘nonstationary’ when the occurrence rate is not constant.

### **6.2.1 Non-Poisson renewal process**

The occurrence of hazards could be time-dependent. For instance, after an earthquake, there can be a long period before the next earthquake, in which the accumulated elastic strain energy is released by the fault. By considering such time-dependent characteristics, a non-Poisson process can be used to model the occurrence of earthquakes over a long period of time (Cornell and Steven 1988; Matthews *et al.* 2002). In the nonstationary renewal processes, different probabilistic models of inter-arrival times are used to quantify the time-dependent characteristics. For instance, several distributions of the inter-arrival time are provided in earthquake engineering, including

lognormal (Michael 2005), gamma (Hainzl *et al.* 2006), and Brownian Passage Time (BPT) distribution (Matthews *et al.* 2002).

### 6.2.2 Non-homogeneous Poisson process

Another nonstationary model used for the long-term loss assessment is the non-homogeneous Poisson process, with a time-dependent occurrence rate. A renewal process is not necessarily limited to the exponentially distributed inter-arrival times, while the Poisson process is not subjected to the time-independent occurrence rate. For instance, the non-homogeneous Poisson process can be used to model hurricane landfalls in a changing climate (Ellingwood and Lee 2016; Lin and Shullman 2017). The frequency of hurricanes may increase due to the impact of the warming climate. For this process, the occurrence rate is time-varying, e.g.,  $\lambda(t)$ . The expected number of hazard arrivals over the time interval  $(0, t_{\text{int}}]$  can be computed as

$$E[N(t_{\text{int}})] = \int_0^{t_{\text{int}}} \lambda(t) dt \quad (6-1)$$

The probability of having  $n$  number of arrivals within the time interval  $(0, t_{\text{int}}]$  is computed as

$$P[N(t_{\text{int}}) = n] = \frac{\left( \int_0^{t_{\text{int}}} \lambda(t) dt \right)^n \exp\left(-\int_0^{t_{\text{int}}} \lambda(t) dt\right)}{n!}, n = 0, 1, 2, \dots \quad (6-2)$$

### 6.2.3 Mixed Poisson process

In the homogeneous and non-homogenous Poisson processes, the occurrence rate is restricted to a deterministic intensity function (i.e., either a constant  $\lambda$  or the time-dependent  $\lambda(t)$ ). However, the deterministic function may not be sufficient to capture the uncertainty in a long-term trend. The mixed Poisson process, which covers uncertainty within the intensity function, is receiving increased attention in the hazard model and should also be evaluated. For instance, Xiao *et al.* (2015) suggested using a stochastic intensity function to model hurricane occurrence when considering seasonal variability, based on the recorded hurricane activities along the U.S. Gulf and Atlantic coasts between 1900 and 2010.

The mixed Poisson process is known as a special case of the cox process. A cox process is a Poisson process, in which the occurrence rate is a stochastic process (denoted as  $\{G(t_{\text{int}}), t_{\text{int}} > 0\}$ ). A cox process becomes a mixed Poisson process when the rate is a random variable, e.g.,  $\{G(t_{\text{int}})\} = \Lambda$ . Given the rate  $\Lambda$ , increments in the mixed Poisson process stay stationary (Ross 2014). However, these increments are no longer independent, as the number of arrivals relies on the distribution of  $\Lambda$ . Herein, the stochastic rate  $\Lambda$  is assigned to follow a gamma distribution with shape parameter  $\alpha$  and rate parameter  $\beta$ . The rate  $\Lambda$  is continuous with a probability density function  $g(x)$ . Hence, the probability density function of the gamma distributed rate  $\Lambda \sim \Gamma(\alpha, \beta)$  can be assessed as

$$g(x) = \frac{\beta^\alpha x^{\alpha-1}}{\Gamma(\alpha)} e^{-\beta x} \quad (6-3)$$

Consequently, the probability of having  $n$  number of arrivals within the time interval  $(0, t_{\text{int}}]$  is

$$P(N(t_{\text{int}}) = n) = \int_0^{\infty} e^{-xt_{\text{int}}} \frac{(xt_{\text{int}})^n}{n!} \frac{\beta^\alpha x^{\alpha-1}}{\Gamma(\alpha)} e^{-\beta x} dx \quad (6-4)$$

### 6.3 Long-term loss under nonstationary hazards

Based on the stochastic models, the long-term loss of civil infrastructure subjected to hazards can be formulated. The time interval  $(0, t_{\text{int}}]$  is defined as the service life of civil infrastructure. During the time interval, hazard arrivals are modeled as a stochastic process and the total number of hazard events is  $N(t_{\text{int}}) = n$  with  $N(0) = 0$ . The arriving time and inter-arrival time of the  $k$ th event can be defined as  $T_k$  and  $W_k$ , respectively. The arriving time  $T_k$  equals the sum of inter-arrival times, i.e.,  $T_k = W_1 + W_2 + \dots + W_k$ , as described previously.  $L$  is the loss severity.  $L_k$  refers to the financial loss due to structural damage/failure under the  $k$ th hazard event. The loss severity  $L_k$  and the inter-arrival time  $W_k$  are assumed to be independent. The long-term loss, denoted as  $LTL(t_{\text{int}})$ , is the hazard-induced financial loss of civil infrastructure subjected to hazards within the investigated period  $t_{\text{int}}$ . The loss is discounted to the present value using a monetary discount rate  $r$ , as indicated in Figure 6-1. The long-term loss  $LTL(t_{\text{int}})$  gives

$$LTL(t_{\text{int}}) = \sum_{k=1}^{N(t_{\text{int}})} L_k e^{-rT_k} \quad (6-5)$$

The long-term loss  $LTL(t_{\text{int}})$  is related to the stochastic models of the hazard. For instance, if a homogeneous Poisson process is implemented for loss assessment,

the inter-arriving time  $W_k$  follows an exponential distribution, and the number of arrivals  $N(t_{\text{int}})$  has a Poisson distribution. These parameters are different under different models.

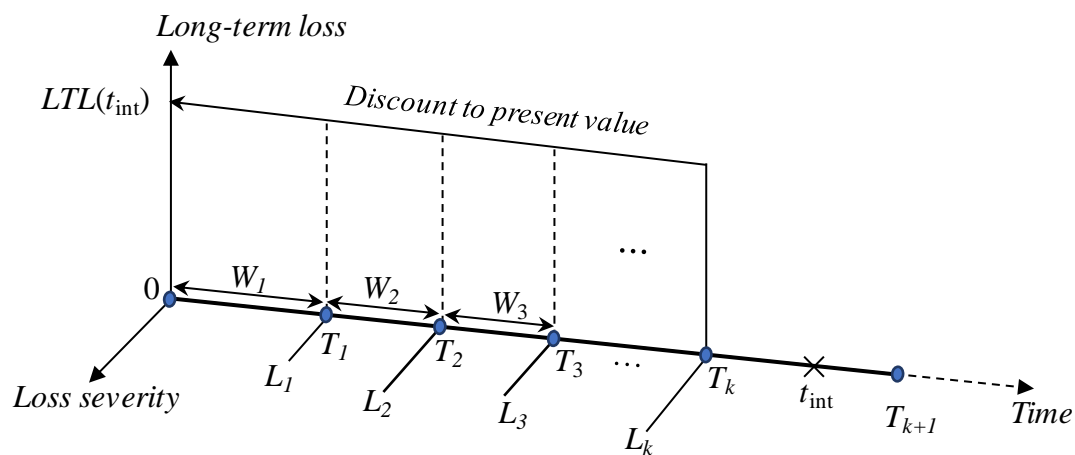


**Figure 6-1** Long-term loss model by considering discounting and hazard arrival process.

#### 6.4 Higher-order analysis using moment generating function

This section introduces the theoretical fundamentals of the proposed moment generating function-based approach. Analytical derivations of moment generating functions and statistical moments of long-term loss under the homogeneous Poisson process, non-homogeneous Poisson process, mixed Poisson process, and renewal process are presented. The merit, capability, and limitations of the developed approach are also discussed.

### 6.4.1 Moment generating function approach

The moment generating function uniquely dictates the probability distribution of a random variable. This property can be adopted to formulate probability distributions of random variables. For instance, random variables will have the same probability distributions if they have identical moment generating functions. Another property of the moment generating function is that raw moments (e.g., mean, second moment) can be obtained by taking derivatives (Ross 2014; Shreve 2004). This property is utilized to formulate statistical moments of long-term loss.

For a random variable  $X$ , its moment generating function about  $\eta$  ( $\eta \in \mathbb{R}$ ) is defined as  $\Phi_X(\eta)$

$$\Phi_X(\eta) = E[e^{\eta X}] \quad (6-6)$$

The first two raw moments of  $X$  can be obtained by taking the first and second derivatives of the moment generating function at zero

$$\Phi_X'(\eta) = \frac{d}{d\eta} E[e^{\eta X}] = E\left[\frac{d}{d\eta} e^{\eta X}\right] = E[Xe^{\eta X}] \Rightarrow \Phi_X'(0) = E[X] \quad (6-7)$$

$$\Phi_X''(\eta) = \frac{d}{d\eta} E[Xe^{\eta X}] = E[X^2 e^{\eta X}] \Rightarrow \Phi_X''(0) = E[X^2] \quad (6-8)$$

Similarly, the  $m$ th-order moment can be assessed by taking the  $m$ th derivative at zero

$$\Phi_X^{(m)}(0) = E[X^m], \quad m \geq 1 \quad (6-9)$$

Based on this concept, the key to derive higher-order moments of long-term loss  $LTL(t_{\text{int}})$  is to compute its moment generating function  $\Phi_{LTL(t_{\text{int}})}$ .

#### 6.4.2 Moment generating function for homogeneous Poisson case

With respect to the homogeneous Poisson case, the moment generating function of long-term loss can be derived in terms of a compound Poisson process. By conditioning on the number of arrivals (i.e.,  $N(t_{\text{int}}) = n$ ) with the Poisson distribution, the moment generating function of long-term loss  $\Phi_{LTL(t_{\text{int}})}$  can be evaluated using the law of total expectation.

The moment generating function of the long-term loss is

$$\Phi_{LTL(t_{\text{int}})}(\eta) = E\left[e^{\eta LTL(t_{\text{int}})}\right] = E\left[\prod_{k=1}^{N(t_{\text{int}})} \Phi_L(\eta e^{-rT_k})\right] \quad (6-10)$$

According to the properties of moment generating functions (Mikosch 2009), the Eq. (6-10) can be expressed as

$$\begin{aligned} & \Phi_{LTL(t_{\text{int}})}(\eta) \\ &= \exp(-\lambda t_{\text{int}}) + \sum_{n=1}^{\infty} E\left[\exp\left(\eta \prod_{k=1}^n L_k e^{-rT_k}\right) \middle| N(t_{\text{int}}) = n\right] \mathbb{P}(N(t_{\text{int}}) = n) \\ &= \exp(-\lambda t_{\text{int}}) + \sum_{n=1}^{\infty} E\left[\prod_{k=1}^n \Phi_L(\eta e^{-rT_k}) \middle| N(t_{\text{int}}) = n\right] \left[\frac{(\lambda t_{\text{int}})^n}{n!} e^{-\lambda t_{\text{int}}}\right] \\ &= \exp(-\lambda t_{\text{int}}) \\ &+ \sum_{n=1}^{\infty} \left\{ \int_0^{t_{\text{int}}} \int_{s_1}^{t_{\text{int}}} \cdots \int_{s_{n-1}}^{t_{\text{int}}} \prod_{k=1}^n \Phi_L(\eta e^{-rs_k}) f_{T_1, \dots, T_n}(s_1, \dots, s_n | N(t_{\text{int}})) ds_n \cdots ds_1 \right\} \frac{(\lambda t_{\text{int}})^n}{n!} e^{-\lambda t_{\text{int}}} \end{aligned} \quad (6-11)$$

Eq. (6-11) requires the joint probability density function of the arriving times  $T_1, T_2, \dots, T_k$ . The loss severity is independent of the number of arrivals  $N(t_{\text{int}})$ . Hence, for the homogeneous Poisson process, the conditional joint probability density function of the arriving times  $T_1, T_2, \dots, T_k$  given  $N(t_{\text{int}}) = n$  can be represented by

$$f_{T_1, T_2, \dots, T_n}((s_1, s_2, \dots, s_n) | N(t_{\text{int}}) = n) = n! \cdot \frac{1}{t_{\text{int}}^n} \quad (6-12)$$

in which  $0 < s_1 < s_2 < \dots < s_n < t_{\text{int}}$ . The result shown in Eq. (6-12) can be alternatively explained by the order statistics (Mikosch 2009; Ross 2014). Given  $N(t_{\text{int}}) = n$ , the arriving time can be expressed by a sequence of independently identically uniformly distributed random variables  $\{U_1, U_2, \dots, U_n\}$

$$((T_1, T_2, \dots, T_n) | N(t_{\text{int}}) = n) \stackrel{d}{=} (t_{\text{int}} U_1, t_{\text{int}} U_2, \dots, t_{\text{int}} U_n) \quad (6-13)$$

where  $\stackrel{d}{=}$  refers to that the same probability distribution is maintained on both sides. Random variables  $U_1, U_2, \dots, U_n$  have a uniform distribution over  $(0, 1)$ . Consequently, substituting Eq. (6-12) into Eq. (6-11), the moment generating function of long-term loss can be rearranged as

$$\begin{aligned} & \Phi_{LTL(t_{\text{int}})}(\eta) - \exp(-\lambda t_{\text{int}}) \\ &= \sum_{n=1}^{\infty} \left\{ \int_0^{t_{\text{int}}} \int_{s_1}^{t_{\text{int}}} \dots \int_{s_{n-1}}^{t_{\text{int}}} \prod_{k=1}^n \Phi_L(\eta e^{-rs_k}) \left( \frac{n!}{t_{\text{int}}^n} \right) ds_n \dots ds_1 \right\} \left[ \frac{(\lambda t_{\text{int}})^n}{n!} e^{-\lambda t_{\text{int}}} \right] \\ &= \exp(-\lambda t_{\text{int}}) \sum_{n=1}^{\infty} \lambda^n \int_0^{t_{\text{int}}} \int_0^{s_n} \dots \int_0^{s_2} \prod_{k=1}^n \Phi_L(\eta e^{-rs_k}) ds_1 \dots ds_n \end{aligned} \quad (6-14)$$

Within the period of  $(0, t_{\text{int}}]$ , the right-hand side of Eq. (6-14) is noted as  $\Omega$ . Taking derivatives on both sides with respect to  $t_{\text{int}}$ , Eq. (6-14) can be rearranged as Eq. (6-15)

$$\begin{aligned}
\frac{d}{dt_{\text{int}}} \Phi_{LTL(t_{\text{int}})}(\eta) &= -\lambda \exp(-\lambda t_{\text{int}}) - \lambda \exp(-\lambda t_{\text{int}}) \Omega + \exp(-\lambda t_{\text{int}}) \Omega' \\
&= -\lambda \exp(-\lambda t_{\text{int}}) (1 + \Omega) + \exp(-\lambda t_{\text{int}}) \Omega' \\
&= -\lambda \Phi_{LTL(t_{\text{int}})}(\eta) + \exp(-\lambda t_{\text{int}}) \Omega' \\
&= -\lambda \Phi_{LTL(t_{\text{int}})}(\eta) + \lambda \Phi_L(\eta e^{-rs}) \exp(-\lambda t_{\text{int}}) \\
&\quad \left[ 1 + \sum_{n=1}^{\infty} \lambda^n \int_0^{t_{\text{int}}} \int_0^{s_n} \cdots \int_0^{s_2} \prod_{k=1}^n \Phi_L(\eta e^{-rs_k}) ds_1 \cdots ds_n \right] \\
&= -\lambda \Phi_{LTL(t_{\text{int}})}(\eta) + \lambda \Phi_L(\eta e^{-rs}) \Phi_{LTL(t_{\text{int}})}(\eta)
\end{aligned} \tag{6-15}$$

By solving this linear differential equation Eq. (6-15), the moment generating function can be obtained as

$$\Phi_{LTL(t_{\text{int}})}(\eta) = \exp \left[ \lambda \int_0^{t_{\text{int}}} [\Phi_L(\eta e^{-rs}) - 1] ds \right] \tag{6-16}$$

in which  $\Phi_L$  refers to the moment generating function of loss severity  $L$ . The derivation of  $\Phi_L$  requires the information with respect to the probabilistic distribution of loss severity. In general, the process of deriving moment generating function is

$$\begin{aligned}
\Phi_{LTL(t_{\text{int}})}(\eta) &= E \left[ e^{\eta LTL(t_{\text{int}})} \right] = E \left[ \exp(\eta \sum_{k=1}^{N(t_{\text{int}})} L_k e^{-rT_k} | N(t_{\text{int}}) = n \right] \\
&= e^{-\lambda t_{\text{int}}} + \sum_{n=1}^{\infty} E \left[ \exp(\eta \prod_{k=1}^n L_k e^{-rT_k}) \right] \left[ \frac{(\lambda t_{\text{int}})^n e^{-\lambda t_{\text{int}}}}{n!} \right] \\
&= \exp(-\lambda t_{\text{int}}) + \exp(-\lambda t_{\text{int}}) \sum_{n=1}^{\infty} [\Phi_L(\eta e^{-rs_k})]^n \left[ \frac{(\lambda t_{\text{int}})^n}{n!} \right] \\
&= \exp \left[ \lambda \int_0^{t_{\text{int}}} [\Phi_L(\eta e^{-rs}) - 1] ds \right]
\end{aligned} \tag{6-17}$$

Previous studies indicated that the probabilistic loss severity can be modeled by the exponential distribution (Read and Vogel 2016; Smith 2003). Herein, the loss severity  $L$  is assumed to follow an exponential distribution  $L \sim \text{EXP}(\theta)$ , with the mean

$E[L] = 1/\theta$ . By substituting  $\Phi_L$  into Eq. (6-17), the moment generating function of long-term loss  $\Phi_{LTL(t_{\text{int}})}$  under the homogeneous Poisson process gives

$$\Phi_{LTL(t_{\text{int}})}(\eta) = \exp \left[ \lambda \int_0^{t_{\text{int}}} \left[ \frac{\theta}{\theta - \eta e^{-rs}} - 1 \right] ds \right] = \left( \frac{\theta - \eta e^{-rt_{\text{int}}}}{\theta - \eta} \right)^{\frac{\lambda}{r}} \quad (6-18)$$

By taking the first and second derivatives at zero, the expectation and variance of long-term loss can be obtained

$$E[LTL(t_{\text{int}})] = \Phi'_{LTL(t_{\text{int}})}(0) = \frac{\lambda}{\theta r} (1 - e^{-rt_{\text{int}}}) \quad (6-19)$$

$$Var[LTL(t_{\text{int}})] = \Phi''_{LTL(t_{\text{int}})}(0) - (\Phi'_{LTL(t_{\text{int}})}(0))^2 = \frac{\lambda}{\theta^2 r} (1 - e^{-2rt_{\text{int}}}) \quad (6-20)$$

Likewise, the  $m$ th order moment can be assessed using Eq. (6-16). The expressions of skewness and kurtosis are associated with the third and fourth-order raw moments. For instance, the skewness  $u_3$  and kurtosis  $u_4$  are

$$u_3 = \frac{E[LTL^3(t_{\text{int}})] - 3\mu\sigma^2 - \mu^3}{\sigma^3} \quad (6-21)$$

$$u_4 = \frac{E[LTL^4(t_{\text{int}})] - 4\mu E[LTL^3(t_{\text{int}})] + 6\mu^2 E[LTL^2(t_{\text{int}})] - 3\mu^4}{\sigma^4} \quad (6-22)$$

in which  $\mu$  refers to the expected long-term loss  $E[LTL(t_{\text{int}})]$  and  $\sigma$  is the standard deviation of  $LTL(t_{\text{int}})$ . Consequently, skewness and kurtosis of long-term loss can be obtained

$$u_3 = \frac{2\lambda r^{1/2}(1 - e^{-3rt_{\text{int}}})}{(\lambda - \lambda e^{-2rt_{\text{int}}})^{3/2}} \quad (6-23)$$

$$u_4 = \frac{(6r + 3\lambda) + (6r - 3\lambda)e^{-2rt_{\text{int}}}}{\lambda(1 - e^{-2rt_{\text{int}}})} \quad (6-24)$$

Eqs. (6-23) and (6-24) show the skewness and kurtosis of long-term loss are not affected by  $\theta$ . Hence, the skewness and kurtosis under the homogeneous Poisson process are independent of the exponentially distributed loss severity. When other distributions are used for the loss severity, the higher-order moments may be affected.

#### 6.4.3 Moment generating function for non-homogeneous Poisson case

The same technique can be used for the non-homogeneous model by applying the law of total expectation. For the non-homogeneous Poisson process, the expected number of arrivals  $Q(t_{\text{int}})$  becomes

$$Q(t_{\text{int}}) = E[N(t_{\text{int}})] = \int_0^{t_{\text{int}}} \lambda(t) dt \quad (6-25)$$

Given the number of arrivals, the moment generating function of long-term loss can be derived as

$$\begin{aligned}
& \Phi_{LTL(t_{\text{int}})}(\eta) \\
&= \exp(-Q(t_{\text{int}})) + \sum_{n=1}^{\infty} E \left[ \prod_{k=1}^n \Phi_L(\eta e^{-rT_k}) \middle| N(t_{\text{int}}) = n \right] \mathbf{P}(N(t_{\text{int}}) = n) \\
&= \exp(-Q(t_{\text{int}})) \\
&+ \exp(-Q(t_{\text{int}})) \sum_{n=1}^{\infty} \int_0^{t_{\text{int}}} \int_{s_1}^{t_{\text{int}}} \cdots \int_{s_{n-1}}^{t_{\text{int}}} \prod_{k=1}^n [\lambda(s_k) \Phi_L(\eta e^{-rs_k})] ds_n \cdots ds_1 \\
&= \exp \left[ \int_0^{t_{\text{int}}} \lambda(s) [\Phi_L(\eta e^{-rs}) - 1] ds \right]
\end{aligned} \tag{6-26}$$

For the non-homogeneous Poisson process, the conditional probability density function of arriving times is

$$f_{T_1, T_2, \dots, T_n}((s_1, s_2, \dots, s_n) | N(t_{\text{int}}) = n) = \frac{n!}{Q^n(t_{\text{int}})} \prod_{k=1}^n \lambda(s_k) \tag{6-27}$$

where  $Q(t_{\text{int}})$  is the expected number of hazard events (Léveillé and Hamel 2018), as indicated in Eq. (6-25). Following a similar computation procedure, as shown in Eq. (6-11), the moment generating function can be expressed as

$$\begin{aligned}
& \Phi_{LTL(t_{\text{int}})}(\eta) \\
&= \exp(-Q(t_{\text{int}})) + \sum_{n=1}^{\infty} \left\{ \int_0^{t_{\text{int}}} \int_{s_1}^{t_{\text{int}}} \cdots \int_{s_{n-1}}^{t_{\text{int}}} \prod_{k=1}^n \Phi_L(\eta e^{-rs_k}) \right. \\
&\quad \left. f_{T_1, \dots, T_n}(s_1, \dots, s_n | N(t_{\text{int}})) ds_n \cdots ds_1 \right\} \\
&\quad \left[ \frac{Q^n(t_{\text{int}})}{n!} e^{-Q(t_{\text{int}})} \right] \\
&= \exp(-Q(t_{\text{int}})) + \exp(-Q(t_{\text{int}})) \sum_{n=1}^{\infty} \int_0^{t_{\text{int}}} \int_0^{s_n} \cdots \int_0^{s_2} \prod_{k=1}^n [\lambda(s_k) \Phi_L(\eta e^{-rs_k})] ds_1 \cdots ds_n
\end{aligned} \tag{6-28}$$

Taking derivatives at two sides of Eq. (6-28), the moment generating function of long-term loss associated with the non-homogeneous Poisson process can be expressed as

$$\Phi_{LTL(t_{int})}(\eta) = \exp \left[ \int_0^{t_{int}} \lambda(s) [\Phi_L(\eta e^{-rs}) - 1] ds \right] \quad (6-29)$$

If a linear function is used for the increasing occurrence rate, e.g.,  $\lambda(t_{int}) = \lambda_0(1 + ct_{int})$ , the moment generating function becomes

$$\Phi_{LTL(t_{int})}(\eta) = \exp \left[ \int_0^{t_{int}} \lambda_0(1 + cs) [\Phi_L(\eta e^{-rs}) - 1] ds \right] \quad (6-30)$$

in which  $\lambda_0$  is the initial stationary occurrence rate and  $c$  refers to an annual increase rate of hazard occurrence. For the given linear rate function, the moment generating function may not be differentiable at zero. Under this circumstance, the moments can be computed by taking derivatives and finding limits by approaching zero. Accordingly, the raw moments can be computed as

$$E[LTL^m(t_{int})] = \lim_{\eta \rightarrow 0} \left( \frac{d^m \Phi_{LTL(t_{int})}(\eta)}{d\eta^m} \right) \quad (6-31)$$

#### 6.4.4 Moment generating function for mixed Poisson case

As mentioned earlier, the mixed Poisson process has a stochastic occurrence rate  $\Lambda$ . Though the random variable  $\Lambda$  affects the probability of the number of arrivals, the inter-arrival times are not influenced by time. Hence, the derivation of the moment generating function for the mixed Poisson case is similar to that for the homogeneous case, as shown in Eq. (6-11). The deterministic rate in the homogeneous model is

switched to the stochastic random variable, e.g.,  $\lambda = E[\Lambda]$  and  $\lambda^2 = E[\Lambda^2]$ . Therefore, the moment generating function of long-term loss under the mixed Poisson model gives

$$\Phi_{LTL(t_{\text{int}})}(\eta) = \Phi_{\Lambda} \left[ \int_0^{t_{\text{int}}} [\Phi_L(\eta e^{-rs}) - 1] ds \right] \quad (6-32)$$

For the illustrative purpose, the random variable  $\Lambda$  follows a gamma distribution  $\Lambda \sim \Gamma(\alpha, \beta)$ , as shown in Eq. (6-3). The loss severity  $L$  remains the exponential distribution  $L \sim \text{EXP}(\theta)$ . The moment generating function of the gamma distributed rate is

$$\Phi_{\Lambda}(x) = \left( \frac{\beta}{\beta - x} \right)^{\alpha} \quad (6-33)$$

Substituting Eq. (6-33) into Eq. (6-32), the moment generating function of long-term loss gives

$$\Phi_{LTL(t_{\text{int}})}(\eta) = \beta^{\alpha} \left[ \beta - \frac{1}{r} \ln \left( \frac{\theta - \eta e^{-rt_{\text{int}}}}{\theta - \eta} \right) \right]^{-\alpha} \quad (6-34)$$

According to Eq. (6-34), the moments of long-term loss under a mixed Poisson process can be assessed.

## 6.5 Higher-order moments for renewal case

### 6.5.1 Higher-order moments using moment generating function

For some stochastic models, properties of the models can be used to formulate the moment generating functions. In this section, statistical moments of long-term loss

under a renewal process are assessed by incorporating the renewal function and convolution technique. Under this scenario, the provided derivations are based on a general renewal process and the probability distribution of the inter-arrival time  $W$  is not specified. The formulation of moment generating function of long-term loss remains the same as presented before

$$\Phi_{LTL(t_{int})}(\eta) = E\left[e^{\eta LTL(t_{int})}\right] = E\left[\prod_{k=1}^{N(t_{int})} \Phi_L(\eta e^{-rT_k})\right] \quad (6-35)$$

According to the renewal theorem (Ross 2014), Eq. (6-35) can be written as

$$\Phi_{LTL(t_{int})}(\eta) = \int_{t_{int}}^{\infty} dF_W(s) + \int_0^{t_{int}} \Phi_L(\eta e^{-rs}) \Phi_{LTL(t_{int}-s)}(\eta e^{-rs}) dF_W(s) \quad (6-36)$$

where  $F_W$  indicates the cumulative distribution function of the inter-arrival time. Consequently, the moments of long-term loss under the renewal process can be obtained by taking derivatives of Eq. (6-36) at zero. The  $m$ th-order derivative of the moment generating function gives

$$\begin{aligned} \frac{d^m \Phi_{LTL(t_{int})}(\eta)}{d\eta^m} &= \Phi_{LTL(t_{int})}^{(m)}(\eta) \\ &= \sum_{k=0}^{m-1} \binom{m}{k} \int_0^{t_{int}} e^{-mrs} \Phi_L^{(m-k)}(\eta e^{-rs}) \Phi_{LTL(t_{int}-s)}^{(k)}(\eta e^{-rs}) dF_W(s) \\ &\quad + \int_0^{t_{int}} e^{-mrs} \Phi_L(\eta e^{-rs}) \Phi_{LTL(t_{int}-s)}^{(m)}(\eta e^{-rs}) dF_W(s) \end{aligned} \quad (6-37)$$

When  $\eta$  equals zero, the  $m$ th-order moments of long-term loss is

$$\begin{aligned}
E[LTL^m(t_{\text{int}})] &= \sum_{k=0}^{m-1} \binom{m}{k} E[L^{m-k}] \int_0^{t_{\text{int}}} e^{-mrs} \Phi_{LTL(t_{\text{int}}-s)}^{(k)}(0) dF_W(s) \\
&\quad + \int_0^{t_{\text{int}}} e^{-mrs} \Phi_{LTL(t_{\text{int}}-s)}^{(m)}(0) dF_W(s)
\end{aligned} \tag{6-38}$$

The convolution technique and the renewal function are used to solve Eq. (6-38). The renewal function refers to the expected number of events in a renewal process. Based on the cumulative distribution function of the inter-arrival time  $F_W$ , a defective distribution function can be defined as (Li *et al.* 2020a)

$$D(t_{\text{int}}) = D_{mr}(t_{\text{int}}) = \int_0^{t_{\text{int}}} e^{-mrs} dF_W(s) \tag{6-39}$$

The convolution power of Eq. (6-39) can be rewritten using the renewal function  $\Theta$ . The summed  $i$ -fold convolution power gives

$$\sum_{i=1}^{\infty} D^{*i}(t_{\text{int}}) = \int_0^{t_{\text{int}}} e^{-mrs} d \sum_{i=1}^{\infty} F_W^{*i}(s) = \int_0^{t_{\text{int}}} e^{-mrs} d\Theta(s) \tag{6-40}$$

where  $*$  is a convolution operator. Substituting Eqs. (6-39) and (6-40) into Eq. (6-38), the  $m$ th-order moment can be formulated as follows

$$\begin{aligned}
E[LTL^m(t_{\text{int}})] &= \sum_{k=0}^{m-1} \binom{m}{k} E[L^{m-k}] \Phi_{LTL}^{(k)}(0) * D(t_{\text{int}}) + \Phi_{LTL}^{(m)}(0) * D(t_{\text{int}}) \\
&= \sum_{k=0}^{m-1} \binom{m}{k} E[L^{m-k}] \Phi_{LTL}^{(k)}(0) * \sum_{i=1}^{\infty} D^{*i}(t_{\text{int}}) \\
&= \sum_{k=0}^{m-1} \binom{m}{k} E[L^{m-k}] \int_0^{t_{\text{int}}} e^{-mrs} \Phi_{LTL(t_{\text{int}}-s)}^{(k)}(0) d\Theta(s) \\
&= \sum_{k=0}^{m-1} \binom{m}{k} E[L^{m-k}] \int_0^{t_{\text{int}}} e^{-mrs} E[LTL^k(t_{\text{int}}-s)] d\Theta(s)
\end{aligned} \tag{6-41}$$

The first four moments of long-term loss can be effectively obtained by using this recursive equation, i.e., Eq. (6-41). This recursive equation is validated by comparing the first two moments with the results provided by (Pandey and Van Der Weide 2017), in which the analytical expressions of the mean and variance using the regenerative property were provided. The moments of long-term loss assessed by Eq. (6-41) are based on a general renewal process. The loss under renewal processes with different probabilistic models of the inter-arrival times can be computed by employing different renewal functions. The implementation of the renewal function circumvents complicated derivations starting from a stochastic process.

The homogeneous Poisson process, as a typical renewal process, has a renewal function defined as  $d\Theta(s)/ds = \lambda$ . Consequently, the  $m$ th-order moment of long-term loss under the homogeneous Poisson model is

$$E[LTL^m(t_{\text{int}})] = \lambda \sum_{k=0}^{m-1} \binom{m}{k} E[L^{m-k}] \int_0^{t_{\text{int}}} e^{-mrs} E[LTL^k(t_{\text{int}} - s)] ds \quad (6-42)$$

The expectation and variance of the long-term loss are assessed

$$E[LTL(t_{\text{int}})] = \frac{E[L]\lambda}{r} (1 - e^{-rt_{\text{int}}}) \quad (6-43)$$

$$\text{Var}[LTL(t_{\text{int}})] = \frac{E[L^2]\lambda}{2r} (1 - e^{-2rt_{\text{int}}}) \quad (6-44)$$

The third and fourth-order moments obtained from the renewal function are also validated by comparing with the values computed using the moment generating function, as shown in Eqs. (6-19) and (6-20).

### **6.5.2 Comparison between renewal approach and moment generating function approach**

As introduced in CHAPTER 5, the renewal approach is efficient in solving the homogeneous Poisson process and renewal processes using the renewal function. Identifying the distribution type of loss severity is not necessary under the renewal condition. Compared with the renewal approach, the moment generating function approach model is more computationally demanding but also has a wider application range. The moment generating function efficiently solves higher-order moments of long-term loss under different stochastic models (the renewal process, homogeneous Poisson process, non-homogeneous Poisson process, and mixed Poisson process). Based on the law of total expectation, the proposed approach expands the application scope of the moment approach, which was formerly used for the homogeneous Poisson model only. Using the convolution technique, the higher-order moments of loss under a renewal process are successfully derived from the developed approach. During the computational process, if the limit function of the moment generating function is difficult to solve, the raw moments can be assessed using Eq. (6-31).

The developed approach is validated by Monte Carlo simulation and more details are shown in illustrative examples. Some of the derivations may not be applicable to stochastic processes without Poisson properties, e.g., when inter-arrival times are not independent identically distributed. Additionally, by considering the mathematical definition, the moment generating function may not exist due to divergent integrals. These issues should be carefully considered during the application process. Apart from the loss assessment, higher-order moments can be used to compute long-

term reliability (Zhao and Ono 2001). For instance, skewness was involved in the third-order moment method to assess the long-term reliability of reinforced concrete structures under chloride-induced corrosion (Zhang *et al.* 2015). Reliability analysis involving skewness and kurtosis was also conducted in Lu *et al.* (Lu *et al.* 2019). Another application of the moment generating function is that statistical moments can be used if there is insufficient information. For instance, Zhao and Lu (2007) used statistical moments to describe probabilistic characteristics of random variables.

## 6.6 Illustrative example

The occurrence of hurricanes can be modeled as a stochastic process using observation data (Elsner *et al.* 2001; Katz 2002). For instance, a homogeneous Poisson process can be used to model hurricane arrivals in a stationary environment (Elsner *et al.* 2001). However, stochastic models using historical observations only may not be sufficient to project future scenarios, as the variability in characteristics of hazards is not considered (Hallegatte *et al.* 2011). In recent decades, hurricane arrivals in a changing environment considering the effects of climate change and variability have been modeled by the non-homogeneous and mixed Poisson models (Elsner and Bossak 2001; Lin and Shullman 2017). This example aims to assess the impact of climate change and variability on hurricane-induced losses, from a long-term perspective.

The homogeneous Poisson process is widely used to model hurricane arrivals in a stationary environment, which assumes a constant occurrence rate  $\lambda$  based on historical observations (Elsner *et al.* 2001; Katz 2002). This rate is typically determined by dividing the total number of hurricane landfalls by the observation period (Elsner *et*

*al.* 2001). Recent studies observe the increasing trend in hurricane frequency in the warming climate (Emanuel 2005). For such scenarios, the non-homogeneous Poisson process with an increasing occurrence rate, i.e.,  $\lambda(t_{int})$ , could be used to predict the increase in the number of hurricane arrivals (Ellingwood and Lee 2016; Lin and Shullman 2017).

In a changing environment, in addition to the potential increasing trend, the occurrence of hurricanes can be significantly influenced by climate variability. Climate variability refers to variations in the mean state and characteristics of climate (Kossin *et al.* 2007). Previous studies stated the importance of considering the occurrence rate as a random variable in the Poisson process (i.e., the mixed Poisson process) for future hurricane predictions. For instance, Elsner and Bossak (2001) projected the occurrence rate of the U.S. hurricane landfalls using the mixed Poisson model. Villarini *et al.* (2010) assessed changes in hurricane frequency using the mixed Poisson process, by modeling the dependence of hurricane occurrence on different climate indices. In this example, a gamma distributed stochastic rate is utilized (Elsner and Bossak 2001).

The long-term loss analysis is performed on a multi-span simply supported girder bridge (Li and Dong 2019). The bridge has six spans equally distributed with a length of 146 *m*. This type of bridge is most susceptible to deck unseating damage (Zhu and Dong 2020). The given annual occurrence rate of hurricane  $\lambda_0$  is 0.245 for the investigated area in the stationary environment (i.e., with a homogeneous Poisson process). The rate is determined by counting the total number of 27 hurricane landfalls in the investigated region from 1900 to 2100, i.e.,  $\lambda_0 = 27/110$  per year (Wang *et al.* 2017a). The expected loss severity  $E[L]$  is 1.283 million USD (Li and Dong 2019). The

detailed computation of  $\lambda_0$  and loss severity under hurricane hazards can be performed according to the process as described in CHAPTER 3 and CHAPTER 5. The monetary discount rate  $r$  is 2% for the long-term evaluation (Lee and Ellingwood 2015). The loss severity follows an exponential distribution.

In a stationary environment, the occurrence of hurricanes is modeled as a homogeneous Poisson process, with a rate of  $\lambda = \lambda_0$  throughout the lifetime. In a changing climate, the non-homogeneous Poisson process is adopted and the occurrence rate is assumed to follow an increasing linear relationship  $\lambda(t_{\text{int}}) = \lambda_0(1 + ct_{\text{int}})$ , in which  $c$  refers to an annual increase rate of hurricane landfalls (Ellingwood and Lee 2016). The annual increase rate of 0.2% indicates that the number of hurricanes is increased by 20% in the next century (Bender *et al.* 2010; Ellingwood and Lee 2016). The mixed Poisson process is also adopted to compute the long-term loss of the bridge under hurricanes considering climate variability. Herein, the parameters within the stochastic occurrence rate  $\Lambda \sim \Gamma(\alpha, \beta)$  are based on the information presented in Elsner and Bossak (2001). The rate has a mean of  $E[\Lambda] = \lambda_0$  (the same value as the rate in the homogeneous model) and the gamma parameters are assumed as  $\Lambda \sim \Gamma(0.49, 2)$ . Given more information (e.g., climate information), the parameters used in the non-homogenous and mixed Poisson processes can be upgraded and the relevant results would be computed.

The expectation, standard deviation, coefficient of variation, skewness, and kurtosis of the long-term loss under the homogeneous, non-homogeneous, and mixed Poisson processes are obtained for the investigated bridge by using the proposed approach, as shown in Table 6-1. When the service life reaches 150 years, the expected

long-term loss of bridge under the non-homogeneous Poisson model is approximately increased by 5.0% in the changing climate. As a relatively small increase in the occurrence rate is assumed in this example, the loss results with respect to the non-homogeneous model do not show large differences from those of the homogeneous model.

According to Table 6-1, all skewness values are positive (right-skewed), which indicates a longer tail on the right side of the distribution of long-term loss. Homogeneous and non-homogeneous models are moderately skewed (skewness between 0.5 and 1), while the mixed model is highly skewed (skewness greater than 1). Meanwhile, all kurtosis values are greater than 3, indicating that all the tails are heavier and longer than a normal distribution. For the case using the mixed Poisson process, the expected loss is the same as that using the homogeneous Poisson process, but the standard deviation, skewness, and kurtosis are much larger, which indicated potential heavy tail risks. Special attention should be paid to this aspect within the decision-making process.

**Table 6-1** Statistical moments, i.e., mean, standard deviation (SD), skewness (ske), and kurtosis (kur), of Long-term loss of the bridge under homogeneous, non-homogeneous (NHPP), and mixed Poisson processes.

Model	Lifetime	Mean	SD	COV	Ske	Kur
	(years)	(10 <sup>6</sup> USD)	(10 <sup>6</sup> USD)			
Homogeneous	75	12.2099	4.3773	0.36	0.61	3.54
NHPP		12.9048	4.4686	0.35	0.59	3.51

Mixed		12.2099	17.9835	1.47	2.86	15.27
Homogeneous		14.9343	4.4849	0.30	0.57	3.49
NHPP	150	16.1929	4.5941	0.28	0.55	3.46
Mixed		14.9343	21.8010	1.46	2.86	15.26

The proposed analytical method is validated by the Monte Carlo simulation. In the simulation approach, the homogeneous model is generated using the exponentially distributed inter-arrival times, while a non-homogeneous process is simulated using the thinning method (Gerhardt and Nelson 2009). The mixed Poisson process is simulated based on the stochastic occurrence rate (Burnecki and Weron 2005). The results of the mean and standard deviation of the long-term loss under the homogenous and non-homogeneous models are indicated in Figure 6-2. Figure 6-3 shows the standard deviation of long-term loss of the investigated bridge under different hurricane occurrence models. The loss under the mixed Poisson process has the largest dispersion, as the mixed model involves large uncertainties of climate variability, compared with the other two Poisson models. In the figures, the comparison between the analytical and simulation results is also provided. A good agreement among the results indicates the accuracy and effectiveness of the proposed analytical method. Compared with the analytical approach, the simulation of a single run with respect to an assigned lifetime takes about one to two hours. The simulation was conducted on a computer with *Intel Core i7-6700 CPU (4 core, 3.40 GHz, 16 GB RAM)* and *Intel HD Graphics 530 GPU*. In this example, the simulation approach is time-consuming and computationally expensive.

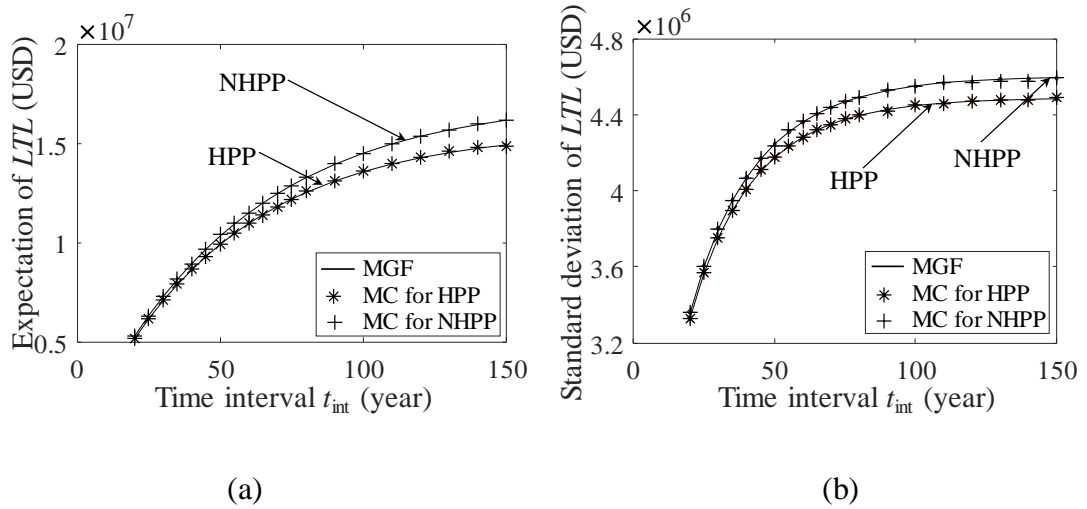


**Figure 6-2** (a) Expectation and (b) standard deviation of hurricane-induced long-term loss under homogeneous (HPP) and non-homogeneous model (NHPP) by moment generating function (MGF) method and Monte Carlo (MC) simulation.

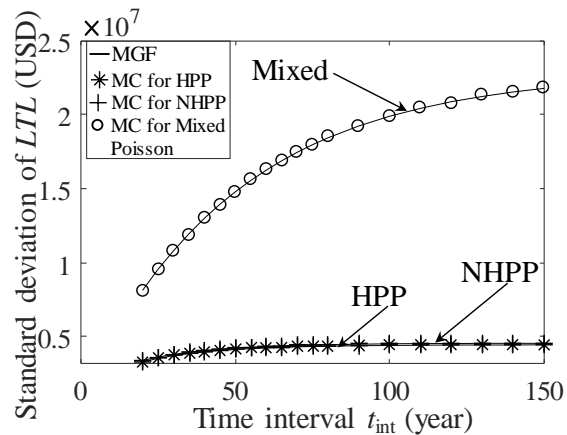


**Figure 6-3** Standard deviation of hurricane-induced long-term loss under homogeneous (HPP), non-homogeneous (NHPP), and mixed Poisson model by moment generating function (MGF) method and Monte Carlo (MC) simulation.

A parametric study is developed to measure the sensitivity of long-term loss to the monetary discount rate and variability of loss severity. A series of incremental

monetary discount rates from 1% to 5% is considered for the homogeneous Poisson model. Figure 6-4(a) illustrates that the expected long-term loss decreases rapidly with the increase of the monetary discount rate. The same trend is also observed for the standard deviation of long-term loss. However, the tendency is opposite with respect to skewness and kurtosis. Figure 6-4(b) shows that skewness increases with the discount rates. Hence, appropriate predictions of the monetary discount rate are significant for long-term loss estimation.

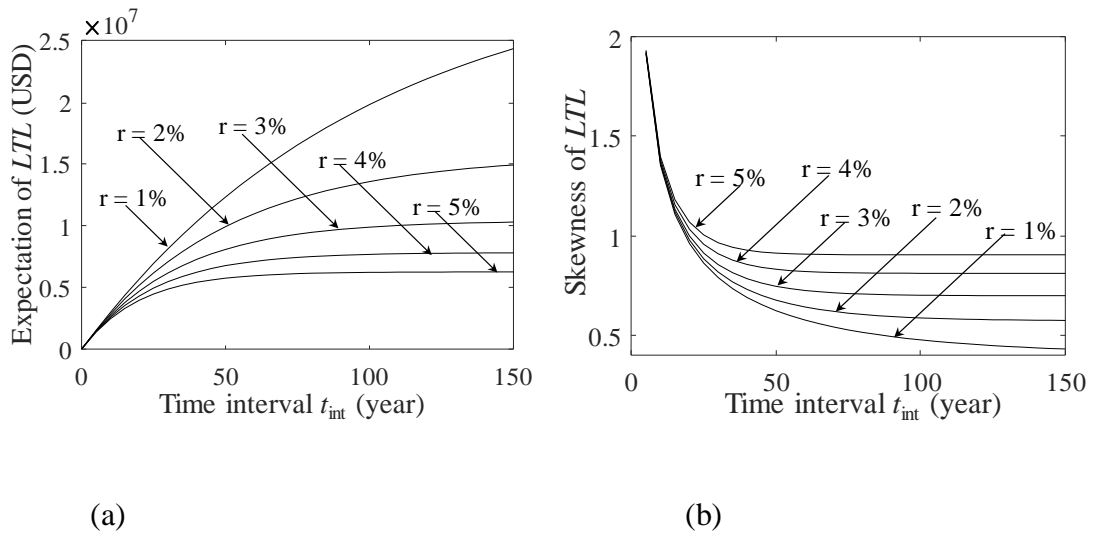


**Figure 6-4** (a) Expectation and (b) skewness of the long-term loss considering different monetary discount rates.

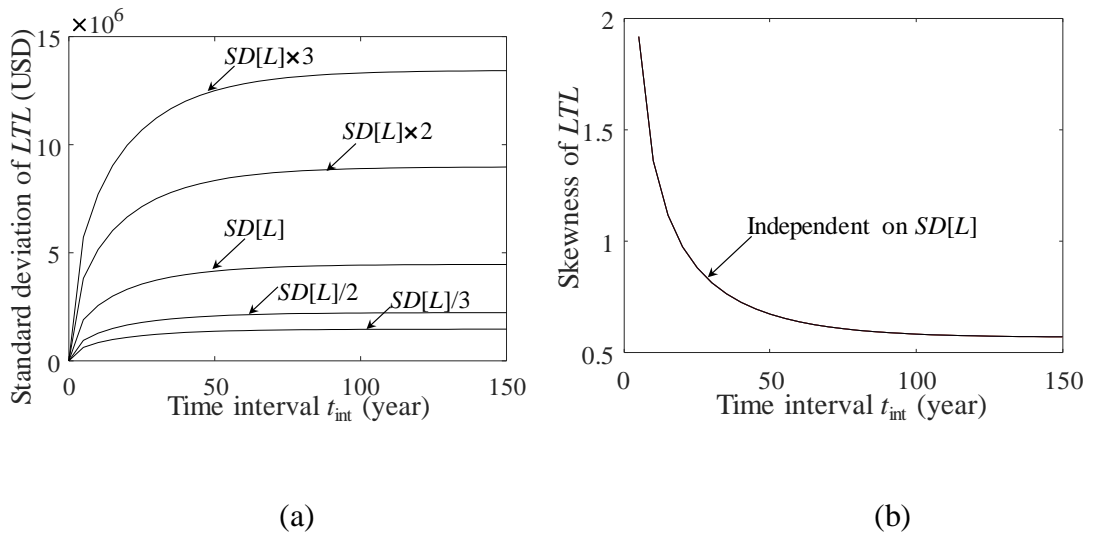


**Figure 6-5** (a) Impact of the variability of loss severity on the long-term loss considering identical expectation  $E[L]$  with different standard deviations of loss severity  $SD[L]$  and (b) the effect of variability of loss severity on the skewness of long-term loss.

The loss severity is another key input for the loss assessment, as its mean  $E[L]$  and standard deviation  $SD[L]$  are associated with large uncertainty in hazard characteristics and climate environments. The impact of the variability of loss severity on the long-term loss is assessed. The long-term loss with the initial standard deviation  $SD[L]$  is taken as the reference value. The long-term loss under the other four cases with triple, double, one-half, and one-third  $SD[L]$  is assessed. The associated standard deviations are presented in Figure 6-5(a). It shows that the dispersion of long-term loss is significantly enlarged with the increase of loss severity. However, the skewness of long-term loss is not influenced, as shown in Figure 6-5(b). From Eqs. (6-23) and (6-24), the skewness and kurtosis are independent of the exponentially distributed loss severity.

In the illustrative examples, structures are assumed to be fully restored to the pre-hazard stage. This assumption is commonly used in the loss assessment (Padgett *et al.* 2010; Wen and Kang 2001; Yeo and Cornell 2009). The level of restoration usually depends on many factors, e.g., the acceptable level of structural performance, investment, and tradeoffs between appropriate performance levels and investment. Further studies are needed to incorporate different restoration models.

## **6.7 Summary**

This chapter develops a novel moment generating function-based analytical approach to perform higher-order analysis in a life-cycle context. The moment generating function-based approach is proposed for the higher-order analysis of long-term loss. By using the law of total expectation, the developed approach successfully expands the application scope of the moment generating function. Explicit expressions of moment generating functions are presented for the homogeneous, non-homogeneous, and mixed Poisson processes. When the derivations of moment generating functions are complex, e.g., in a renewal process, properties of the stochastic process can be utilized. The renewal function and the convolution technique are used to derive moments under the renewal model. A new stochastic model of the mixed Poisson process is introduced, which is associated with a random variable for the rate function. Statistical moments of long-term loss under this new model are also effectively assessed using the moment generating function. In addition to the lower-order moments (i.e., mean and standard deviation), higher-order moments (i.e., skewness and kurtosis) of the long-term loss can be successfully derived using the proposed moment generating function. The proposed

approach is flexible to solve various stochastic processes. For instance, apart from the stationary model (e.g., homogeneous Poisson process), statistical moments associated with non-homogeneous Poisson, mixed Poisson, and renewal processes can be effectively attained. The analytical approach is validated by the Monte Carlo simulations. With a satisfactory agreement of the results, the effectiveness and accuracy of the proposed approach are validated.

The proposed approach is applied to an illustrative example to assess the long-term loss of highway bridges subjected to hurricanes. The long-term loss of the investigated civil infrastructure under different stochastic occurrence models of hazard is computed. In particular, the homogeneous Poisson, non-homogeneous Poisson, and mixed Poisson processes are investigated. The impact of climate change and variability on hurricane-induced loss is assessed. Due to the stochastic occurrence rate within the mixed Poisson process, the relevant standard deviation, skewness, and kurtosis of long-term loss are much larger than those associated with other models. In addition, the long-term loss is sensitive to the change of loss severity and monetary discount rate. Appropriate evaluations of these parameters are required for the loss assessment.

# CHAPTER 7 LIFE-CYCLE ANALYSIS SUBJECTED TO MULTIPLE DEPENDENT DETERIORATION PROCESSES

## 7.1 Introduction

Civil infrastructure systems are subjected to multiple deterioration processes during the lifetime, such as gradual deterioration caused by environmental influence (e.g., corrosion and crack growth) and shock deterioration due to extreme events (e.g., hurricanes and earthquakes). These deterioration processes may affect the performance of systems and interrupt service. The combination effects of deterioration processes may lead to damage and failure, thus threatening public safety and resulting in considerable financial and social losses. During the life-cycle analysis, due to various uncertainties associated with deterioration, rational stochastic models and reliability analysis can be essential. Although numerous studies have accounted for both gradual and shock deterioration processes (Giouvanidis and Dong 2020; Gong and Frangopol 2019; Li *et al.* 2015), while interaction and correlation between them are commonly neglected (i.e., assume they are independent), e.g., Ghosh and Padgett (2010) and Peng and Stewart (2014).

This chapter evaluates the structural performance of civil infrastructure under multiple deterioration processes. In addition to a gradual deterioration process and an external deterioration process, a fatal shock process is considered to incorporate uncertainties associated with extreme events. The fatal shock results from extreme

events such as earthquakes and hurricanes, and their occurrence can be modeled by stochastic processes presented in CHAPTER 5 and CHAPTER 6. The fatal shock leads to immediate failure of the system. Interactions among different deterioration processes are explored and the associated impact on the system is assessed by time-dependent reliability. The effect of interaction among deterioration processes and the effect of fatal shocks are investigated.

## **7.2 Structural deterioration over life-cycle**

Stochastic models associated with system deterioration are described in this section. The gradual deterioration is modeled by a stochastic gamma process. Two types of shock processes, i.e., external shocks and fatal shocks, are considered in this chapter. Reliability-based maintenance policies are proposed considering the interaction between deterioration processes.

### **7.2.1 Gradual deterioration**

The stochastic gamma process has been widely used to model gradual deterioration (Iervolino *et al.* 2013; Sanchez-Silva *et al.* 2011). Compared with the conventional deterministic time-dependent model, e.g., using a deterioration function (Guo *et al.* 2020), a gamma process describes the auto correlation and monotonous (non-increasing) characteristics in terms of the system deterioration, thus providing considerable effectiveness and convenience during mathematical calculations (Cheng *et al.* 2012). Furthermore, the stochastic process associated with the gradual deterioration allows the

mathematical computation of dependent multiple deterioration processes, thus providing sufficient efficiency during the modeling. The gradual deterioration of an infrastructure system can be modeled by a stochastic gamma process  $\{Q(s), s \geq 0\}$ . Over an interval  $(0, s]$ , the cumulative degradation  $Q(s)$  follows the gamma distribution, and its PDF  $ga(q; \alpha s, \beta)$  and CDF  $Ga(q; \alpha s, \beta)$  are given by

$$ga(q; \alpha s, \beta) = \frac{q^{\alpha s - 1} \exp(-q / \beta)}{\beta^{\alpha s} \Gamma(\alpha s)} \quad (7-1)$$

$$Ga(q; \alpha s, \beta) = \frac{\Upsilon(\alpha s, q / \beta)}{\Gamma(\alpha s)} \quad (7-2)$$

where  $\alpha s$  and  $\beta$  are shape and scale parameters, respectively;  $\Upsilon(\alpha s, \beta) = \int_0^\beta x^{\alpha s - 1} e^{-x} dx$  is the lower incomplete gamma function; and  $\Gamma(\alpha s) = \int_0^\infty x^{\alpha s - 1} e^{-x} dx$  is the complete gamma function.

### 7.2.2 Shock deterioration: external shock and fatal shock

Different from gradual deterioration, shock deterioration indicates the abrupt decrease in the performance of a system caused by a shock event (Caballé and Castro 2017; Guo *et al.* 2020). There are two shock processes considered herein. One is the external shock process, which leads to the accumulation of shock deterioration and results in failure when the failure threshold is reached. The other one refers to a fatal shock process, which leads to immediate failure of the system. It is necessary to account for random fatal shocks, as the system can be subjected to extreme events with low-frequency and

high-consequence during the lifetime. Two shock processes are modeled by the Poisson processes, in which the occurrence rate of a fatal shock process  $\lambda_{FaS}$  is much smaller than that of an external shock process  $\lambda_{ExS}$ . For a single shock process, the number of shocks follows a Poisson distribution, which gives

$$P[N(t) = x] = \frac{(\lambda t)^x \exp(-\lambda t)}{x!} \quad (7-3)$$

where  $q$  is the number of shocks with  $x = 0, 1, 2, \dots$  and  $\lambda$  is the occurrence rate of a shock process.

### 7.3 System reliability analysis

As the system degrades due to gradual deterioration and shocks, reliability assessment is essential to evaluate the structural performance during life-cycle analysis. Recent studies have paid more attention to investigate multiple deterioration processes and their interaction on structural reliability. For instance, Kumar *et al.* (2015) proposed a stochastic framework for engineering systems to estimate the time to failure considering exposure to gradual degradation and sudden events. Wang *et al.* (2017b) developed a dependence framework to assess the time-dependent reliability of deteriorating structures considering the correlation between gradual and shock deterioration processes. Jia *et al.* (2021) investigated the stochastic deterioration of reinforced concrete structures considering compound effects of corrosion, earthquakes, and ASR. In addition to interactive effects, the system can be exposed to various extreme events

associated with low probability and high consequence. Therefore, the impact of extreme events on structural performance should be evaluated.

### 7.3.1 Stochastic demand and capacity

The deterioration of a system has a direct influence on structural reliability. The time-dependent reliability analysis relies on the assessment of demand and capacity subjected to stochastic deterioration. During the service life of a system  $(0, s]$ , the random occurrence of external loads  $\{U_i\}$  with  $i = 1, 2, \dots, n$  impose demand  $\{D_{t_n}\}$  upon the system. The arriving times of external loads are  $t_1, t_2, \dots, t_n$ . Subsequently, the period  $(0, s]$  is divided into  $n + 1$  intervals by  $n$  number of load events, i.e.,  $(0, t_1]$ ,  $(t_1, t_2]$ ,  $\dots$ ,  $(t_{n-1}, t_n]$ ,  $(t_n, t_{n+1} = s]$ . Meanwhile, the system suffers from gradual and external shock deterioration, thus reducing the capacity. The system resistance at time  $t_n$  can be denoted as  $R_{t_n}$

$$R_{t_n^-} = R_0 - \sum_{i=1}^n \Delta R_{t_i}^{Gra} - \sum_{i=1}^{n-1} \Delta R_{t_i}^{ExS} \quad (7-4)$$

$$R_{t_n^+} = R_0 - \sum_{i=1}^n \Delta R_{t_i}^{Gra} - \sum_{i=1}^{n-1} \Delta R_{t_i}^{ExS} - \Delta R_{t_n}^{ExS} \quad (7-5)$$

where  $R_0$  represents the initial capacity of the system;  $t_n^-$  and  $t_n^+$  are the time immediately before and after  $t_n$ ;  $\Delta R_{t_i}^{ExS}$  is the external shock deterioration at time  $t_i$ ; and

$\Delta R_{t_i}^{Gra}$  is gradual deterioration within time interval  $(t_{i-1}, t_i]$ . Figure 7-1 describes the impact of gradual and shock deterioration on the system capacity at  $t_n$  ( $t_n^-$  and  $t_n^+$ ).

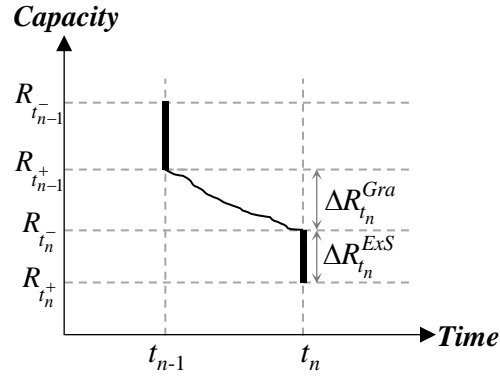


**Figure 7-1** Schematic diagram of deterioration of system capacity.

For normalization, the capacity can be defined as the product of the deterioration function  $G(t)$  and the initial capacity  $R_0$ , i.e.,  $R(t) = R_0 \cdot G(t)$ . Accordingly, the time-dependent deterioration function can be defined as

$$G_{t_n^-} = 1 - \sum_{i=1}^n \Delta R_{t_i}^{Gra} / R_0 - \sum_{i=1}^{n-1} \Delta R_{t_i}^{ExS} / R_0 \quad (7-6)$$

$$G_{t_n^+} = 1 - \sum_{i=1}^n \Delta R_{t_i}^{Gra} / R_0 - \sum_{i=1}^n \Delta R_{t_i}^{ExS} / R_0 \quad (7-7)$$

For the system with a lifetime of  $(0, s]$ , the deterioration function at time  $s$  becomes

$$G(s^-) = 1 - \sum_{i=1}^{N^+1} \Delta R_{t_i}^{Gra} / R_0 - \sum_{i=1}^{N^-} \Delta R_{t_i}^{ExS} / R_0 \quad (7-8)$$

$$G(s^+) = 1 - \sum_{i=1}^{N^++1} \Delta R_{t_i}^{Gra} / R_0 - \sum_{i=1}^{N^+} \Delta R_{t_i}^{ExS} / R_0 \quad (7-9)$$

where  $N^-$  is the maximum integer  $j$  with  $t_j < s$  and  $N^+$  is the maximum integer  $j$  with  $t_j \leq s$ .  $N^+ = N^- + 1$  only when  $s = t_i$  ( $i = 1, 2, \dots, n$ ) otherwise  $N^+ = N^-$ . Based on Eqs. (7-8) and (7-9), within the lifetime  $(0, s]$ , the deterioration function at time  $s$  can be given as

$$G(s) = G_{s^-} = G_{s^+} = 1 - \sum_{i=1}^n \Delta R_{t_i}^{Gra} / R_0 - \sum_{i=1}^{n+1} \Delta R_{t_i}^{ExS} / R_0 \quad (7-10)$$

### 7.3.2 Failure mechanisms and limit state function

Two possible failure modes of the system are considered: one is that failure occurs when the demand exceeds its capacity, and the other one defines that the system fails when the cumulative deterioration or damage exceeds the threshold. For the first scenario, the system fails at the  $n$ th shock event with  $R_{t_n^-} < D_{t_n}$  and the limit state function can be computed as

$$LS_n = R_0 - \sum_{i=1}^n \Delta R_{t_i}^{Gra} - \sum_{i=1}^{n-1} \Delta R_{t_i}^{ExS} - D_{t_n} \quad (7-11)$$

Given Eq. (7-11), the failure occurs when  $LS_n$  is smaller than zero, i.e.,  $LS_n < 0$ .

An illustrative diagram is shown in Figure 7-2 to describe the demand and time-dependent resistance subjected to gradual deterioration and external shocks.

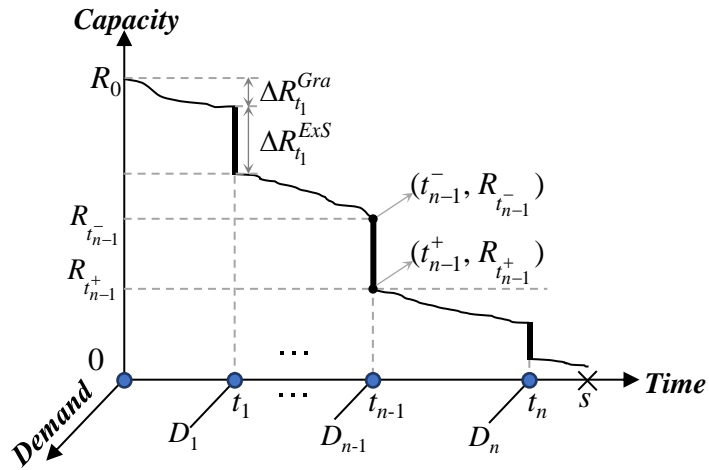


**Figure 7-2** Capacity and demand of a system subjected to gradual deterioration and external shock process.

The other type of failure occurs at an arbitrary time when the total deterioration exceeds the maximum deterioration level (Kumar *et al.* 2015; Wang *et al.* 2017b). As the fatal shock process is taken into account, a fatal event results in immediate failure of the system. Additionally, the failure occurs when the total amount of deterioration caused by gradual deterioration and external shock exceeds the threshold, as shown in Eq. (7-12)

$$\sum_{i=1}^{N^++1} \Delta R_{t_i}^{Gra} / R_0 - \sum_{i=1}^{N^+} \Delta R_{t_i}^{ExS} / R_0 > g_{\max} \quad (7-12)$$

### 7.3.3 Dependence between deterioration processes

In previous studies, different deterioration processes and the demand are commonly assumed to be independent. However, deterioration processes usually have interactive

effects. For instance, cracks caused by external activities may accelerate the initiation and corrosion rate of reinforcement steel in terms of reinforced concrete structures (Otieno *et al.* 2010). Therefore, for the reliability analysis, the interactive effects should be considered. As the deterioration of one process is typically aggravated by the other, the interaction among deterioration processes should be evaluated by positive correlation (Jia and Gardoni 2019; Wang *et al.* 2017b). Herein, the effects are quantified by dependent demands and deterioration. For instance, a series of demands  $\{ D_{t_n} \}$  are associated with external shock deterioration. Meanwhile, the shock-induced deterioration interacts with the gradual deterioration.

The interaction among different deterioration processes can be modeled by a multivariate probability distribution function. Herein, the interaction in terms of shock deterioration focuses on the external shock deterioration, as the fatal shock deterioration always results in immediate failure of the system. Let  $A_{t_i} = \Delta R_{t_i}^{Gra} / R_0$ ,  $B_{t_i} = \Delta R_{t_i}^{ExS} / R_0$ , and  $\Psi_{t_i} = D_{t_i} / R_0$  represent the normalized gradual deterioration, external shock deterioration, and demand at time  $t_i$ , respectively. The joint CDF of the three correlated random variables  $(A_{t_i}, B_{t_i}, \Psi_{t_i})$  can be denoted as  $F_{A,B,\Psi}(a,b,d)$ . The CDF of the random vector  $(A_{t_i}, B_{t_i}, \Psi_{t_i})$  can either be derived by empirical models or the advanced copula approach. This chapter adopts a copula to model their dependency as the copula tool allows a separate assessment of the dependence structure and marginal distributions. For instance, the joint CDF of the random vector can be expressed as

$$F_{A,B,\Psi}(a,b,d) = C_{\theta}(F_A(a), F_B(b), F_{\Psi}(d)) \quad (7-13)$$

where  $C_{\theta}$  is the copula model with dependence parameter  $\theta$ ;  $F_A(a)$ ,  $F_B(b)$ , and  $F_{\Psi}(d)$  are the CDFs of the normalized gradual deterioration, external shock deterioration, and demand. The detailed modeling of  $F_{A,B,\Psi}(a,b,d)$  is provided in the illustrative example.

#### 7.4 Illustrative example

The proposed framework is applied to an illustrative example. The example aims to assess the time-dependent reliability of a bridge subjected to dependent deterioration processes. The gradual deterioration, external shock deterioration, and fatal shock deterioration are considered. In this example, a gamma process is employed to model the gradual deterioration of the investigated bridge. The expectation of the cumulative gradual deterioration changes linearly with time (Wang *et al.* 2015). The initial resistance of the investigated system is  $R_0$ . At the end of a time period of 40 years, the expected cumulative gradual deterioration is  $0.2R_0$  with a coefficient of variation of 0.4. The maximum deterioration level  $g_{\max}$  is 0.4. Random external shocks are caused by hazards and modeled by a Poisson process, with an annual occurrence rate of  $\lambda_{ExS} = 0.3$ . Meanwhile, hazards impose demands acting on the bridge. It is assumed that demands follow a Gumbel distribution with a mean of  $0.3L$  and a coefficient of variation of 0.3. The resulting deterioration in terms of the external shock process is lognormally distributed. It has a mean of  $0.03L$  and a coefficient of variation of 0.4. Herein, it

assumes  $L = R_0/3$ . The occurrence of fatal shocks is also modeled by a Poisson process with an annual occurrence rate  $\lambda_{FaS} = 1 \times 10^{-5}$ . A low-frequency fatal event leads to the immediate failure of a system and results in essential maintenance.

The dependence structure for the normalized gradual deterioration, external shock deterioration, and demand  $(A_{t_i}, B_{t_i}, \Psi_{t_i})$ , as shown in Eq. (7-14) is modeled by a Gaussian copula. The joint CDF of the correlated random vector  $(A_{t_i}, B_{t_i}, \Psi_{t_i})$  can be written as

$$F_{A,B,\Psi}(a,b,d) = \Theta_{\zeta}(\Theta^{-1}(F_A(a)), \Theta^{-1}(F_B(b)), \Theta^{-1}(F_{\Psi}(d))) \quad (7-14)$$

in which  $\Theta(\cdot)$  is the CDF of a multivariate normal distribution;  $\zeta$  is the correlation matrix; and  $\Theta^{-1}(\cdot)$  is the inverse CDF of the standard normal distribution. The correlation between random vectors is positive (Dieulle *et al.* 2003), as a stronger external load results in a larger decrease in resistance due to damage (e.g., crack). Meanwhile, changes in resistance further accelerate the gradual deterioration process (e.g., corrosion in terms of reinforcement). Herein, the associations between every two random variables are described by Pearson's correlation coefficient with  $\gamma_d = 0.3$ . The assigned values are presented here for illustrative purposes and can be upgraded with specific problems.

Given these inputs, the probability of failure of the system within 100 years can be computed by using Monte Carlo simulation with  $10^6$  replications, as shown in Figure 7-3. The system is subjected to multiple deterioration processes, including gradual deterioration, external shock, fatal shock, and their interactions. After a short rapid increase period, the logarithm failure probability nearly increases linearly with time at

the first forty years. If the failure threshold is given as 0.01, the system reaches the threshold at about 37 years, which is the expected service life.

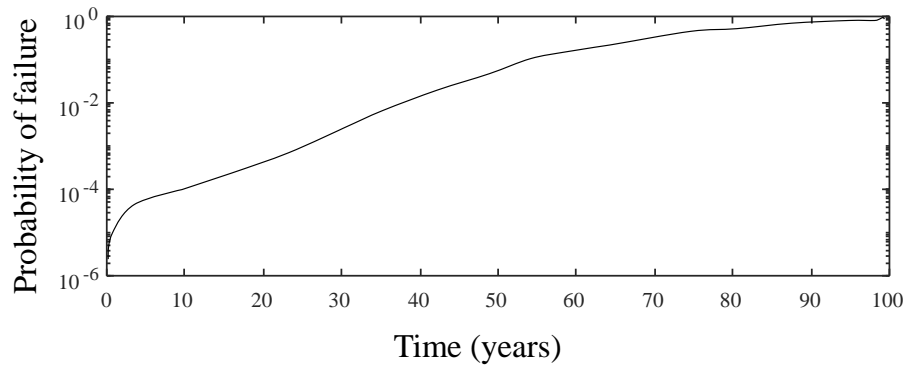


**Figure 7-3** Probability of failure considering gradual deterioration, external shock, fatal shock processes, and their interactions.

There are various uncertainties associated with different deterioration processes. Therefore, the effect of uncertainties from different deterioration processes on structural performance is investigated. Firstly, the effect of interaction among processes is explored. The investigated scenario with  $\gamma_d = 0.3$  is compared with the case with no dependence, as shown in Figure 7-4. The failure probability of the dependent case is consistently higher than the independent case. It is reasonable as deterioration among different processes is positively correlated and leads to more severe damage. For the investigated case, if the failure threshold is 0.01, the lifetime of the dependent case is 38 years while the independent case is 42 years, as described in Figure 7-4.

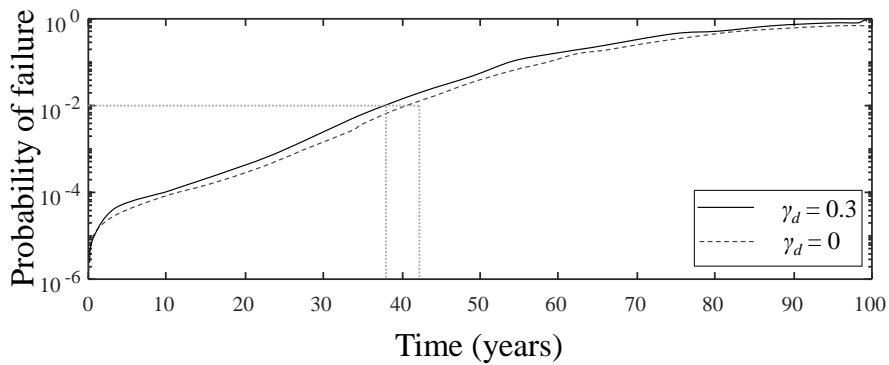


**Figure 7-4** Effect of dependence among different deterioration processes by considering with dependence ( $\gamma_d = 0.3$ ) and without dependence ( $\gamma_d = 0$ ).

In addition to interaction among processes, stochastic characteristics may have an impact on the system failure probability. Figure 7-5 shows the effect of gradual deterioration. By considering different rates of gradual deterioration (i.e., the expected cumulative gradual deterioration is  $0.1R_0$ ,  $0.3R_0$ , and  $0.5R_0$  within a 40-year time interval, respectively), the failure probability varies significantly. When the threshold of 0.01 is reached, the case with a mean gradual deterioration amount of  $0.5R_0$  has a service life of 13 years, while the case with  $0.1R_0$  fails at 57 years. In addition to the mean, the effect of the coefficient of variation (i.e., the ratio of standard deviation to the mean) with respect to gradual deterioration is investigated. Compared with the initial scenario as described in Figure 7-3 with a coefficient of variation of 0.4, changing the coefficient of variation also leads to a considerable difference in the failure probability, as described in Figure 7-6.

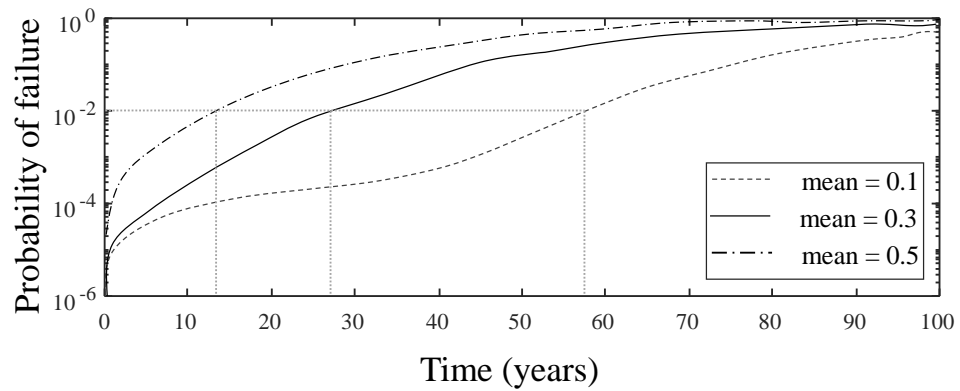


**Figure 7-5** Effect of gradual deterioration on the failure probability by considering different expectations of the cumulative gradual deterioration ( $0.1R_0$ ,  $0.3R_0$ , and  $0.5R_0$ ).

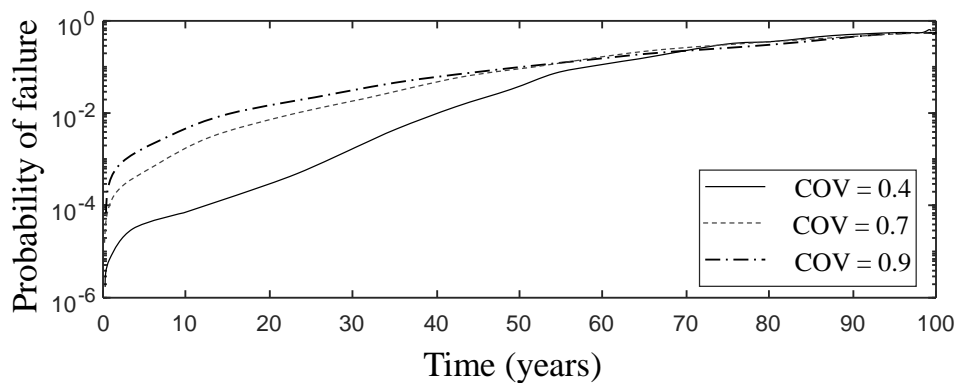


**Figure 7-6** Effect of gradual deterioration on the failure probability by considering different COV associated with gradual deterioration.

The effect of the external shock is also explored. Figure 7-7 shows the failure probability with respect to three different mean values associated with the external shock deterioration. It shows that a larger mean value, e.g., with the expected mean of  $0.1L_n$ , results in a higher failure probability. Figure 7-8 illustrates the impact of different COV associated with the external shock deterioration. It shows that changing the coefficient of variation of the external shock process does not have an apparent effect

on system reliability. Besides, the effect of the stochastic occurrence is investigated by considering different occurrence rates. Figure 7-9 shows the probability of failure with respect to different occurrence rates of external shock processes. The occurrence rate also refers to the occurrence rate  $\lambda_{ExS}$  associated with the Poisson process. It shows that the system subjected to a more frequent external shock process has a higher failure probability during the lifetime.

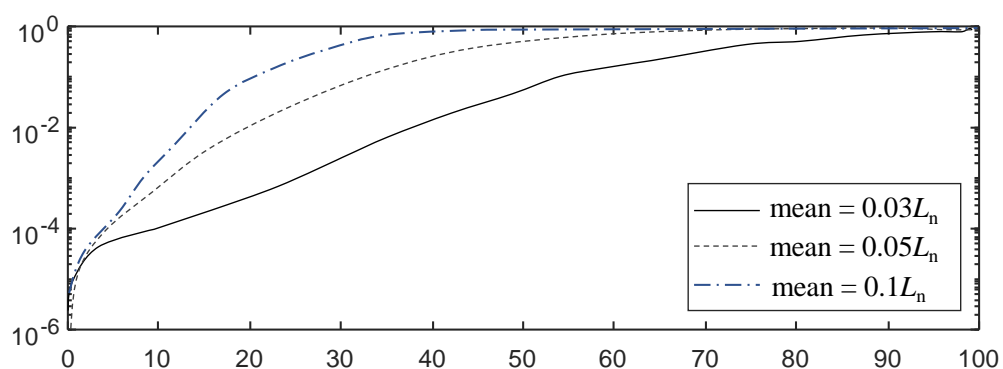


**Figure 7-7** Effect of the external shock deterioration process on the failure probability by considering different mean values of the deterioration amount.

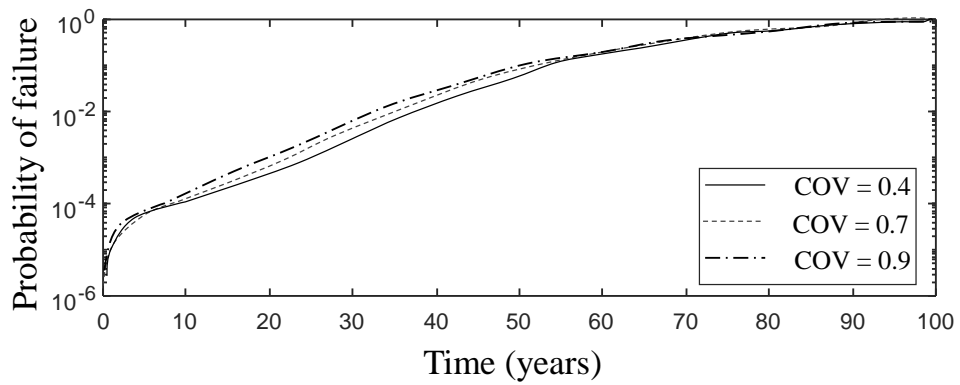


**Figure 7-8** Effect of the external shock deterioration process on the failure probability by considering different COV of the deterioration amount.

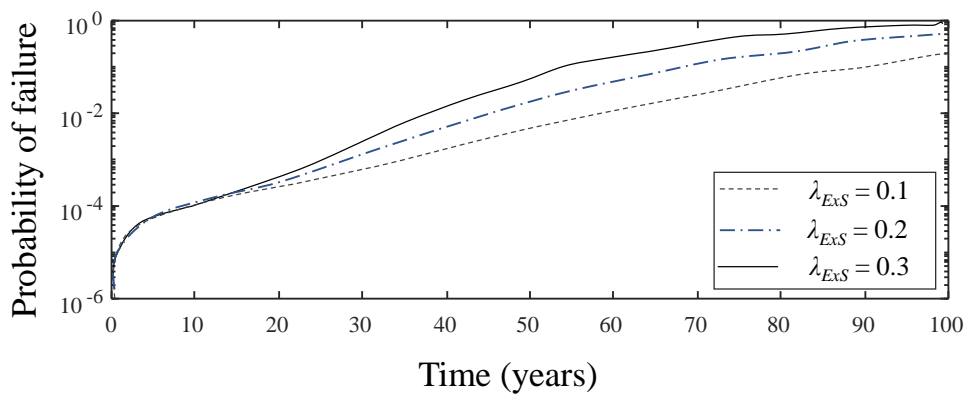


**Figure 7-9** Effect of external shock process on the failure probability by considering different occurrence rates.

In the proposed approach, the occurrence of extreme events is modeled by the fatal shock process and results in immediate failure of the system. For the investigated example, the impact of the fatal shock is reflected at the early stage (i.e., within the 50-year service life), as described in Figure 7-10. Compared with the scenario without fatal shock deterioration, the other two cases with fatal shock processes lead to a larger

failure probability. The failure probability of the system is increased with the occurrence rate of fatal shock deterioration. Thus, the impact of extreme events should be carefully considered during reliability analysis and life-cycle management.

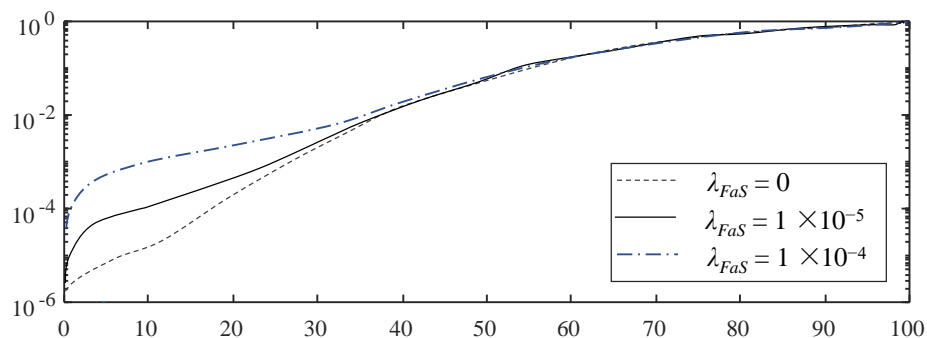


**Figure 7-10** Effect of fatal shock process on the failure probability by considering different occurrence rates.

## 7.5 Summary

This chapter provides a life-cycle analysis approach to assess the performance of civil infrastructure systems subjected to dependent multiple deterioration processes. The gradual deterioration process, external shock process, and fatal shock process are considered. The uncertainties associated with extreme events are considered within the life-cycle analysis framework. The system experiences an immediate failure after a fatal shock. A gamma process has been utilized to model the gradual deterioration of the system. The Poisson process is employed to model shock deterioration associated with the external shock process and the fatal shock process. The stochastic processes show considerable effectiveness in terms of deterioration modeling and dependence modeling. Interactions among processes are incorporated by modeling dependence

among gradual deterioration, external shock deterioration, and external load process. An illustrative example is provided to explore the effect of different deterioration processes on time-dependent reliability. Results show that the system reliability can be sensitive to the change in frequency and magnitude associated with different deterioration processes. It also indicates that interaction among processes can be significant, as neglecting the associated correlation may mis-specify the structural performance. For the investigated case, compared with the no correlation scenario, the positive correlation among deterioration processes results in a larger failure probability. The failure probability of the system can also be increased due to fatal shock. Therefore, the impact of fatal shock deterioration caused by extreme events should be carefully evaluated during reliability analysis and life-cycle analysis. In practice, the correlation among different deterioration processes relies on multiple factors. Further studies are needed to incorporate the quantification of the dependence relationship and to investigate the associated variability.

# CHAPTER 8 A COPULA-BASED LIFE-CYCLE MANAGEMENT FRAMEWORK OF DETERIORATING SYSTEMS

## 8.1 Introduction

Civil infrastructure is vulnerable to hazards such as hurricanes, earthquakes, and continuous deterioration during the lifetime. Hazards may result in the sudden and gradual reduction of structural capacity, and various maintenance actions are required to maintain the safety and functionality of the infrastructure. The resulting maintenance cost increases the life-cycle cost and directly affects the decision-making process. Therefore, the assessment of the life-cycle maintenance cost is essential. There is a need to explore the effect of these actions on the life-cycle performance of the system.

Despite considerable efforts on deterioration modeling and cost assessment, these studies commonly assume that the maintenance interval and cost are independent. The independence assumption has been widely used to simplify the analytical formulation associated with the renewal theory (Cheng *et al.* 2012; Liu *et al.* 2020; Yang and Frangopol 2019a). However, the assumption is less likely to be realistic, as increasing the maintenance cost (by conducting more frequent maintenance actions) commonly extends the maintenance interval. Furthermore, neglecting the dependence and the associated uncertainties may result in an inappropriate estimation of the accumulative cost, thus misleading decision-makers during the life-cycle management. Pandey and Van Der Weide (2017) also indicated that dependence between

maintenance cost and renewal cycle cannot be ignored, especially when preventive maintenance is considered. To the best of the authors' knowledge, the dependent maintenance interval and cost have not been considered in the life-cycle cost analysis.

This chapter presents a copula-based life-cycle analysis framework for deteriorating civil infrastructure systems. Multiple deterioration processes and their interaction are considered. The developed copula-based approach allows various complex dependence structures between the maintenance interval and the cost in a renewal process. A copula-based multivariate renewal model is proposed to assess the life-cycle maintenance cost analytically and numerically. In addition to the expected cost, statistical moments (standard deviation, skewness, and kurtosis) are calculated to quantify uncertainties from higher-order moments. Results show that the dependence structure and uncertainties can have a large impact on the life-cycle cost. Decisions can be altered by considering statistical moments of the cost. An analytical model, the Farlie-Gumbel-Morgenstern (FGM) copula, is provided to derive statistical moments of the life-cycle maintenance cost. Two illustrative examples are provided to highlight the importance of statistical moments and copula within the life-cycle analysis and decision-making processes.

## **8.2 A copula-based life-cycle analysis framework**

This section proposes a copula-based life-cycle analysis framework based on renewal processes. By characterizing deterioration of the system and performing maintenance actions, the life-cycle maintenance cost can be assessed using the proposed approach.

Dependence between maintenance interval and cost is incorporated by using the multivariate copula model. Based on the deterioration model and reliability analysis described in Sections 7.2 and 7.3, the maintenance policy and life-cycle maintenance cost are proposed and assessed.

### **8.2.1 Maintenance policy**

The maintenance policy relies on appropriate modeling of structural deterioration and performance evaluation. In terms of the life-cycle cost analysis, most of the existing studies focus on one type of deterioration (either under gradual deterioration or shocks) and ignore their combined effects. For instance, Cheng *et al.* (2012) presented an analytical framework to derive the probability distribution of maintenance cost of ageing engineering systems subjected to gradual degradation by using the gamma process. Yang and Frangopol (2019a) assessed the life-cycle maintenance cost subjected to independent shock and deterioration processes using renewal models. A few recent studies take correlated deterioration effects into account. For instance, Jia and Gardoni (2019) introduced state-dependent models to the life-cycle cost analysis subjected to earthquake and corrosion damage. Liu *et al.* (2020) investigated dependent degradation processes using copulas and the resulting impact on the life-cycle cost. In this chapter, three deterioration processes are considered, including gradual deterioration, external shock, and fatal shock. The detailed modeling of multiple deterioration processes and structural reliability have been modeled in CHAPTER 7. Interactions between deterioration processes are considered, following the model presented in Section 7.3.3.

As multiple deterioration processes reduce the performance (e.g., reliability) of a system, maintenance actions are required to minimize potential risks and damage. Herein, a reliability-based maintenance policy is proposed, consisting of preventive and essential maintenance interventions. The probability of failure is taken as a performance indicator to determine the maintenance policy. Herein, preventive maintenance gives minimal repairs, while essential maintenance provides major repairs or replacement to enhance the system reliability to the initial level. Preventive maintenance is conducted when the probability of the system failing exceeds  $P_{PM}$ . After a preventive maintenance event, the rate of gradual deterioration is reduced. Essential maintenance is performed when the probability of failure exceeds a threshold  $P_{EM}$  or a fatal-induced failure occurs. Following the essential maintenance, the structural resistance is enhanced and restored to the initial level  $C_0$ . In other words, the system is resumed and a renewal process is formed (Cheng *et al.* 2012; Liu *et al.* 2020). The time-dependent limit state function becomes

$$LS_n = C_0 - \omega \cdot \sum_{i=1}^n \Delta C_{t_i}^{Gra} - \sum_{i=1}^{n-1} \Delta C_{t_i}^{ExS} - D_{t_n} \quad (8-1)$$

in which  $\omega$  ( $\omega < 1$ ) is the changing rate in terms of the gradual deterioration after a preventive maintenance action. Figure 8-1 provides an illustrative diagram to describe the impact of preventive and essential maintenance actions on the probability of failure of the system.

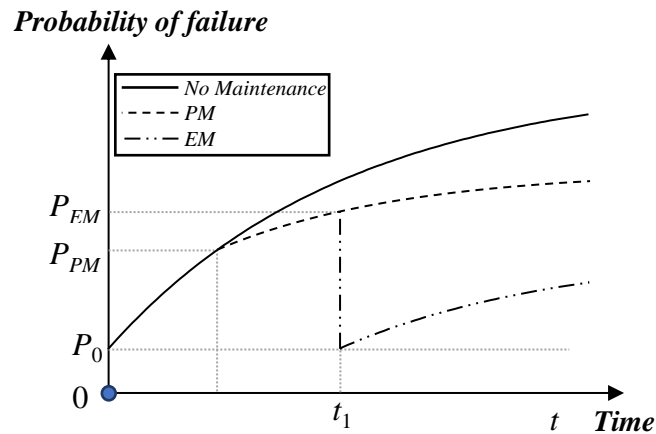


**Figure 8-1** An illustrative diagram of reliability-based preventive maintenance (PM) and essential maintenance (EM) actions.

### 8.2.2 Life-cycle maintenance cost

The assessment of life-cycle maintenance cost can be based on a stochastic renewal process (Li *et al.* 2020b; Yang and Frangopol 2019a). Sánchez-Silva *et al.* (2016) reviewed the renewal-based models for shock-based degradation, periodic-replacement maintenance strategy, and the quantification of maintenance cost based on renewal theory. Sánchez-Silva and Klutke (2016) also discussed the application of renewal process for the reliability and life-cycle analysis of deteriorating engineering systems. As a system is resumed to its initial level (i.e.,  $R_0$ ) after each essential maintenance, a stochastic renewal process is formed. The maintenance interval is a renewal cycle  $W$ , which can be defined as the time interval from the system operation to the essential maintenance. The maintenance cost  $Z$  within a renewal cycle is the total cost incurred by preventive and essential maintenance. The maintenance cost and renewal cycle can be correlated (Pandey and Van Der Weide 2017). For instance, increasing the

maintenance cost by conducting more frequent preventive maintenance actions commonly extends the maintenance interval (i.e., a longer renewal cycle).

To incorporate the correlation between the maintenance interval and cost, statistical modeling of the joint probability distribution is essential. A conventional approach of multivariate modeling relies on an empirical multivariate joint distribution or a joint normal distribution (Ataei and Padgett 2013; Lucas and Soares 2015), but the approach is limited to a certain correlation relationship. Herein, a copula-based method is proposed. As an advanced mathematical tool, the copula model offers sufficient efficiency and flexibility in multivariate dependence modeling by separately considering the joint distribution and marginal distributions. Due to this advantage, copulas have been increasingly applied in deterioration processes and reliability analysis. For instance, Goda (2010) employed copulas to model dependence between peak and permanent displacement seismic demand. Li *et al.* (2020c) assessed the vulnerability of coastal bridges subjected to hurricane hazards by modeling dependent peak water level and wave height based on historical records.

In addition to uncertainties resulting from the dependence model, uncertainties associated with statistical moments (mean, standard deviation, skewness, and kurtosis) of the life-cycle cost have not been thoroughly explored. Although the minimum expected cost has been utilized as a standard decision criterion, the impact of the other statistical moments on the life-cycle cost and decision-making process has been rarely discussed. Pandey and Van Der Weide (2017) indicated that the variance of the life-cycle damage cost can be significant to indicate the variability. Li *et al.* (2020b) stated the importance of higher-order moments (skewness and kurtosis) of the repair cost

during system lifetime, as skewness and kurtosis imply potential tail risks. Hence, it is necessary to assess the statistical moments of the life-cycle maintenance cost. This section presents a life-cycle analysis framework incorporating correlated maintenance interval and cost using copula models.

During the service life  $(0, t_{\text{int}}]$  of a system, there can be a series of renewal cycles  $\{W_1, W_2, \dots, W_k\}$  associated with  $k$  number of maintenance events. The chronological time in terms of the  $k$ th renewal can be written as  $T_k$ , with  $T_k = W_1 + W_2 + \dots + W_k$ . The incurred maintenance costs can be denoted as  $\{Z_1, Z_2, \dots, Z_k\}$ .  $W_k$  and  $Z_k$  ( $k = 1, 2, \dots$ ) are non-negative random variables. The life-cycle maintenance cost incurred from maintenance actions can be defined as  $LCC(t_{\text{int}})$ , which is a compound renewal process consisting of a set of random vectors  $(Z_1, W_1), (Z_2, W_2), \dots, (Z_k, W_k)$ . The key component in this model is that the renewal cycle  $W_k$  and maintenance cost  $Z_k$  are dependent, while the joint probability distributions of  $(Z_i, W_i)$  are independent of  $(Z_k, W_k)$  for any  $i \neq k$ . Given these parameters, the life-cycle maintenance cost  $LCC(t_{\text{int}})$  is the accumulative cost of all the renewal cycles and gives

$$LCC(t_{\text{int}}) = \sum_{k=1}^{N(t_{\text{int}})} Z_k e^{-rT_k} \quad (8-2)$$

in which  $N(t_{\text{int}})$  is the total number of maintenance events and a discount rate  $r$  is used to discount the future expense to the present.

The dependence structure between the renewal cycle  $W_k$  and maintenance cost  $Z_k$  can be described by a joint CDF  $F_{Z,W}(z, t)$ . Although the joint CDF  $F_{Z,W}(z, t)$  can be conditioned on an empirical model from historical maintenance records, the dependence is only limited to a certain correlation relationship. In the life-cycle cost

analysis, a flexible multivariate analysis tool is needed. In this section, a copula-based approach is proposed to establish the dependency structure between  $W_k$  and  $Z_k$ . The advantage of using copula is that the simulation of multivariate probability distributions is separate from the univariate random variables, thus providing sufficient effectiveness during statistical modeling (Joe 2014; Zhang *et al.* 2018b).

To model the dependence between the renewal cycle and maintenance cost, the bivariate copula is focused. Based on the copula theory, the joint CDF of the bivariate random vector  $(Z_k, W_k)$  can be written as

$$F_{Z,W}(z,t) = C_{\theta}(F_Z(z), F_W(t)) \quad (8-3)$$

in which  $F_Z(z)$  and  $F_W(t)$  are CDFs of maintenance cost and renewal cycle, respectively.  $C_{\theta}$  is the CDF of a copula function with a dependence parameter  $\theta$ . The PDF of the random vector  $f_{Z,W}(z, t)$  is given as

$$f_{Z,W}(z,t) = c_{\theta}(F_Z(z), F_W(t)) f_Z(z) f_W(t) \quad (8-4)$$

where  $c_{\theta}$  describes the PDF of a copula;  $f_Z$  and  $f_W$  are the univariate PDFs of maintenance cost and renewal cycle, respectively.

As described in CHAPTER 4, there is a wide range of copula functions indicating different dependence structures between variables. Herein, the dependence structure between the renewal cycle and maintenance cost can be measured by the correlation coefficient: Pearson's correlation coefficient, Kendall's tau, and Spearman's rho. Although Pearson's correlation coefficient may be the most popular

one in previous studies, it is limited to a linear relationship (Joe 2014). Pearson's correlation coefficient for correlated random vector  $(Z_k, W_k)$  can be derived as

$$\gamma = \frac{\int (z - \bar{z})(w - \bar{w}) f_{Z,W}(z, t) dz dt}{\sqrt{\int (z - \bar{z})^2 f_Z(z) dz \int (w - \bar{w})^2 f_W(t) dt}} \quad (8-5)$$

Due to the linear limitation, Kendall's tau  $\tau$  and Spearman's rho  $\rho$  can be described using copulas (Nelsen 2006)

$$\tau(\theta) = 4 \int_{[0,1]^2} C_\theta(u, v) dC_\theta(u, v) - 1 \quad (8-6)$$

$$\rho(\theta) = 12 \int_{[0,1]^2} uv dC_\theta(u, v) - 3 \quad (8-7)$$

Both these two coefficients are developed from the concept of concordance and give a similar interpretation of association in most cases (Nelsen 2006). Given the correlation coefficient, the dependence parameter  $\theta$  associated with a copula can be estimated. For instance, the maximum pseudo-likelihood method can be applied to compute the dependence parameter by maximizing the pseudo log-likelihood function (Genest *et al.* 1995)

$$L_{pl}(\theta) = \sum_{i=1}^n \log \left[ c_\theta \left( \frac{R_{Z_i}}{n+1}, \frac{R_{W_i}}{n+1} \right) \right] \quad (8-8)$$

where  $R_{Z_i}$  and  $R_{W_i}$  are ranks of the maintenance cost and renewal cycle, respectively.

To determine the copula function, there are generally two methods in terms of the cases with and without data, as shown in Figure 8-2. When there are detailed

historical records of maintenance interval and cost, the selection of the copula model can be data-based (Jane *et al.* 2018; Li *et al.* 2020c). The data-based method requires two main parts: quantification of marginal distributions (i.e.,  $F_Z(z)$  and  $F_W(t)$ ) and selection of the most fitted copula by using the goodness-of-fit test. While there are limited data available, the dependence structure between variables is commonly determined according to correlation coefficients (Hong *et al.* 2014; Wang *et al.* 2020). Detailed descriptions of the two methods are shown in the section of illustrative examples. As practical data can be incorporated, the proposed copula approach can be significant for data-based decision-making during the life-cycle management of civil infrastructure.

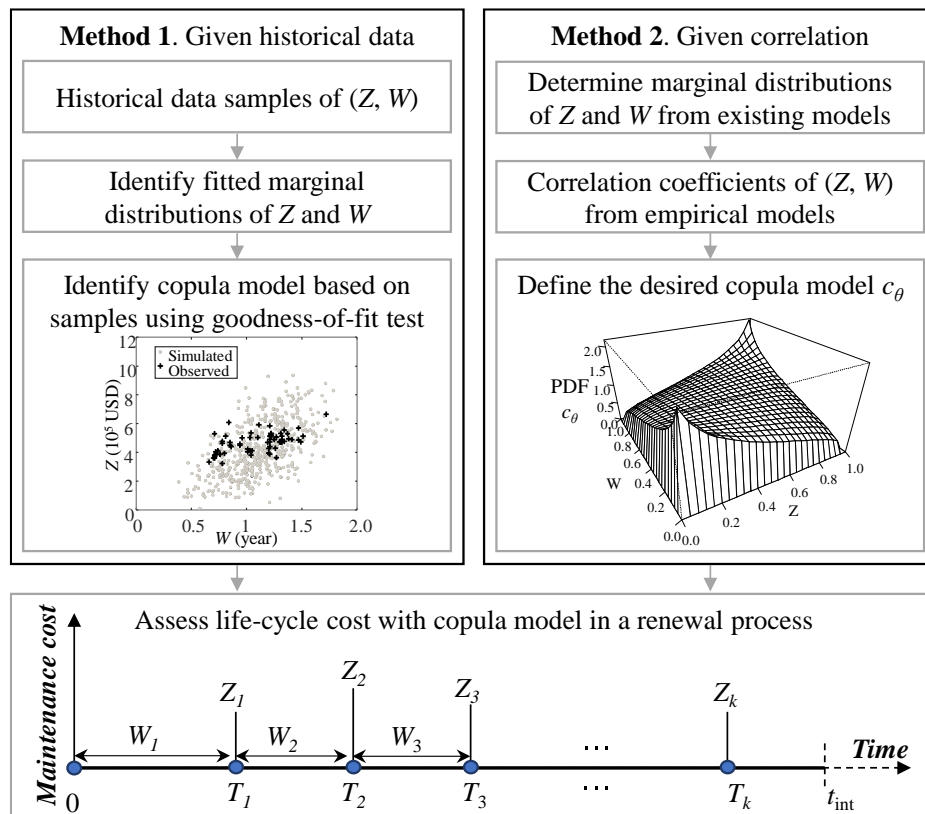


**Figure 8-2** Assessment of life-cycle maintenance cost using the proposed copula-based multivariate renewal model.

After the selection of the copula model and estimation of dependence parameter, the life-cycle maintenance cost incorporating dependent maintenance cost and renewal cycle can be assessed. Due to complicated expressions of copulas, statistical modeling generally relies on numerical simulations. Simulations are flexible with various copulas but can be time-consuming and expensive. The algorithm to assess the life-cycle maintenance cost using a Monte Carlo simulation is summarized as follows:

*Simulation algorithm*

- (1) Inputs:  $t_{\text{int}}$ ,  $r$ , marginal PDFs and CDFs of  $Z$  and  $W$  (e.g.,  $F_Z(z)$ ,  $f_Z(z)$ ,  $F_W(t)$ ,  $f_W(t)$ );
- (2) Establish dependence structure of the copula function  $c_\theta$  and generate dependent random vectors  $(Z_k, W_k)$ ;
- (3) Simulate a stochastic renewal process  $\{N(t_{\text{int}})\}$  by using  $\{W_1, W_2, \dots, W_k\}$  generated from Step (2);
- (4) Compute  $\{T_1, T_2, \dots, T_k\}$  of the process based on Step (3);
- (5) Compute  $LCC(t_{\text{int}})$  based on Eq. (8-2) by using  $\{T_1, T_2, \dots, T_k\}$  of Step (4), the associated  $\{Z_1, Z_2, \dots, Z_k\}$  generated from Step (2), and the number of events  $N(t_{\text{int}})$  from Step (3);
- (6) Repeat Step (2) to (5) for  $N_{MC}$  times based on Monte Carlo simulation; and
- (7) Outputs: the mean  $\mu_{LCC}(t_{\text{int}})$ , standard deviation, skewness, and kurtosis of  $LCC(t_{\text{int}})$  based on  $N_{MC}$  samples.

### 8.3 Analytical case: life-cycle analysis with FGM copula

In addition to numerical modeling, an analytical case is developed. In this section, the closed-form expressions of statistical moments of the life-cycle maintenance cost considering an FGM copula are derived. Derivations are based on the renewal theory and Laplace Transform. Due to its analytical characteristics, the FGM copula was employed by Eryilmaz (2016) to model dependent degradation rates for reliability

analysis of systems. The FGM copula is the first-order Taylor approximation of the Frank copula and belongs to neither the elliptical family nor the Archimedean family (Eryilmaz 2016).

The FGM copula demonstrates a weak correlation, including both positive and negative. The PDF of the FGM copula  $c_\theta^{FGM}$  is given as

$$c_\theta^{FGM}(u, v) = 1 + \theta(1 - 2u)(1 - 2v) \quad (8-9)$$

where the dependence parameter  $\theta$  is between  $[-1, 1]$  and  $(u, v) \in [0, 1] \times [0, 1]$ .

The joint probability of  $(Z, W)$  can be expressed as follows using the copula

$$\begin{aligned} f_{Z,W}(z, t) &= c_\theta^{FGM}(F_Z(z), F_W(t))f_Z(z)f_W(t) \\ &= [1 + \theta(1 - 2F_Z(z))(1 - 2F_W(t))]f_Z(z)f_W(t) \end{aligned} \quad (8-10)$$

### 8.3.1 Expectation and variance of life-cycle maintenance cost

The expected life-cycle maintenance cost under a renewal process can be formulated by conditioning on the first arrival time  $y$

$$\begin{aligned} \mu_{LCC}(t_{\text{int}}) &= E[LCC(t_{\text{int}})] \\ &= E\left[E[e^{-ry}Z_1 + e^{-ry}LCC(t_{\text{int}} - y) \mid W_1 = y]\right] \\ &= \int_0^{t_{\text{int}}} e^{-ry} E[Z \mid W = y] f_W(y) dy \\ &\quad + \int_0^{t_{\text{int}}} e^{-ry} E[LCC(t_{\text{int}} - y)] f_W(y) dy \end{aligned} \quad (8-11)$$

in which the first arrival time is equal to the first inter-arrival time  $T_1 = W_1$ . The conditional expectation of maintenance cost  $E[Z|W = y]$  can be expressed by the conditional probability

$$E[Z|W = y] = \int_0^{\infty} z f_{Z|W=y}(z) dz \quad (8-12)$$

where the conditional density function of maintenance cost  $f_{Z|W=y}$  is associated with the bivariate joint probability  $f_{Z,W}(z, t)$ . Substituting the FGM copula according to Eq. (8-9), the conditional density function gives

$$f_{Z|W=y}(z) = \frac{f_{Z,W}(z, t)}{f_W(t)} = [1 + \theta(1 - 2F_Z(z))(1 - 2F_W(t))] f_Z(z) \quad (8-13)$$

Substituting Eq. (8-13) into Eq. (8-12), the conditional expectation of maintenance cost gives

$$\begin{aligned} E[Z|W = y] &= \int_0^{\infty} z [1 + \theta(1 - 2F_Z(z))(1 - 2F_W(y))] f_Z(z) dx \\ &= E[Z](1 - \theta(1 - 2F_W(y))) + \theta(1 - 2F_W(y))E[\Lambda] \end{aligned} \quad (8-14)$$

in which  $E[\Lambda]$  is defined to combine the identical items

$$E[\Lambda] = \int_0^{\infty} z(2 - 2F_Z(z)) f_Z(z) dz = \int_0^{\infty} (1 - F_Z(z))^2 dz \quad (8-15)$$

A Poisson process is the most common renewal process. It has exponentially distributed inter-arrival times. It gives that the inter-arrival time follows  $W \sim \text{EXP}(\lambda)$  with an occurrence rate  $\lambda$ . Hence, the PDF of the inter-arrival time  $f_W(t)$  gives

$$f_W(t) = \lambda \exp(-\lambda t) \quad (8-16)$$

Herein, let  $\omega(t; \lambda)$  represent the PDF  $f_W(t)$  of  $W$  (Barges *et al.* 2011; Ross 2014).

Consequently, the expected life-cycle maintenance cost can be rearranged as

$$\begin{aligned} \mu_{LCC}(t_{\text{int}}) &= E[Z] \int_0^{t_{\text{int}}} \frac{\lambda}{\lambda+r} \omega(y; \lambda+r) dy \\ &+ \theta(E[\Lambda] - E[Z]) \int_0^{t_{\text{int}}} \frac{2\lambda}{2\lambda+r} \omega(y; 2\lambda+r) dy \\ &- \theta(E[\Lambda] - E[Z]) \int_0^{t_{\text{int}}} \frac{\lambda}{\lambda+r} \omega(y; \lambda+r) dy \\ &+ \int_0^{t_{\text{int}}} \frac{\lambda}{\lambda+r} \omega(y; \lambda+r) \mu_{LCC}(t_{\text{int}} - y) dy \end{aligned} \quad (8-17)$$

Taking the Laplace transform of Eq. (8-17) on both sides, the Laplace transform of the expected life-cycle maintenance cost  $\tilde{\mu}_{LCC}(\tau)$  can be written as

$$\begin{aligned} \tilde{\mu}_{LCC}(\tau) &= E[Z] \frac{\lambda}{\lambda+r} \frac{\tilde{\omega}(\tau; \lambda+r)}{\tau} \\ &+ \theta(E[\Lambda] - E[Z]) \frac{2\lambda}{2\lambda+r} \frac{\tilde{\omega}(\tau; 2\lambda+r)}{\tau} \\ &- \theta(E[\Lambda] - E[Z]) \frac{\lambda}{\lambda+r} \frac{\tilde{\omega}(\tau; \lambda+r)}{\tau} \\ &+ \frac{\lambda}{\lambda+r} \tilde{\omega}(\tau; \lambda+r) \tilde{\mu}_{LCC}(\tau) \end{aligned} \quad (8-18)$$

where the Laplace transform of the PDF of inter-arrival time  $\tilde{\omega}_{LCC}(\tau; \lambda)$  can be computed as

$$\tilde{\omega}(\tau; \lambda) = \frac{\lambda}{\lambda + \tau} \quad (8-19)$$

Substituting Eq. (8-19) into Eq. (8-18), the Laplace transform of expected life-cycle maintenance cost can be rearranged as

$$\tilde{\mu}_{LCC}(\tau) = \frac{E[Z]\lambda}{\tau(\tau+r)} + \frac{\theta\lambda(E[\Lambda]-E[Z])}{\tau(2\lambda+r+\tau)} \quad (8-20)$$

By taking inverse Laplace transform of Eq. (8-20) on both sides, the expected life-cycle maintenance cost under dependency is obtained

$$\mu_{LCC}(t_{\text{int}}) = \frac{E[Z]\lambda}{r}(1-e^{-rt_{\text{int}}}) + \frac{\theta\lambda(E[\Lambda]-E[Z])}{2\lambda+r}(1-e^{-(2\lambda+r)t_{\text{int}}}) \quad (8-21)$$

Following the similar procedure of the first moment, the second moment of life-cycle maintenance cost can be assessed by conditioning on the first arrival time  $y$

$$\begin{aligned} \mu_{LCC}^2(t_{\text{int}}) &= E[LCC^2(t_{\text{int}})] = E\left[E[(e^{-ry}Z_1 + e^{-ry}LCC(t_{\text{int}}-y))^2 | W_1 = y]\right] \\ &= \int_0^{t_{\text{int}}} e^{-2ry} E[Z^2 | W = y] f_W(y) dy \\ &\quad + \int_0^{t_{\text{int}}} e^{-2ry} \mu_{LCC}^2(t_{\text{int}}-y) f_W(y) dy \\ &\quad + 2 \int_0^{t_{\text{int}}} e^{-2ry} E[Z | W = y] \mu_{LCC}(t_{\text{int}}-y) f_W(y) dy \end{aligned} \quad (8-22)$$

Following similar procedures in terms of the Laplace transform approach, the second moment of the life-cycle maintenance cost can be derived accordingly. For instance, the conditional second moment of maintenance cost can be computed and rearranged as

$$E\left[Z^2|W=y\right]=\int_0^{\infty} z^2 f_{Z|W=y}(z) dz = E[Z^2] + \theta\left(E[\Lambda^2]-E[Z^2]\right)(1-2F_W(y)) \quad (8-23)$$

where

$$E[\Lambda^2]=\int_0^{\infty} z^2(2-2F_Z(z))f_Z(z) dz = \int_0^{\infty} 2z(1-F_Z(z))^2 dz \quad (8-24)$$

The PDF of the renewal cycle can be denoted as  $\omega(t, \lambda)$ . Consequently, the second moment of life-cycle maintenance cost can be computed as

$$\begin{aligned} \mu_{LCC}^2(t_{\text{int}}) &= E[Z^2] \int_0^{t_{\text{int}}} \frac{\lambda}{\lambda+2r} \omega(y; \lambda+2r) dy + \theta\left(E[\Lambda^2]-E[Z^2]\right) \\ &\int_0^{t_{\text{int}}} \left[ \frac{2\lambda}{2\lambda+2r} \omega(y; 2\lambda+2r) - \frac{\lambda}{\lambda+2r} \omega(y; \lambda+2r) \right] dy \\ &+ 2E[Z] \int_0^{t_{\text{int}}} \frac{\lambda}{\lambda+2r} \omega(y; \lambda+2r) \mu_{LCC}(t_{\text{int}}-y) dy \\ &+ 2\theta\left(E[\Lambda]-E[Z]\right) \\ &\int_0^{t_{\text{int}}} \left[ \frac{2\lambda}{2\lambda+2r} \omega(y; 2\lambda+r) - \frac{\lambda}{\lambda+2r} \omega(y; \lambda+2r) \right] \mu_{LCC}(t_{\text{int}}-y) dy \\ &+ \int_0^{t_{\text{int}}} \frac{\lambda}{\lambda+2r} \omega(y; \lambda+2r) \mu_{LTL}^2(t_{\text{int}}-y) dy \end{aligned} \quad (8-25)$$

By taking Laplace transform of Eq. (8-25) on both sides and performing the associated inversion, the second moment of life-cycle cost under dependency can be derived as

$$\begin{aligned}
\mu_{LCC}^2(t_{\text{int}}) &= \frac{\lambda E[Z^2]}{2r} (1 - e^{-2rt_{\text{int}}}) + 2\lambda^2 E[Z]^2 \left( \frac{1 - 2e^{-rt_{\text{int}}} + e^{-2rt_{\text{int}}}}{2r^2} \right) \\
&+ \theta\lambda (E[\Lambda^2] - E[L^2]) \left( \frac{1 - e^{-(2\lambda+2r)t_{\text{int}}}}{2\lambda+2r} \right) \\
&+ 2\theta\lambda^2 E[Z] (E[\Lambda] - E[Z]) \\
&\left( \frac{e^{-(2\lambda+r)t_{\text{int}}}}{(2\lambda-r)(2\lambda+r)} - \frac{e^{-2rt_{\text{int}}}}{2r(2\lambda-r)} + \frac{1}{2r(2\lambda+r)} \right) \\
&+ 2\theta\lambda^2 E[Z] (E[\Lambda] - E[Z]) \\
&\left( \frac{e^{-(2\lambda+2r)t_{\text{int}}}}{2(2\lambda+r)(\lambda+r)} + \frac{1}{2r(\lambda+r)} - \frac{e^{-rt_{\text{int}}}}{r(2\lambda+r)} \right) \\
&+ 2\theta^2 \lambda^2 (E[\Lambda] - E[Z])^2 \\
&\left( \frac{1}{2(2\lambda+r)(\lambda+r)} - \frac{e^{-(2\lambda+r)t_{\text{int}}}}{r(2\lambda+r)} + \frac{e^{-(2\lambda+2r)t_{\text{int}}}}{2r(2\lambda+r)} \right)
\end{aligned} \tag{8-26}$$

Consequently, the variance can be evaluated from the first two moments as shown in Eqs. (8-25) and (8-26)

$$\sigma_{LCC}^2(t_{\text{int}}) = \text{Var}[LCC(t_{\text{int}})] = \mu_{LCC}^2(t_{\text{int}}) - (\mu_{LCC}(t_{\text{int}}))^2 \tag{8-27}$$

When the dependence parameter is zero, the maintenance cost and renewal cycle become independent. The associated expectation and variance of life-cycle cost give identical outcomes as described in previous studies (Li *et al.* 2020; Pandey and Van Der Weide 2017), as shown in Eqs. (8-28) and (8-29)

$$\mu_{LCC}(t_{\text{int}}) = \frac{E[Z]\lambda}{r} (1 - e^{-rt_{\text{int}}}) \tag{8-28}$$

$$\sigma_{LCC}^2(t_{\text{int}}) = \frac{\lambda E[Z^2]}{2r} (1 - e^{-2rt_{\text{int}}}) \tag{8-29}$$

### 8.3.2 Higher-order moments of life-cycle maintenance cost

By summarizing the computation process of the first two moments, the  $m$ th order moment can be evaluated using the Laplace transform approach accordingly. The  $m$ th order moment of life-cycle maintenance cost can be derived using the univariate distribution of inter-arrival time

$$\begin{aligned}\mu_{LCC}^m(t_{\text{int}}) &= E[LCC^m(t_{\text{int}})] = \int_0^{t_{\text{int}}} e^{-mry} E[Z^m | W = y] f_W(y) dy \\ &+ \int_0^{t_{\text{int}}} e^{-mry} E[LCC^m(t_{\text{int}} - y)] f_W(y) dy \\ &+ \sum_{i=1}^{m-1} \binom{m}{i} \int_0^{t_{\text{int}}} e^{-mry} E[Z^i | W = y] E[LCC^{m-i}(t_{\text{int}} - y)] f_W(y) dy\end{aligned}\quad (8-30)$$

where  $m \geq 1$  and  $1 \leq i < m$ .

Similar to the first two moments, the  $m$ th order conditional expectation of maintenance cost can be expressed as

$$E[Z^m | W = y] = \int_0^{\infty} z^m f_{Z|W=y}(z) dz = \int_0^{\infty} z^m c_{\theta}^{FGM}(F_Z(z), F_W(t)) f_Z(z) dz \quad (8-31)$$

Substituting Eq. (8-31) into Eq. (8-30), the  $m$ th order moment of life-cycle maintenance cost gives

$$\begin{aligned}\mu_{LCC}^m(t_{\text{int}}) &= \int_0^{t_{\text{int}}} \int_0^{\infty} e^{-mry} z^m f_{Z,W}(z, y) dz dy + \int_0^{t_{\text{int}}} e^{-mry} \mu_{LCC}^m(t_{\text{int}} - y) f_W(y) dy \\ &+ \sum_{i=1}^{m-1} \binom{m}{i} \int_0^{t_{\text{int}}} \int_0^{\infty} e^{-mry} z^i f_{Z,W}(z, y) \mu_{LCC}^{m-i}(t_{\text{int}} - y) dz dy\end{aligned}\quad (8-32)$$

Considering the exponential distribution associated with the inter-arrival time  $f_W(t)$ , the  $m$ th order moment becomes

$$\begin{aligned}
\mu_{LCC}^m(t_{\text{int}}) &= \lambda \int_0^{t_{\text{int}}} \int_0^{\infty} e^{-(\lambda+mr)y} z^m f_Z(z) c_{\theta}(F_Z(z), F_W(y)) dz dy \\
&+ \lambda \int_0^{t_{\text{int}}} e^{-(\lambda+mr)y} \mu_{LCC}^m(t_{\text{int}} - y) dy \\
&+ \lambda \sum_{i=1}^{m-1} \binom{m}{i} \int_0^{t_{\text{int}}} e^{-(\lambda+mr)y} z^{-(m-i)} c_{\theta}(F_Z(z), F_W(y)) \\
&f_Z(z) \mu_{LCC}^{m-i}(t_{\text{int}} - y) dz dy
\end{aligned} \tag{8-33}$$

Consequently, the moments can be derived by using the Laplace transform approach. The analytical case can be more effective than the complicated numerical simulation. Based on the recursive moments (i.e., Eq. (8-33)) using the FGM copula, decision-makers can estimate the life-cycle cost under dependency effectively.

## 8.4 Illustrative examples

There are two illustrative examples provided to apply the proposed copula-based life-cycle analysis framework. The first example incorporates maintenance data records to assess the dependence between maintenance cost and interval. The second one investigates the impact of different dependence structures on the life-cycle maintenance cost by using different copula models.

### 8.4.1 Data-based decision making and higher-order moments

In previous studies, the minimum expected life-cycle cost has been broadly utilized as a standard criterion in the decision-making process. However, decisions exclusively

based on the expected cost may not be optimal, as uncertainties associated with the other three statistical moments have been ignored (Goda 2010). This illustrative example considers statistical moments of the life-cycle maintenance cost in the decision-making process. Based on the proposed copula approach and historical records, a data-based decision-making process is provided to determine an appropriate maintenance policy for a reinforced concrete bridge.

There are two maintenance policies considered for the bridge, as shown in Figure 8-3. Maintenance Policy 1 is provided based on the historical records of 50 similar reinforced concrete bridges from the US National Bridge Inventory (NBI) database (2020). The maintenance interval of Policy 1 has a mean of 16.14 years and a mean maintenance cost per unit deck area of 4298.02 USD/m<sup>2</sup>. As the sizes of bridges vary significantly, the maintenance cost is conditioned on the unit deck area. In contrast, Maintenance Policy 2 is proposed, in which the maintenance interval is extended by increasing the maintenance cost. Policy 2 has a mean maintenance interval of 24.10 years and a mean maintenance cost per unit deck area of 6390.55 USD/m<sup>2</sup>. Data associated with Maintenance Policy 2 are provided for illustrative purposes. Between the two alternatives, decisions should be made to select an appropriate policy for the bridge by considering statistical moments of the life-cycle maintenance cost.

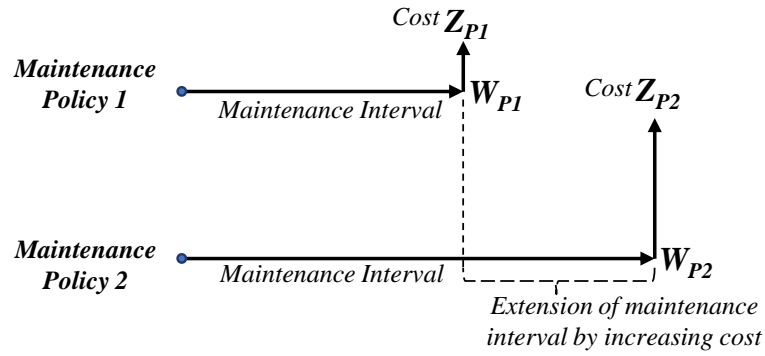


**Figure 8-3** Two maintenance policies with different maintenance interval  $W$  and maintenance cost  $Z$ .

For maintenance policy 1, the dependence structure between the maintenance interval  $W$  and maintenance cost  $Z$  can be examined by using the presented Method 1 as described in Figure 8-2. Firstly, marginal distributions of  $W$  and  $Z$  should be fitted. It is identified that there are many distribution alternatives due to limited data records. Herein, their marginal distributions are fitted into exponential distributions. Subsequently, the copula function for the correlated  $W$  and  $Z$  is assessed using the goodness-of-fit test (Genest *et al.* 2006; Genest *et al.* 2009). Based on the Akaike information criterion and Bayesian information criterion, the Clayton copula is selected among candidates (i.e., Gaussian, Student's  $t$ , Clayton, Gumbel, and Frank copulas) for the two policies. Detailed fitting procedures and the goodness-of-fit test follow the process of copula selection described in Li *et al.* (2020c). The PDF of the Clayton copula can be described as

$$c_{\theta}^{Clay}(u, v) = (\theta + 1)(uv)^{-(\theta+1)}(u^{-\theta} + v^{-\theta} - 1)^{-\frac{2\theta+1}{\theta}} \quad (8-34)$$

where  $\theta$  is the dependence parameter.

The recorded and simulated maintenance interval and maintenance cost based on the fitted Clayton copula associated with two policies are shown in Figure 8-4. For Policy 1 (e.g., Figure 8-4(a)), the dependence parameter for the Clayton copula is 1.24 and the correlation between  $W$  and  $Z$  is measured by Kendall's tau as 0.38. For Policy 2 in Figure 8-4(b), the associated dependence parameter is 0.89 and Kendall's tau is computed to be 0.31. Given the fitted copula models, the life-cycle maintenance costs with respect to two policies can be assessed. The service life of the bridge is defined as 100 years. The associated expectation, standard deviation, skewness, and kurtosis are computed using the Monte Carlo simulation, as shown in Table 8-1.

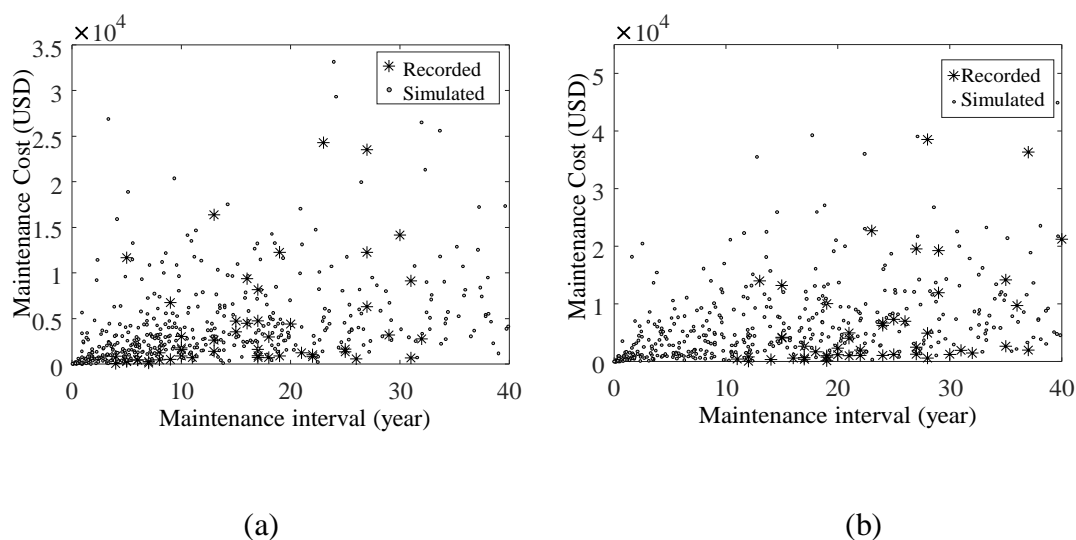


**Figure 8-4** Scatter plots of the recorded and simulated data of the maintenance interval  $W$  and maintenance cost  $Z$  of (a) Maintenance Policy 1 and (b) Maintenance Policy 2.

**Table 8-1** Mean, standard deviation (SD), skewness, and kurtosis of the life-cycle maintenance cost associated with two maintenance policies.

	Mean (USD/m <sup>2</sup> )	SD (USD/m <sup>2</sup> )	Skewness	Kurtosis
Maintenance Policy 1	10231.86	5555.48	1.04	1.89
Maintenance Policy 2	10068.05	7010.80	1.32	2.83

To determine an appropriate maintenance policy, four statistical moments are defined as four different decision criteria. For the investment in maintaining civil infrastructure, decision-makers may tend to be risk-averse (Cha and Ellingwood 2012), as they tend to avoid large variability and extreme cost. For instance, risk averters tend to seek a smaller standard deviation and a positive skewness of the investment return (Brockett and Kahane 1992; Li *et al.* 2020b).

In this example, the decision process is based on the multi-attribute utility theory. The multi-attribute utility theory generally consists of four steps: quantification of attributes, identification of utility functions, assessment of relative weights, and decision on the maximum utility (Jansen 2011). Four statistical moments are considered as four attributes. As smaller expected life-cycle maintenance cost is preferred, the normalized attribute function of the mean can be defined as (Anwar *et al.* 2020; Gumus *et al.* 2020)

$$\varepsilon = \frac{E[LTL]_{\min}}{E[LTL]} \quad (8-35)$$

in which  $E[LTL]_{\min}$  is the minimum mean value between the considered maintenance policies. Based on the risk-averse attitude, a smaller standard deviation should be chosen. Meanwhile, risk averters avoid extreme events associated with low-probability and high-consequence. The extreme situation can be implied by the potential tail risk in terms of skewness and kurtosis (Goda 2010; Li *et al.* 2020b). Therefore, attributes for skewness and kurtosis should be defined based on the aversion of a heavy tail associated with the huge cost. For the investigated case, as the life-cycle maintenance cost indicates negative investment return, smaller skewness and kurtosis are favored (Brockett and Kahane 1992; Maringer and Parpas 2009). Accordingly, similar to the mean attribute described in Eq. (8-35), the minimum values of the other three attributes (i.e., standard deviation, skewness, and kurtosis) are also preferred. Hence, all four attributes can be defined as the ratio of minimum value over the attribute value.

After defining attributes, the utility function of each attribute can be formulated. In this example, the same utility functions are utilized for the four attributes, as they are all statistical characteristics of the life-cycle maintenance cost. The utility function is commonly fitted by a few points in the utility curve, which is typically concave for risk averters (Anwar *et al.* 2020; Wang and Hsu 2009). Herein, a risk-averse utility function is directly given for illustrative purpose (Garmabaki *et al.* 2016), as shown in Eq. (8-36)

$$u(\varepsilon) = 5.5 \exp(-2 / \varepsilon) \quad (8-36)$$

Subsequently, the additive multi-attribute utility function can be formulated. The utility of each attribute is multiplied by the associated weighting factor and then summed over. The multi-attribute utility function can be described as Eq. (8-37)

$$u_{LTL}(mean, sd, skew, kurt) = w_{mean}u_{mean} + w_{sd}u_{sd} + w_{skew}u_{skew} + w_{kurt}u_{kurt} \quad (8-37)$$

where  $u_{mean}$ ,  $u_{sd}$ ,  $u_{skew}$ , and  $u_{kurt}$  are the utility values of the four attributes (i.e., mean, standard deviation, skewness, and kurtosis);  $w_{mean}$ ,  $w_{sd}$ ,  $w_{skew}$ , and  $w_{kurt}$  are weighting factors with respect to the attributes. Typically, weighting factors are allocated considering information provided by decision-makers (Jiménez *et al.* 2003). Herein, the four weighting factors,  $w_{mean}$ ,  $w_{sd}$ ,  $w_{skew}$ , and  $w_{kurt}$ , are allocated as 0.40, 0.25, 0.20, and 0.15, respectively. These values can be adjusted based on the preferences of decision-makers.

Given these inputs of attributes, the utility of Maintenance Policy 1 and Policy 2 can be computed as 0.735 and 0.535, respectively. As Policy 1 gives the maximum utility value between alternatives, Policy 1 should be chosen as the appropriate maintenance policy for the bridge. However, if the decision is purely based on the mean value (i.e., the expected life-cycle maintenance cost) as shown in Table 8-1, Policy 2 should be selected due to a relatively lower expected cost. A different decision outcome is attained due to the consideration of statistical moments. Therefore, statistical moments should be considered during the life-cycle analysis and decision-making process. The proposed copula tool also provides an effective data-based model for decision-making.

#### 8.4.2 Effect of copulas on life-cycle maintenance cost

The impact of different dependence structures between maintenance interval and cost on the life-cycle maintenance cost is investigated by using different copula models. The maintenance actions are based on structural reliability. In this example, the reliability analysis and deterioration modeling of the system use the results in Section 7.4. Parameters remain unchanged unless specified. Maintenance actions are performed when the probability of the system failing hits the associated thresholds, i.e.,  $P_{PM} = 1 \times 10^{-5}$  for preventive maintenance and  $P_{EM} = 1 \times 10^{-3}$  for essential maintenance, respectively. The maximum deterioration level  $g_{\max}$  is 0.5. The changing rate  $\omega$  on gradual deterioration after the preventive maintenance is 0.5, as described in Eq. (8-1). The monetary discount rate is 2% for the life-cycle cost analysis.

The assessment of the life-cycle maintenance cost relies on the quantification of maintenance interval and cost. The two items can be computed from the reliability analysis subjected to deterioration and shocks. In this example, the costs of preventive and essential maintenance actions are given as 50,000 USD and 487,100 USD, respectively (Mondoro *et al.* 2017; Okasha and Frangopol 2010). The bridge has a service life of 100 years. Given these parameters, the maintenance interval and the associated cost are determined by computing the probability of failure of the bridge using Monte Carlo simulation. Deterministic maintenance interval and cost can be assessed with  $10^6$  replications. Figure 8-5 shows the probability of failure subjected to multiple dependent deterioration processes. The bridge experiences nearly four cycles of essential maintenance and resulting in a renewal cycle (i.e., maintenance interval) of  $E[W] = 25.6$  years. The associated maintenance cost within a renewal cycle is computed

as  $E[Z] = 537,100$  USD, which consists of preventive intervention and essential maintenance. The two random variables are assumed to follow exponential distributions herein.

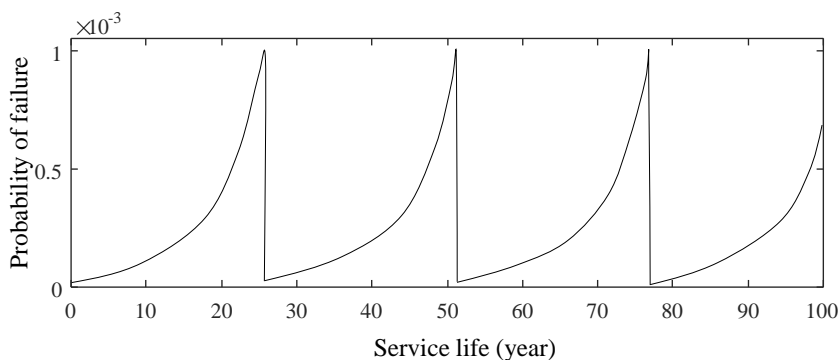


**Figure 8-5** The probability of bridge failing subjected to multiple dependent deterioration processes considering preventive and essential maintenance actions.

In this example, two main statistical parameters of the life-cycle maintenance cost are focused, e.g., the mean  $E[LCC]$  and standard deviation  $Std[LCC]$ . The impact of dependent maintenance interval and cost on the  $E[LCC]$  and  $Std[LCC]$  are explored using the proposed FGM copula. As the FGM copula itself indicates the weak correlation, the maximum positive correlation refers to Kendall's tau at  $2/9$ . The associated expectation and standard deviation of life-cycle maintenance cost are computed as 800,152USD and 588,943 USD, respectively. If considering an independent case (i.e., tau of zero), the expectation and standard deviation of the life-cycle cost can be computed as 907,054 USD and 743,714 USD, respectively. The analytical results have been validated by using numerical modeling based on Monte Carlo simulation. Figure 8-6 demonstrates the difference in the life-cycle maintenance

cost by considering dependent maintenance interval and cost associated with an FGM copula. A negative correlation may exist when there is a different maintenance policy.

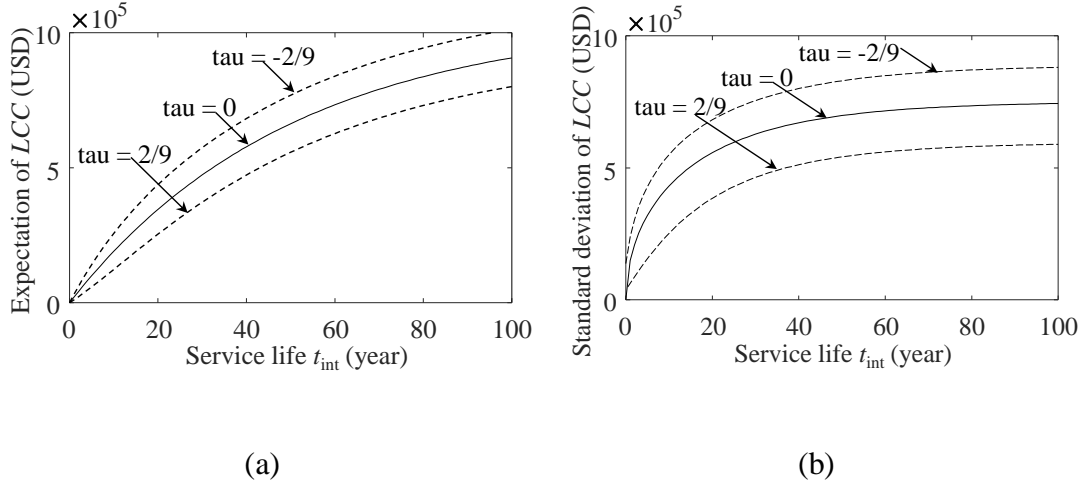


**Figure 8-6** (a) Expectation and (b) standard deviation of life-cycle maintenance cost with the FGM copula subjected to Kendall's tau at  $-2/9$ ,  $0$ , and  $2/9$ .

Apart from the weak correlation associated with the FGM copula, different correlation relationships and different copulas may influence the life-cycle maintenance cost. Herein, the dependence structures described by Gaussian and Clayton copulas are also investigated by using numerical modeling. Figure 8-7 shows the three-dimensional schematic PDFs of FGM, Gaussian, and Clayton copulas with Kendall's tau of  $0.2$ . The PDF of the Gaussian copula can be written as

$$c_{\theta}^{Gau}(u, v) = \frac{1}{\sqrt{(1-\theta^2)}} \exp\left(\frac{2\theta\Phi^{-1}(u)\Phi^{-1}(v) - \theta^2(\Phi^{-1}(u)^2 + \Phi^{-1}(v)^2)}{2(1-\theta^2)}\right) \quad (8-38)$$

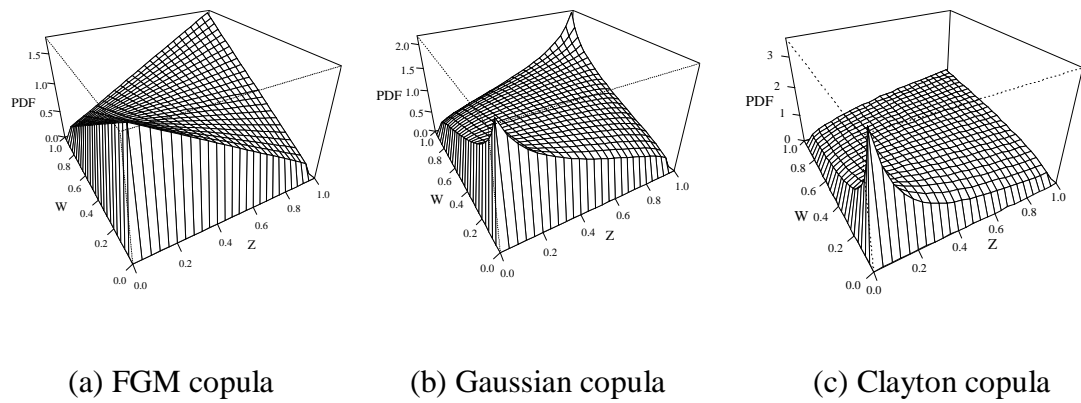


**Figure 8-7** Three-dimensional PDFs of different copulas with Kendall's tau = 0.2.

The expectation and standard deviation of life-cycle maintenance cost with respect to the three copulas are shown in Figure 8-8. Both weak (i.e., Kendall's tau of 0.2) and strong (i.e., Kendall's tau of 0.9) positive correlations are considered. The FGM copula only illustrates the weak correlation. Compared with the independent case, the positive correlation results in decreases in the expected life-cycle maintenance cost and standard deviation. A stronger correlation can lead to a more significant reduction. The interpretation of such a trend is that increasing the maintenance cost (e.g., with more frequent preventive cost) leads to a longer maintenance interval, as more preventive actions delay the occurrence of essential maintenance. Consequently, the life-cycle maintenance cost is reduced. Such findings can assist researchers and decision-makers to explore the optimization of maintenance policy by comparing the life-cycle cost. In Figure 8-8, with the same correlation coefficients (i.e., Kendall's tau), the expectation and standard deviations of the life-cycle maintenance cost are not significantly affected by different copula models. Under the weak correlation, the results associated with the FGM copula show similar estimates compared with the Gaussian and Clayton copulas. Therefore, the proposed analytical approach using an

FGM copula provides an effective tool for decision-makers to estimate the life-cycle cost considering weak correlation. The analytical estimation significantly accelerates the computation process, as numerical modeling of copula functions can be complicated and time-consuming.

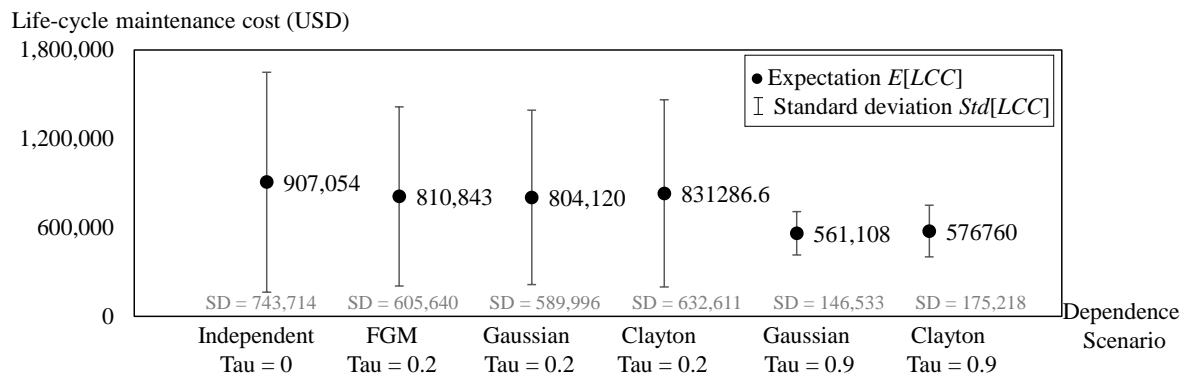


**Figure 8-8** Expected life-cycle cost and standard deviation of different dependence scenarios.

In addition to the dependence structure, the interaction between deterioration processes affects the maintenance interval, maintenance cost, and life-cycle cost. For instance, the length of the renewal cycle (i.e., maintenance interval) is particularly affected by deterioration processes. Figure 8-9 presents the probability of bridge failing subjected to deterioration under three scenarios: dependent deterioration processes (correlation coefficient  $\gamma_d = 0.3$ ) with fatal shocks, dependent deterioration processes ( $\gamma_d = 0.3$ ) without fatal shocks, and independent deterioration process ( $\gamma_d = 0$ ) without fatal shocks. The expected maintenance intervals  $E[W]$  with respect to the three scenarios are 25.6, 26.8, and 29.2 years, respectively. The associated maintenance cost remains unchanged at 537,100 USD. Considering a FGM copula (Kendall's tau = 2/9), the expected life-cycle maintenance costs associated with the three scenarios are

800,153 USD, 760,552 USD, and 691,311 USD, respectively. It shows that dependent deterioration processes and fatal shocks shorten the maintenance interval and increases the life-cycle maintenance cost. Therefore, interaction among deterioration processes should be examined during the life-cycle analysis. In particular, modeling of random fatal shocks can be essential, as neglecting the impact of extreme events may lead to a significant underestimation of the potential risk.

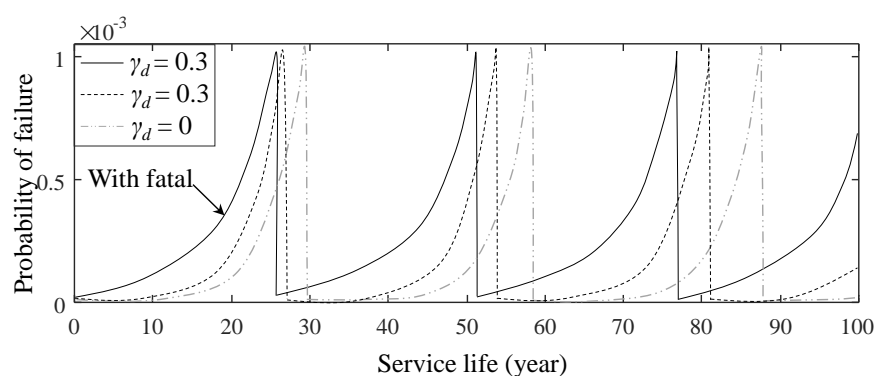


**Figure 8-9** The impact of fatal shocks and dependent deterioration processes on the probability of failure and renewal cycle (scenarios are without fatal shocks unless specified).

The maintenance cost is more likely affected by the maintenance policy, e.g., maintenance threshold. For instance, if maintenance thresholds for preventive and essential action change to  $1 \times 10^{-5}$  and 0.1, respectively, the maintenance interval and cost can be significantly altered. The interval is extended to 56 years, while the maintenance cost remains unchanged. The maintenance cost changes with different preventive and essential maintenance actions. The associated expected life-cycle cost considering the FGM copula (Kendall's tau = 2/9) becomes 328,906 USD with a standard deviation of 369,844 USD. Therefore, the maintenance interval can be

sensitive to the maintenance thresholds. The associated parameters should be carefully examined during the life-cycle analysis.

## **8.5 Summary**

This chapter proposes a copula-based life-cycle analysis framework for deteriorating civil infrastructure systems considering uncertainties and correlation effects (e.g., dependent maintenance interval and maintenance cost). Statistical moments associated with the life-cycle maintenance cost can be effectively estimated analytically and numerically using the copula approach. Multiple dependent deterioration processes are considered in the proposed framework, including gradual deterioration, external shock, and fatal shocks. Reliability-based preventive and essential maintenance actions are performed based on system reliability. Several major conclusions are drawn as follows:

The joint probability distribution of the maintenance interval and the maintenance cost can be effectively modeled by the proposed copula approach. An analytical case, i.e., the FGM copula, is employed to derive statistical moments of the life-cycle cost under the weak correlation, due to its unique mathematically trackable form. Results show that even only with a weak correlation, the dependent consideration significantly affects the life-cycle maintenance cost. The proposed copula-based approach is flexible to incorporate practical data to determine the correlation between the maintenance interval and the cost, thus delivering data-based models for the life-cycle analysis. In addition to the expectation, the other statistical moments (i.e., standard deviation, skewness, and kurtosis) of the life-cycle maintenance cost should

be considered during the life-cycle cost assessment, as different decision results can be attained due to exclusion of the other three statistical moments.

In addition to the FGM copula, the Gaussian and Clayton copulas are also applied to explore the effect of different dependence structures on the life-cycle cost. Results show that the expectation and standard deviation of the life-cycle cost will decrease when the correlation increases. Under the same degree of dependence (i.e., with identical Kendall's tau), the life-cycle maintenance cost is not significantly affected by different copula models. Dependent deterioration processes and maintenance policy affect the maintenance interval and maintenance cost, thus influencing the life-cycle maintenance cost. For instance, in the illustrative example, considering dependent deterioration processes and fatal shocks results in a significant decrease in the maintenance interval and an increase of the life-cycle maintenance cost. Changing maintenance thresholds also cause considerable differences in the maintenance interval and the life-cycle maintenance cost.

# CHAPTER 9 CONCLUSIONS AND FUTURE WORK

## 9.1 Conclusions

This thesis proposes a risk- and resilience-based life-cycle analysis of engineering structures under multiple hazards. Various uncertainties associated with the occurrence and intensity of hazards, structural vulnerability, deterioration processes caused by multiple hazards, long-term resilience and loss assessment, and life-cycle analysis have been taken into account in the proposed framework. The major conclusions of this thesis are summarized.

1. A multivariate approach is developed for civil infrastructure considering the multi-hazard features of hurricanes. The copula model is proposed to model dependent hazard parameters for the vulnerability assessment. The mathematical copula model delivers desired performance in modeling dependent hazard parameters, as the marginal distribution and the correlated effects are considered separately. An illustrative example of a coastal bridge subjected to deck unseating failure is provided to apply the proposed approach. Results show that the structural vulnerability may be underestimated if neglecting the dependence among hazard parameters.
2. An analytical approach using renewal theory is proposed to assess the expected long-term resilience and loss of civil infrastructure under hazards. Uncertainties associated with stochastic occurrence and intensity of hazards are evaluated based on a stochastic renewal process. An illustrative example is provided focusing on highway bridges under multiple independent hazards. Results show

the most harmful scenario determined by the long-term resilience may not be the costliest scenario implied by the long-term loss, thus suggesting different decisions under multiple hazards. Therefore, decision-makers should consider both long-term resilience and loss during the life-cycle analysis.

3. A moment generating function-based approach is proposed for the higher-order analysis of long-term loss. Derivations of statistical moments of the loss are developed for the homogeneous Poisson, non-homogeneous Poisson, mixed Poisson, and renewal processes. An example of a highway bridge is provided to evaluate the long-term impact of climate change and variability on hurricane-induced loss. Results show that the tail risk associated with the higher-order moments may imply extreme losses. Special attention should be paid to the higher-order moments.
4. Finally, a probabilistic life-cycle analysis is developed for ageing infrastructure. The impact of multiple hazards on the system is modeled by multiple dependent deterioration processes (e.g., gradual deterioration, external shock, and fatal shock). Various uncertainties associated with deterioration, system reliability, intervention actions, and maintenance cost are integrated into the proposed framework. In particular, the impact of correlated maintenance interval and cost is investigated by the proposed copula-based multivariate renewal model. Results show their correlation may significantly affect the life-cycle maintenance cost. In terms of the higher-order analysis, examples show that decisions can be altered by considering statistical moments of the life-cycle maintenance cost. Interaction among deterioration processes and the maintenance policy should be carefully considered during life-cycle analysis.

## 9.2 Suggestions for future research

Based on the research work developed in this thesis, several suggestions for future research are provided:

1. The proposed multivariate analysis approach identifies the impact of tail dependence among hazard parameters by considering different copula models. The tail dependence is typically associated with extreme value theory and is commonly captured in extreme events. Future studies may perform extreme value analysis associated with hurricane parameters and incorporate more data records. In addition, the time-dependent reliability assessment during the life-cycle analysis framework shows that the scenario with fatal shock and with interaction among deterioration processes is the most severe. This also implies the need for further analysis in terms of extreme value theory. In addition to the deck unseating failure mode, different failure modes of bridges under hurricanes can be investigated in future studies. The impact of other correlated intensity measures and other multi-hazard effects can be considered in the vulnerability assessment.
2. The long-term performance assessment has employed the commonly used stochastic renewal process. An important assumption associated with the renewal process is that the capacity of a system is fully restored to the initial state after the major repair or replacement (i.e., essential maintenance). This assumption may not be applicable for some civil infrastructure as the entire system is hard to replace. More efforts should be performed to identify the impact of different levels of restoration and incorporate more restoration models.

3. It is recommended to explore the statistical moments of long-term loss with limited information, e.g., with a few observations. In terms of the long-term resilience, future studies can incorporate more detailed investigations associated the restoration modeling, resource availability, constraints, how damage can be mapped to functionality, and restoration actions. Additionally, as the proposed copula approach provides a data-based approach during the decision-making process, more efforts should be made to incorporate more observation data to improve the accuracy of practical applications during the life-cycle analysis.
4. Future work is needed to explore the effect of statistical moments on the life-cycle maintenance cost. More efforts can be made by investigating different risk attitudes and weighting factors during the proposed multi-attribute utility theory model. Moreover, as the higher-order moments are associated with the tail risk, more approaches are needed to investigate the effect of tail risk on the decision-making process. Studies associated with the reduction of the life-cycle cost can also be performed based on the maintenance cost and maintenance policy.
5. The proposed life-cycle analysis framework mainly evaluates the performance based on the economic loss metric. The framework could also be extended to address broader performance metrics, such as social metrics (e.g., downtime, fatalities), and sustainability metrics (e.g., embodied energy, emissions, waste, health impacts). Meanwhile, the impact of potential climate change and nonstationarity associated with climate-related extreme events can also be evaluated.

## REFERENCES

- AASHTO. (2000). *AASHTO LRFD Bridge Design Specifications*. Washington, DC.
- AASHTO. (2008). *AASHTO guide specifications for bridges vulnerable to coastal storms*. Washington, DC.
- Ahmad, R., and Kamaruddin, S. (2012). An overview of time-based and condition-based maintenance in industrial application. *Computers and Industrial Engineering*, 63(1), 135-149.
- Akiyama, M., Frangopol, D. M., and Ishibashi, H. (2019). Toward life-cycle reliability-, risk-and resilience-based design and assessment of bridges and bridge networks under independent and interacting hazards: emphasis on earthquake, tsunami and corrosion. *Structure and Infrastructure Engineering*, 16(1), 26-50.
- Akiyama, M., Frangopol, D. M., and Matsuzaki, H. (2011). Life-cycle reliability of RC bridge piers under seismic and airborne chloride hazards. *Earthquake Engineering and Structural Dynamics*, 40(15), 1671-1687.
- Aksaraylı, M., and Pala, O. (2018). A polynomial goal programming model for portfolio optimization based on entropy and higher moments. *Expert Systems with Applications*, 94, 185-192.
- American Association of State and Highway Transportation Officials (AASHTO). (2008). *AASHTO guide specifications for bridges vulnerable to coastal storms*. Washington, DC.

- American Concrete Institute (ACI). (2005). *Building code requirements for structural concrete and commentary (ACI 318R-05)*. Detroit, MI: American Concrete Institute.
- American Society of Civil Engineers (ASCE). (2021). 2021 Report card for America's Infrastructure. Retrieved from <https://infrastructurereportcard.org/>
- ANSYS. (2009). *ANSYS FLUENT 12.0/12.1 Documentation*. Retrieved from <https://www.afs.enea.it/project/neptunius/docs/fluent/>
- ANSYS. (2016). *ANSYS Fluent Theory Guide, Release 17.2*. Southpointe, Canonsburg: ANSYS Inc.
- Anwar, G. A., Dong, Y., and Li, Y. (2020). Performance-based decision-making of buildings under seismic hazard considering long-term loss, sustainability, and resilience. *Structure and Infrastructure Engineering*, 1-17.
- Ataei, N., and Padgett, J. E. (2013). Probabilistic modeling of bridge deck unseating during hurricane events. *Journal of Bridge Engineering*, 18(4), 275-286.
- Ataei, N., and Padgett, J. E. (2015). Fragility surrogate models for coastal bridges in hurricane prone zones. *Engineering Structures*, 103, 203-213.
- ATC. (1999). Earthquake damage evaluation data for California. Technical Report ATC-13. *Applied Technology Council*.
- Baker, J. W. (2013). An introduction to probabilistic seismic hazard analysis. *White paper version*, 2(1), 79.

- Baker, J. W., Lin, T., Shahi, S. K., and Jayaram, N. (2011). New ground motion selection procedures and selected motions for the PEER transportation research program. *PEER report*, 3.
- Balomenos, G. P., Kameshwar, S., and Padgett, J. E. (2020). Parameterized fragility models for multi-bridge classes subjected to hurricane loads. *Engineering Structures*, 208, 110213.
- Barges, M., Cossette, H., Loisel, S., and Marceau, E. (2011). On the moments of the aggregate discounted claims with dependence introduced by a FGM copula. *Astin Bulletin*, 41(1), 215-238.
- Bastidas-Arteaga, E., Bressolette, P., Chateauneuf, A., and Sánchez-Silva, M. (2009). Probabilistic lifetime assessment of RC structures under coupled corrosion–fatigue deterioration processes. *Structural Safety*, 31(1), 84-96.
- Beck, T. (2020). Finance in the times of coronavirus. *Economics in the Time of COVID-19*, 73.
- Bender, M. A., Knutson, T. R., Tuleya, R. E., Sirutis, J. J., Vecchi, G. A., Garner, S. T., and Held, I. M. (2010). Modeled impact of anthropogenic warming on the frequency of intense Atlantic hurricanes. *Science*, 327(5964), 454-458.
- Biondini, F., and Frangopol, D. M. (2016). Life-cycle performance of deteriorating structural systems under uncertainty. *Journal of structural engineering*, 142(9), F4016001.

- Bjarnadottir, S., Li, Y., and Stewart, M. G. (2014). Regional loss estimation due to hurricane wind and hurricane-induced surge considering climate variability. *Structure and Infrastructure Engineering*, 10(11), 1369-1384.
- Bocchini, P., Frangopol, D. M., Ummenhofer, T., and Zinke, T. (2014). Resilience and sustainability of civil infrastructure: Toward a unified approach. *Journal of Infrastructure Systems*, 20(2), 04014004.
- Boore, D. M., Stewart, J. P., Seyhan, E., and Atkinson, G. M. (2014). NGA-West2 equations for predicting PGA, PGV, and 5% damped PSA for shallow crustal earthquakes. *Earthquake Spectra*, 30(3), 1057-1085.
- Bozorgnia, M., and Lee, J. (2012). Computational fluid dynamic analysis of highway bridges exposed to hurricane waves. *Coastal Engineering Proceedings*, 1(33).
- Brockett, P. L., and Kahane, Y. (1992). Risk, return, skewness and preference. *Management Science*, 38(6), 851-866.
- Bruneau, M., Barbato, M., Padgett, J. E., Zaghi, A. E., Mitrani-Reiser, J., and Li, Y. (2017). State of the art of multihazard design. *Journal of structural engineering*, 143(10), 03117002.
- Burnecki, K., and Weron, R. (2005). Modeling of the risk process. *Statistical tools for finance and insurance* (pp. 319-339). New York: Springer.
- Burnham, K. P., and Anderson, D. R. (2004). Multimodel inference: understanding AIC and BIC in model selection. *Sociological methods & research*, 33(2), 261-304.

- Bushra, N., Trepanier, J. C., and Rohli, R. V. (2019). Joint probability risk modelling of storm surge and cyclone wind along the coast of Bay of Bengal using a statistical copula. *International Journal of Climatology*, 39(11), 4206-4217.
- Caballé, N., and Castro, I. (2017). Analysis of the reliability and the maintenance cost for finite life cycle systems subject to degradation and shocks. *Applied Mathematical Modelling*, 52, 731-746.
- Caballé, N. C., Castro, I. T., Pérez, C. J., and Lanza-Gutiérrez, J. M. (2015). A condition-based maintenance of a dependent degradation-threshold-shock model in a system with multiple degradation processes. *Reliability Engineering and System Safety*, 134, 98-109.
- Cha, E. J., and Ellingwood, B. R. (2012). Risk-averse decision-making for civil infrastructure exposed to low-probability, high-consequence events. *Reliability Engineering & System Safety*, 104, 27-35.
- Charvet, I., Suppasri, A., Kimura, H., Sugawara, D., and Imamura, F. (2015). A multivariate generalized linear tsunami fragility model for Kesenuma City based on maximum flow depths, velocities and debris impact, with evaluation of predictive accuracy. *Natural Hazards*, 79(3), 2073-2099.
- Chebana, F., and Ouarda, T. B. M. J. (2011). Multivariate extreme value identification using depth functions. *Environmetrics*, 22(3), 441-455.
- Cheng, T., Pandey, M. D., and van der Weide, J. A. (2012). The probability distribution of maintenance cost of a system affected by the gamma process of degradation: Finite time solution. *Reliability Engineering and System Safety*, 108, 65-76.

- Chow, V. T. (1965). Bibliography: 1) Handbook of applied hydrology. *International Association of Scientific Hydrology. Bulletin*, 10(1), 82-83.
- Coastal Engineering Research Center (CERC). (1984). Shore Protection Manual. Department of the Army, Waterways Experiment Station, Corps of Engineers.
- Corbella, S., and Stretch, D. D. (2012). Multivariate return periods of sea storms for coastal erosion risk assessment. *Natural Hazards and Earth System Sciences*, 12(8), 2699-2708.
- Cornell, A. C., and Steven, W. (1988). Temporal and magnitude dependence in earthquake recurrence models. 78(4), 1522-1537.
- Cornell, C. A., Jalayer, F., Hamburger, R. O., and Foutch, D. A. (2002). Probabilistic basis for 2000 SAC federal emergency management agency steel moment frame guidelines. *Journal of structural engineering*, 128(4), 526-533.
- De Michele, C., and Salvadori, G. (2003). A generalized Pareto intensity - duration model of storm rainfall exploiting 2-copulas. *Journal of Geophysical Research: Atmospheres*, 108 (D2).
- De Risi, M. T., Del Gaudio, C., and Verderame, G. M. (2020). A component-level methodology to evaluate the seismic repair costs of infills and services for Italian RC buildings. *BULLETIN OF EARTHQUAKE ENGINEERING*, 18(14), 6533-6570.
- Decò, A. (2013). *Risk-based approach for life-cycle assessment and management of bridges and ship structures*. Lehigh University,

- Decò, A., Frangopol, D., and Bocchini, P. (2013). Probabilistic seismic resilience of bridge networks. *Proceedings of the Eleventh International Conference on Structural Safety and Reliability, ICOSSAR2013*, 621-628.
- Decò, A., and Frangopol, D. M. (2011). Risk assessment of highway bridges under multiple hazards. *Journal of Risk Research*, 14(9), 1057-1089.
- DET NORSKE VERITAS (DNV). (2014). *DNV-RP-C205: Environmental Conditions and Environmental Loads*. Høvik, Norway.: DET NORSKE VERITAS
- Dieulle, L., Bérenguer, C., Grall, A., and Roussignol, M. (2003). Sequential condition-based maintenance scheduling for a deteriorating system. *European Journal of operational research*, 150(2), 451-461.
- Dong, Y., and Frangopol, D. M. (2015). Risk and resilience assessment of bridges under mainshock and aftershocks incorporating uncertainties. *Engineering Structures*, 83, 198-208.
- Dong, Y., and Frangopol, D. M. (2016). Probabilistic time-dependent multihazard life-cycle assessment and resilience of bridges considering climate change. *Journal of Performance of Constructed Facilities*, 30(5), 04016034.
- Dong, Y., and Frangopol, D. M. (2017). Probabilistic assessment of an interdependent healthcare–bridge network system under seismic hazard. *Structure and Infrastructure Engineering*, 13(1), 160-170.
- Dong, Y., Frangopol, D. M., and Sabatino, S. (2015). Optimizing bridge network retrofit planning based on cost-benefit evaluation and multi-attribute utility associated with sustainability. *Earthquake Spectra*, 31(4), 2255-2280.

- Dong, Y., Frangopol, D. M., and Saydam, D. (2013). Time-variant sustainability assessment of seismically vulnerable bridges subjected to multiple hazards. *Earthquake Engineering & Structural Dynamics*, 42(10), 1451-1467.
- Dong, Y., Frangopol, D. M., and Saydam, D. (2014). Sustainability of highway bridge networks under seismic hazard. *Journal of Earthquake Engineering*, 18(1), 41-66.
- Douglass, S. L., Hughes, S., Rogers, S., and Chen, Q. (2004). The impact of Hurricane Ivan on the coastal roads of Florida and Alabama: a preliminary report. *Rep. to Coastal Transportation Engineering Research Education Center, Univ. of South Alabama, Mobile, Ala.*
- Eligehausen, R., Mallee, R., and Silva, J. F. (2006). *Anchorage in concrete construction*. Berlin: Ernst & Sohn.
- Ellingwood, B., and Hwang, H. (1985). Probabilistic descriptions of resistance of safety-related structures in nuclear plants. *Nuclear Engineering and Design*, 88(2), 169-178.
- Ellingwood, B. R. (2001). Earthquake risk assessment of building structures. *Reliability Engineering and System Safety*, 74(3), 251-262.
- Ellingwood, B. R., and Lee, J. Y. (2016). Managing risks to civil infrastructure due to natural hazards: communicating long-term risks due to climate change. *Risk Analysis of Natural Hazards* (pp. 97-112): Springer.
- Ellsworth, W. L., Matthews, M. V., Nadeau, R. M., Nishenko, S. P., Reasenber, P. A., and Simpson, R. W. (1999). A physically-based earthquake recurrence model

- for estimation of long-term earthquake probabilities. *US Geological Survey Open-File Report*, 99(522), 22.
- Elsner, J. B., and Bossak, B. H. (2001). Bayesian analysis of US hurricane climate. *Journal of Climate*, 14(23), 4341-4350.
- Elsner, J. B., Bossak, B. H., and Niu, X. F. (2001). Secular changes to the ENSO-US hurricane relationship. *Geophysical Research Letters*, 28(21), 4123-4126.
- Emanuel, K. (2005). Increasing destructiveness of tropical cyclones over the past 30 years. *Nature*, 436(7051), 686-688.
- Eryilmaz, S. (2016). A reliability model for a three-state degraded system having random degradation rates. *Reliability Engineering and System Safety*, 156, 59-63.
- Federal Highway Administration (FHWA). (2020). US Department of Transportation: National Bridge Inventory Data. Retrieved Jan 8, 2021 <https://www.fhwa.dot.gov/bridge/nbi/ascii.cfm>
- Field, E. H., Biasi, G. P., Bird, P., Dawson, T. E., Felzer, K. R., Jackson, D. D., . . . Michael, A. J. (2015). Long-term time-dependent probabilities for the third Uniform California Earthquake Rupture Forecast (UCERF3). *Bulletin of the Seismological Society of America*, 105(2A), 511-543.
- Franchin, P., Cavalieri, F. J. C. A. C., and Engineering, I. (2015). Probabilistic assessment of civil infrastructure resilience to earthquakes. *Computer-Aided Civil and Infrastructure Engineering*, 30(7), 583-600.

- Frangopol, D. M., Dong, Y., and Sabatino, S. (2017). Bridge life-cycle performance and cost: analysis, prediction, optimisation and decision-making. *Structure Infrastructure Engineering*, 13(10), 1239-1257.
- Frangopol, D. M., Lin, K.-Y., and Estes, A. C. (1997). Reliability of reinforced concrete girders under corrosion attack. *Journal of structural engineering*, 123(3), 286-297.
- Frangopol, D. M., and Soliman, M. (2016). Life-cycle of structural systems: recent achievements and future directions. *Structure and Infrastructure Engineering*, 12(1), 1-20.
- Gardoni, P. (2017). Risk and reliability analysis. *Theory and Applications* (pp. 3-24). New York: Springer.
- Gardoni, P., Murphy, C., and Rowell, A. (2016). Interdisciplinary challenges and integrated solutions. *Risk analysis of natural hazards* (pp. 1-7). New York: Springer.
- Garmabaki, A., Ahmadi, A., and Ahmadi, M. (2016). Maintenance optimization using multi-attribute utility theory. *Current trends in reliability, availability, maintainability and safety* (pp. 13-25): Springer.
- Gautam, D. (2017). On seismic vulnerability of highway bridges in Nepal: 1988 Udaypur earthquake (MW 6.8) revisited. *Soil Dynamics and Earthquake Engineering*, 99, 168-171.

- Gautam, D., and Dong, Y. (2018). Multi-hazard vulnerability of structures and lifelines due to the 2015 Gorkha earthquake and 2017 central Nepal flash flood. *Journal of Building Engineering*, 17, 196-201.
- Genest, C., Ghoudi, K., and Rivest, L.-P. (1995). A semiparametric estimation procedure of dependence parameters in multivariate families of distributions. *Biometrika*, 82(3), 543-552.
- Genest, C., Quessy, J. F., and Rémillard, B. (2006). Goodness - of - fit procedures for copula models based on the probability integral transformation. *Scandinavian Journal of Statistics*, 33(2), 337-366.
- Genest, C., Rémillard, B., and Beaudoin, D. (2009). Goodness-of-fit tests for copulas: A review and a power study. *Insurance: Mathematics and economics*, 44(2), 199-213.
- Genest, C., and Rivest, L. P. (1989). A characterization of Gumbel's family of extreme value distributions. *Statistics & Probability Letters*, 8(3), 207-211.
- Gerhardt, I., and Nelson, B. L. (2009). Transforming renewal processes for simulation of nonstationary arrival processes. *INFORMS Journal on Computing*, 21(4), 630-640.
- Ghosh, J., and Padgett, J. E. (2010). Aging considerations in the development of time-dependent seismic fragility curves. *Journal of structural engineering*, 136(12), 1497-1511.

- Ghosh, J., Padgett, J. E., and Dueñas-Osorio, L. (2013). Surrogate modeling and failure surface visualization for efficient seismic vulnerability assessment of highway bridges. *Probabilistic Engineering Mechanics*, 34, 189-199.
- Gidaris, I., Padgett, J. E., Barbosa, A. R., Chen, S., Cox, D., Webb, B., and Cerato, A. (2017). Multiple-hazard fragility and restoration models of highway bridges for regional risk and resilience assessment in the United States: state-of-the-art review. *Journal of structural engineering*, 143(3), 04016188.
- Giouvanidis, A., and Dong, Y. (2020). Seismic loss and resilience assessment of single-column rocking bridges. *BULLETIN OF EARTHQUAKE ENGINEERING*, 18, 4481-4513.
- Goda, K. (2010). Statistical modeling of joint probability distribution using copula: application to peak and permanent displacement seismic demands. *Structural Safety*, 32(2), 112-123.
- Goda, K., and Hong, H. (2006). Optimal seismic design considering risk attitude, societal tolerable risk level, and life quality criterion. *Journal of structural engineering*, 132(12), 2027-2035.
- Gong, C., and Frangopol, D. M. (2019). An efficient time-dependent reliability method. *Structural Safety*, 81, 101864.
- Gouldby, B., Méndez, F., Guanche, Y., Rueda, A., and Mínguez, R. (2014). A methodology for deriving extreme nearshore sea conditions for structural design and flood risk analysis. *Coastal Engineering*, 88, 15-26.

- Gudendorf, G., and Segers, J. (2010). Extreme-value copulas. *Copula theory and its applications*. New York, NY: Springer.
- Gumus, H., Aydemir, D., Altuntas, E., Kurt, R., and Imren, E. (2020). Cellulose nanofibrils and nano-scaled titanium dioxide-reinforced biopolymer nanocomposites: Selecting the best nanocomposites with multicriteria decision-making methods. *Journal of Composite Materials*, 54(7), 923-935.
- Guo, H. Y., Dong, Y., and Gu, X. L. (2020). Two-step translation method for time-dependent reliability of structures subject to both continuous deterioration and sudden events. *Engineering Structures*, 225, 111291.
- Gutenberg, B., and Richter, C. F. (1944). Frequency of earthquakes in California. *Bulletin of the Seismological Society of America*, 34(4), 185-188.
- Hainzl, S., Scherbaum, F., and Beauval, C. (2006). Estimating background activity based on interevent-time distribution. *Bulletin of the Seismological Society of America*, 96(1), 313-320.
- Hallegatte, S., Henriot, F., and Corfee-Morlot, J. (2011). The economics of climate change impacts and policy benefits at city scale: a conceptual framework. *Climatic Change*, 104(1), 51-87.
- HAZUS. (1999). Earthquake loss estimation methodology—technical and user manuals. *Federal Emergency Management Agency, Washington*.
- Heo, J. H., Kho, Y. W., Shin, H., Kim, S., and Kim, T. (2008). Regression equations of probability plot correlation coefficient test statistics from several probability distributions. *Journal of Hydrology*, 355(1-4), 1-15.

- Hepburn, C. (2007). *Valuing the far-off future: discounting and its alternatives*. Cheltenham, UK: Edward Elgar.
- Hong, H. P., Zhou, W., Zhang, S., and Ye, W. (2014). Optimal condition-based maintenance decisions for systems with dependent stochastic degradation of components. *Reliability Engineering and System Safety*, 121, 276-288.
- Hosking, J. R. M., and Wallis, J. R. (1997). *Regional frequency analysis: an approach based on L-moments*. New York: Cambridge university press.
- Huang, Q., Gardoni, P., Trejo, D., and Pagnotta, A. (2014). Probabilistic model for steel–concrete bond behavior in bridge columns affected by alkali silica reactions. *Engineering Structures*, 71, 1-11.
- Hüsler, J., and Reiss, R. D. (1989). Maxima of normal random vectors: between independence and complete dependence. *Statistics Probability Letters*, 7(4), 283-286.
- Iervolino, I., Giorgio, M., and Chioccarelli, E. (2013). Gamma degradation models for earthquake-resistant structures. *Structural Safety*, 45, 48-58.
- ISO. (2009). *Risk management – Principles and guidelines*. Retrieved from Geneva, Switzerland:
- Jagger, T. H., and Elsner, J. B. (2006). Climatology models for extreme hurricane winds near the United States. *Journal of Climate*, 19(13), 3220-3236.
- Jalayer, F., Asprone, D., Prota, A., and Manfredi, G. (2011). Multi-hazard upgrade decision making for critical infrastructure based on life-cycle cost criteria. *Earthquake Engineering and Structural Dynamics*, 40(10), 1163-1179.

- Jane, R. A., Simmonds, D. J., Gouldby, B. P., Simm, J. D., Dalla Valle, L., and Raby, A. C. (2018). Exploring the potential for multivariate fragility representations to alter flood risk estimates. *Risk Analysis*, 38(9), 1847-1870.
- Jansen, S. J. (2011). The multi-attribute utility method. *The Measurement and Analysis of Housing Preference and Choice* (pp. 101-125): Springer.
- Jia, G., and Gardoni, P. (2019). Stochastic life-cycle analysis: Renewal-theory life-cycle analysis with state-dependent deterioration stochastic models. *Structure and Infrastructure Engineering*, 15(8), 1001-1014.
- Jia, G., Gardoni, P., and Trejo, D. (2017). *Stochastic modelling of deterioration of reinforced concrete structures considering joint effects of earthquakes, corrosion and ASR*. Paper presented at the ICOSAR 2017: 12th International Conference on Structural Safety & Reliability, Vienna, Austria.
- Jia, G., Gardoni, P., Trejo, D., and Mazarei, V. (2021). Stochastic Modeling of Deterioration and Time-Variant Performance of Reinforced Concrete Structures under Joint Effects of Earthquakes, Corrosion, and ASR. *Journal of structural engineering*, 147(2), 04020314.
- Jiménez, A., Rios-Insua, S., and Mateos, A. (2003). A decision support system for multiattribute utility evaluation based on imprecise assignments. *Decision Support Systems*, 36(1), 65-79.
- Jin, J., and Meng, B. (2011). Computation of wave loads on the superstructures of coastal highway bridges. *Ocean Engineering*, 38(17-18), 2185-2200.

- Joe, H. (1997). *Multivariate models and multivariate dependence concepts*. New York: CRC Press.
- Joe, H. (2014). *Dependence modeling with copulas*. Boca Raton, FL: CRC press.
- Joint Committee on Structural Safety (JCSS). (2001). Probabilistic model code. Part 3: Resistance Models.
- Kameshwar, S., and Padgett, J. E. (2014). Multi-hazard risk assessment of highway bridges subjected to earthquake and hurricane hazards. *Engineering Structures*, 78, 154-166.
- Katz, R. W. (2002). Stochastic modeling of hurricane damage. *Journal of Applied Meteorology*, 41(7), 754-762.
- Kelly, B., and Jiang, H. (2014). Tail risk and asset prices. *The Review of Financial Studies*, 27(10), 2841-2871.
- Kilanitis, I., and Sextos, A. (2019). Integrated seismic risk and resilience assessment of roadway networks in earthquake prone areas. *BULLETIN OF EARTHQUAKE ENGINEERING*, 17(1), 181-210.
- Kim, H., Sim, S. H., Lee, J., Lee, Y. J., and Kim, J. M. (2017). Flood fragility analysis for bridges with multiple failure modes. *Advances in Mechanical Engineering*, 9(3), 1687814017696415.
- Kim, S. H., and Shinozuka, M. (2004). Development of fragility curves of bridges retrofitted by column jacketing. *Probabilistic Engineering Mechanics*, 19(1-2), 105-112.

- Koduru, S., and Haukaas, T. (2010). Probabilistic seismic loss assessment of a Vancouver high-rise building. *Journal of structural engineering*, 136(3), 235-245.
- Kohnke, P. (1994). *ANSYS Theory Reference Manual*. Retrieved from Canonsburg, USA:
- Kossin, J., Knapp, K., Vimont, D., Murnane, R., and Harper, B. (2007). A globally consistent reanalysis of hurricane variability and trends. *Geophysical Research Letters*, 34(4).
- Kulicki, J. M. (2010). *Development of the AASHTO guide specifications for bridges vulnerable to coastal storms*. Paper presented at the Proc., 5th Int. Conf. on Bridge Maintenance, Safety and Management, IABMAS 2010, London,.
- Kumar, R., Cline, D. B., and Gardoni, P. (2015). A stochastic framework to model deterioration in engineering systems. *Structural Safety*, 53, 36-43.
- Kumar, R., and Gardoni, P. (2014a). Effect of seismic degradation on the fragility of reinforced concrete bridges. *Engineering Structures*, 79, 267-275.
- Kumar, R., and Gardoni, P. (2014b). Renewal theory-based life-cycle analysis of deteriorating engineering systems. *Structural Safety*, 50, 94-102.
- Lee, J. Y., and Ellingwood, B. R. (2015). Ethical discounting for civil infrastructure decisions extending over multiple generations. *Structural Safety*, 57, 43-52.
- Lee, J. Y., and Ellingwood, B. R. (2017). A decision model for intergenerational life-cycle risk assessment of civil infrastructure exposed to hurricanes under climate change. *Reliability Engineering and System Safety*, 159, 100-107.

- Léveillé, G., and Garrido, J. (2001). Recursive moments of compound renewal sums with discounted claims. *Scandinavian Actuarial Journal*, 2001(2), 98-110.
- Léveillé, G., and Hamel, E. (2018). Conditional, non-homogeneous and doubly stochastic compound Poisson processes with stochastic discounted claims. *Methodology and Computing in Applied Probability*, 20(1), 353-368.
- Levy, H. (2015). *Stochastic dominance: Investment decision making under uncertainty*: Springer.
- Li, Q., Wang, C., and Ellingwood, B. R. (2015). Time-dependent reliability of aging structures in the presence of non-stationary loads and degradation. *Structural Safety*, 52, 132-141.
- Li, Q., Wang, C., and Zhang, H. (2016). A probabilistic framework for hurricane damage assessment considering non-stationarity and correlation in hurricane actions. *Structural Safety*, 59, 108-117.
- Li, Y., and Dong, Y. (2019). Risk-informed hazard loss of bridges in a life-cycle context. *Proceedings of the 13th International Conference on Applications of Statistics and Probability in Civil Engineering*.
- Li, Y., Dong, Y., Frangopol, D. M., and Gautam, D. (2020a). Long-term resilience and loss assessment of highway bridges under multiple natural hazards. *Structure and Infrastructure Engineering*, 16(4), 626-641.
- Li, Y., Dong, Y., and Qian, J. (2020b). Higher-order analysis of probabilistic long-term loss under nonstationary hazards. *Reliability Engineering and System Safety*, 203, 107092.

- Li, Y., Dong, Y., and Zhu, D. (2020c). Copula-Based Vulnerability Analysis of Civil Infrastructure subjected to Hurricanes. *Frontiers in Built Environment*, 6, 170.
- Li, Y., and Ellingwood, B. R. (2006). Hurricane damage to residential construction in the US: Importance of uncertainty modeling in risk assessment. *Engineering Structures*, 28(7), 1009-1018.
- Liang, M. S., and Julius, S. (2017). *On the coastal topography and storm surge for infrastructure risk assessment and adaptation*. Paper presented at the World Environmental and Water Resources Congress 2017, California.
- Liao, K.-W., Muto, Y., and Gitomarsono, J. (2018). Reliability analysis of river bridge against scours and earthquakes. *Journal of Performance of Constructed Facilities*, 32(3), 04018017.
- Lin, N., Emanuel, K., Oppenheimer, M., and Vanmarcke, E. (2012). Physically based assessment of hurricane surge threat under climate change. *Nature Climate Change*, 2(6), 462-467.
- Lin, N., Emanuel, K. A., Smith, J. A., and Vanmarcke, E. (2010). Risk assessment of hurricane storm surge for New York City. *Journal of Geophysical Research: Atmospheres*, 115(D18).
- Lin, N., and Shullman, E. (2017). Dealing with hurricane surge flooding in a changing environment: part I. Risk assessment considering storm climatology change, sea level rise, and coastal development. *Stochastic Environmental Research and Risk Assessment*, 31(9), 2379-2400.

- Liu, B., Zhao, X., Liu, G., and Liu, Y. (2020). Life cycle cost analysis considering multiple dependent degradation processes and environmental influence. *Reliability Engineering and System Safety*, 197, 106784.
- Longuet-Higgins, M. S. (1980). On the distribution of the heights of sea waves: some effects of nonlinearity and finite band width. *Journal of Geophysical Research: Oceans*, 85(C3), 1519-1523.
- Lu, Z. H., Leng, Y., Dong, Y., Cai, C. H., and Zhao, Y. G. (2019). Fast integration algorithms for time-dependent structural reliability analysis considering correlated random variables. *Structural Safety*, 78, 23-32.
- Lucas, C., and Soares, C. G. (2015). Bivariate distributions of significant wave height and mean wave period of combined sea states. *Ocean Engineering*, 106, 341-353.
- Malmstadt, J. C., Elsner, J. B., and Jagger, T. H. (2010). Risk of strong hurricane winds to Florida cities. *Journal of Applied Meteorology and Climatology*, 49(10), 2121-2132.
- Maringer, D., and Parpas, P. (2009). Global optimization of higher order moments in portfolio selection. *Journal of Global optimization*, 43(2), 219-230.
- Markowitz, H. M., and Todd, G. P. (2000). *Mean-variance analysis in portfolio choice and capital markets* Vol. 66: John Wiley & Sons.
- Masina, M., Lamberti, A., and Archetti, R. (2015). Coastal flooding: A copula based approach for estimating the joint probability of water levels and waves. *Coastal Engineering*, 97, 37-52.

- Matthews, M. V., Ellsworth, W. L., and Reasenber, P. A. (2002). A Brownian model for recurrent earthquakes. *Bulletin of the Seismological Society of America*, 92(6), 2233-2250.
- McCullough, M., Kareem, A., and Kwon, D. K. (2011). *Advanced modeling and simulation tools: From surrogates to copulas*. Paper presented at the Applications of Statistics Probability in Civil Engineering.
- McInnes, K. L., Macadam, I., Hubbert, G., and O'Grady, J. (2013). An assessment of current and future vulnerability to coastal inundation due to sea - level extremes in Victoria, southeast Australia. *International Journal of Climatology*, 33(1), 33-47.
- McKenna, F., Fenves, G., Filippou, F. C., and Mazzoni, S. (2009). Open System for Earthquake Engineering Simulation (OpenSees). Retrieved from [http://opensees.berkeley.edu/wiki/index.php/Main\\_Page](http://opensees.berkeley.edu/wiki/index.php/Main_Page) website:
- Michael, A. J. (2005). Viscoelasticity, postseismic slip, fault interactions, and the recurrence of large earthquakes. *Bulletin of the Seismological Society of America*, 95(5), 1594-1603.
- Mikosch, T. (2009). *Non-Life Insurance Mathematics: An Introduction with the Poisson Processes*. New York: Springer Science and Business Media.
- Minaie, E., and Moon, F. (2017). Practical and simplified approach for quantifying bridge resilience. *Journal of Infrastructure Systems*, 23(4), 04017016.

- Moftakhari, H. R., Salvadori, G., AghaKouchak, A., Sanders, B. F., and Matthew, R. A. (2017). Compounding effects of sea level rise and fluvial flooding. *Proceedings of the National Academy of Sciences*, 114(37), 9785-9790.
- Mondoro, A., and Frangopol, D. M. (2018). Risk-based cost-benefit analysis for the retrofit of bridges exposed to extreme hydrologic events considering multiple failure modes. *Engineering Structures*, 159, 310-319.
- Mondoro, A., Frangopol, D. M., and Soliman, M. (2017). Optimal risk-based management of coastal bridges vulnerable to hurricanes. *Journal of Infrastructure Systems*, 23(3).
- Mousavi, M. E., Irish, J. L., Frey, A. E., Olivera, F., and Edge, B. L. (2011). Global warming and hurricanes: the potential impact of hurricane intensification and sea level rise on coastal flooding. *Climatic Change*, 104(3-4), 575-597.
- Nelsen, R. B. (2006). *An introduction to copulas*. New York: Springer Science & Business Media.
- Nielson, B. G. (2005). *Analytical fragility curves for highway bridges in moderate seismic zones*. Georgia Institute of Technology,
- Nielson, B. G., and DesRoches, R. (2007). Analytical seismic fragility curves for typical bridges in the central and southeastern United States. *Earthquake Spectra*, 23(3), 615-633.
- NOAA National Centers for Environmental Information (NECI). (2020). U.S. Billion-Dollar Weather and Climate Disasters. Retrieved from <https://www.ncdc.noaa.gov/billions/>.

- Obeyssekera, J., and Park, J. (2013). Scenario-based projection of extreme sea levels. *Journal of Coastal Research*, 29(1), 1-7.
- Okasha, N. M., and Frangopol, D. M. (2010). Novel approach for multicriteria optimization of life-cycle preventive and essential maintenance of deteriorating structures. *Journal of structural engineering*, 136(8), 1009-1022.
- Otieno, M., Alexander, M., and Beushausen, H. D. (2010). Corrosion in cracked and uncracked concrete—influence of crack width, concrete quality and crack reopening. *Magazine of Concrete Research*, 62(6), 393-404.
- Padgett, J., DesRoches, R., Nielson, B., Yashinsky, M., Kwon, O. S., Burdette, N., and Tavera, E. (2008). Bridge damage and repair costs from Hurricane Katrina. *Journal of Bridge Engineering*, 13(1), 6-14.
- Padgett, J. E., Dennemann, K., and Ghosh, J. (2010). Risk-based seismic life-cycle cost–benefit (LCC-B) analysis for bridge retrofit assessment. *Structural Safety*, 32(3), 165-173.
- Padgett, J. E., Ghosh, J., and Dennemann, K. (2009). Sustainable infrastructure subjected to multiple threats. *TCLÉE 2009: Lifeline Earthquake Engineering in a Multihazard Environment* (pp. 1-11).
- Pandey, M. D., and Van Der Weide, J. (2017). Stochastic renewal process models for estimation of damage cost over the life-cycle of a structure. *Structural Safety*, 67, 27-38.
- Pandey, M. D., and van der Weide, J. (2018). Probability distribution of the seismic damage cost over the life cycle of structures. *Structural Safety*, 72, 74-83.

- Peng, L., and Stewart, M. G. (2014). Spatial time-dependent reliability analysis of corrosion damage to RC structures with climate change. *Magazine of Concrete Research*, 66(22), 1154-1169.
- Pescaroli, G., Wicks, R., Giacomello, G., and Alexander, D. (2018). Increasing resilience to cascading events: The M. OR. D. OR. scenario. *Safety Science*, 110, 131-140.
- Phan, L. T., Mcinerney, M. A., Taylor, A. A., and Glahn, B. (2007). *Methodology for development of design criteria for joint hurricane wind speed and storm surge events: Proof of concept*. Retrieved from Gaithersburg, MD:
- Porter, K. A. (2003). An overview of PEER's performance-based earthquake engineering methodology. *Proceedings of ninth international conference on applications of statistics and probability in civil engineering (ICASP9)*.
- Qian, J., and Dong, Y. (2020). Multi - criteria decision making for seismic intensity measure selection considering uncertainty. *Earthquake Engineering & Structural Dynamics*, 49(11), 1095-1114.
- Raymond, C., Horton, R. M., Zscheischler, J., Martius, O., AghaKouchak, A., Balch, J., . . . Kornhuber, K. (2020). Understanding and managing connected extreme events. *Nature Climate Change*, 10, 611-621.
- Read, L. K., and Vogel, R. M. (2016). Hazard function analysis for flood planning under nonstationarity. *Water resources research*, 52(5), 4116-4131.
- Rolski, T., Schmidli, H., Schmidt, V., and Teugels, J. L. (2009). *Stochastic processes for insurance and finance*. Vol. 505: John Wiley & Sons.

- Ross, S. M. (2014). *Introduction to probability models*. Amsterdam: Academic press.
- Saeidpour, A., Chorzepa, M. G., Christian, J., and Durham, S. (2019). Probabilistic hurricane risk analysis of coastal bridges incorporating extreme wave statistics. *Engineering Structures*, 182, 379-390.
- Salvadori, G., De Michele, C., Kottegoda, N. T., and Rosso, R. (2007). *Extremes in nature: an approach using copulas*. Netherlands: Springer Science & Business Media.
- Sánchez-Silva, M., Frangopol, D. M., Padgett, J., and Soliman, M. (2016). Maintenance and operation of infrastructure systems. *Journal of structural engineering*, 142(9), F4016004.
- Sánchez-Silva, M., and Klutke, G.-A. (2016). *Reliability and life-cycle analysis of deteriorating systems* Vol. 182: Springer.
- Sanchez-Silva, M., Klutke, G.-A., and Rosowsky, D. V. (2011). Life-cycle performance of structures subject to multiple deterioration mechanisms. *Structural Safety*, 33(3), 206-217.
- Schott, T., Landsea, C., Hafele, G., Lorens, J., Taylor, A., Thurm, H., . . . Zaleski, W. (2019). The Saffir-Simpson Hurricane Wind Scale. *National Weather Services, National Hurricane Centre, National Oceanic and Atmospheric Administration (NOAA) factsheet*. Retrieved from <https://www.nhc.noaa.gov/pdf/sshws.pdf>.
- Segura, R., Padgett, J. E., and Paultre, P. (2020). Metamodel-Based Seismic Fragility Analysis of Concrete Gravity Dams. *Journal of structural engineering*, 146(7), 04020121.

- Seiffert, B., Hayatdavoodi, M., and Ertekin, R. C. (2014). Experiments and computations of solitary-wave forces on a coastal-bridge deck. Part I: Flat plate. *Coastal Engineering*, 88, 194-209.
- Serafin, K. A., Ruggiero, P., and Parker, K. (2019). What's streamflow got to do with it? A probabilistic simulation of the competing oceanographic and fluvial processes driving extreme along-river water levels. *Natural Hazards and Earth System Sciences*, 19, 1415-1431.
- Shreve, S. E. (2004). *Stochastic calculus for finance II: Continuous-time models*. Vol. 11: Springer Science & Business Media.
- Sklar, A. (1959). Fonctions de Répartition à n Dimensions et Leurs Marges. *Publications de l'Institut Statistique de l'Université de Paris*, 8, 229-231.
- Smith, R. L. (2003). Statistics of extremes, with applications in environment, insurance and finance. *Extreme values in finance, telecommunications, and the environment*, 1, 78.
- Takahashi, Y., Kiureghian, A. D., and Ang, A. H. S. (2004). Life - cycle cost analysis based on a renewal model of earthquake occurrences. *Earthquake Engineering and Structural Dynamics*, 33(7), 859-880.
- Technical Lifelines Council for Earthquake Engineering (TCLEE). (2006). Hurricane Katrina: Performance of transportation systems. R. DesRoches (Ed.), *ASCE Technical Council on Lifeline Earthquake Engineering Monograph No. 29*: American Society of Civil Engineers.

- Temam, R. (2001). *Navier-Stokes equations: theory and numerical analysis* Vol. 343: American Mathematical Soc.
- Thoft-Christensen, P., Jensen, F., Middleton, C., and Blackmore, A. (2011). Revised rules for concrete bridges. *Safety of bridges* (pp. 175-188): Thomas Telford Publishing.
- Tramblay, Y., Neppel, L., Carreau, J., and Najib, K. (2013). Non-stationary frequency analysis of heavy rainfall events in southern France. *Hydrological Sciences Journal*, 58(2), 280-294.
- Trepanier, J., Yuan, J., and Jagger, T. (2017). The combined risk of extreme tropical cyclone winds and storm surges along the US Gulf of Mexico Coast. *Journal of Geophysical Research: Atmospheres*, 122(6), 3299-3316.
- Tu, B., Fang, Z., Dong, Y., and Frangopol, D. M. (2017). Time-variant reliability analysis of widened deteriorating prestressed concrete bridges considering shrinkage and creep. *Engineering Structures*, 153, 1-16.
- Um, M. J., Joo, K., Nam, W., and Heo, J. H. (2017). A comparative study to determine the optimal copula model for the wind speed and precipitation of typhoons. *International Journal of Climatology*, 37(4), 2051-2062.
- United States Geological Survey (USGS). (2003). Earthquake Probabilities in the San Francisco Bay Region: 2002–2031. *Open File Report 03-214*.
- van Noortwijk, J. M., and Frangopol, D. M. (2004). Two probabilistic life-cycle maintenance models for deteriorating civil infrastructures. *Probabilistic Engineering Mechanics*, 19(4), 345-359.

- Vickery, P. J., Skerlj, P. F., and Twisdale, L. A. (2000). Simulation of hurricane risk in the US using empirical track model. *Journal of structural engineering*, 126(10), 1222-1237.
- Villarini, G., Vecchi, G. A., and Smith, J. A. (2010). Modeling the dependence of tropical storm counts in the North Atlantic basin on climate indices. *Monthly Weather Review*, 138(7), 2681-2705.
- Vishnu, N., Kameshwar, S., and Padgett, J. E. (2021). Road transportation network hazard sustainability and resilience: correlations and comparisons. *Structure and Infrastructure Engineering*, 1-21.
- Vogel, R. M., and Kroll, C. N. (1989). Low-flow frequency analysis using probability-plot correlation coefficients. *Journal of water resources planning management*, 115(3), 338-357.
- Vorogushyn, S., Merz, B., Lindenschmidt, K. E., and Apel, H. (2010). A new methodology for flood hazard assessment considering dike breaches. *Water resources research*, 46(8).
- Vrouwenvelder, A., Holicky, B., Tanner, C., Lovegrove, D., and Canisius, E. (2001). *Risk assessment and risk communication in civil engineering*. Rotterdam, Netherlands: International Council for Research and Innovation in Building and Construction (CIB).
- Wahl, T., Jain, S., Bender, J., Meyers, S. D., and Luther, M. E. (2015). Increasing risk of compound flooding from storm surge and rainfall for major US cities. *Nature Climate Change*, 5(12), 1093-1097.

- Wahl, T., Plant, N. G., and Long, J. W. (2016). Probabilistic assessment of erosion and flooding risk in the northern Gulf of Mexico. *Journal of Geophysical Research: Oceans*, 121(5), 3029-3043.
- Wang, C., Li, Q. W., Zou, A. M., and Zhang, L. (2015). A realistic resistance deterioration model for time-dependent reliability analysis of aging bridges. *Journal of Zhejiang University-SCIENCE A*, 16(7), 513-524.
- Wang, C., Zhang, H., Feng, K., and Li, Q. (2017a). Assessing hurricane damage costs in the presence of vulnerability model uncertainty. *Natural Hazards*, 85(3), 1621-1635.
- Wang, C., Zhang, H., and Li, Q. (2017b). Reliability assessment of aging structures subjected to gradual and shock deteriorations. *Reliability Engineering and System Safety*, 161, 78-86.
- Wang, H. F., and Hsu, F. C. (2009). An integrated operation module for individual risk management. *European Journal of operational research*, 198(2), 610-617.
- Wang, M. X., Huang, D., Wang, G., Du, W., and Li, D. Q. (2020). Vine Copula-Based Dependence Modeling of Multivariate Ground-Motion Intensity Measures and the Impact on Probabilistic Seismic Slope Displacement Hazard Analysis. *Bulletin of the Seismological Society of America*, 110(6), 2967-2990.
- Wang, Y., and Pham, H. (2011). Modeling the dependent competing risks with multiple degradation processes and random shock using time-varying copulas. *IEEE Transactions on Reliability*, 61(1), 13-22.

- Wang, Z., Padgett, J. E., and Dueñas-Osorio, L. (2014). Risk-consistent calibration of load factors for the design of reinforced concrete bridges under the combined effects of earthquake and scour hazards. *Engineering Structures*, 79, 86-95.
- Wen, Y. K., and Kang, Y. (2001). Minimum building life-cycle cost design criteria. I: Methodology. *Journal of structural engineering*, 127(3), 330-337.
- Xiao, S., Kottas, A., and Sansó, B. (2015). Modeling for seasonal marked point processes: An analysis of evolving hurricane occurrences. *The Annals of Applied Statistics*, 353-382.
- Xu, G., Cai, C., Hu, P., and Dong, Z. (2016). Component level-based assessment of the solitary wave forces on a typical coastal bridge deck and the countermeasure of air venting holes. *Practice Periodical on Structural Design Construction*, 21(4), 04016012.
- Yang, D. Y., and Frangopol, D. M. (2019a). Life-cycle management of deteriorating civil infrastructure considering resilience to lifetime hazards: A general approach based on renewal-reward processes. *Reliability Engineering and System Safety*, 183, 197-212.
- Yang, D. Y., and Frangopol, D. M. (2019b). Societal risk assessment of transportation networks under uncertainties due to climate change and population growth. *Structural Safety*, 78, 33-47.
- Yang, L., Ma, X., and Zhao, Y. (2017). A condition-based maintenance model for a three-state system subject to degradation and environmental shocks. *Computers and Industrial Engineering*, 105, 210-222.

- Yanmaz, A. M. (2001). Uncertainty of local scouring parameters around bridge piers. *Turkish Journal of Engineering and Environmental Sciences*, 25(2), 127-137.
- Yeo, G. L., and Cornell, C. A. (2005). *Stochastic characterization and decision bases under time-dependent aftershock risk in performance-based earthquake engineering*: Pacific Earthquake Engineering Research Center Berkeley, CA.
- Yeo, G. L., and Cornell, C. A. (2009). Building life-cycle cost analysis due to mainshock and aftershock occurrences. *Structural Safety*, 31(5), 396-408.
- Zaghi, A. E., Padgett, J. E., Bruneau, M., Barbato, M., Li, Y., Mitrani-Reiser, J., and McBride, A. (2016). Establishing common nomenclature, characterizing the problem, and identifying future opportunities in multihazard design. *Journal of structural engineering*, 142(12), H2516001.
- Zhang, N., Alipour, A., and Coronel, L. (2018a). Application of novel recovery techniques to enhance the resilience of transportation networks. *Transportation research record*, 2672(1), 138-147.
- Zhang, W., Wang, N., and Nicholson, C. (2017). Resilience-based post-disaster recovery strategies for road-bridge networks. *Structure and Infrastructure Engineering*, 13(11), 1404-1413.
- Zhang, X., Wang, J., Zhao, Y., Tang, L., and Xing, F. (2015). Time-dependent probability assessment for chloride induced corrosion of RC structures using the third-moment method. *Construction and Building Materials*, 76, 232-244.

- Zhang, Y., Kim, C.-W., Beer, M., Dai, H., and Soares, C. G. (2018b). Modeling multivariate ocean data using asymmetric copulas. *Coastal Engineering*, 135, 91-111.
- Zhao, Y. G., and Lu, Z. H. (2007). Fourth-moment standardization for structural reliability assessment. *Journal of structural engineering*, 133(7), 916-924.
- Zhao, Y. G., and Ono, T. (2001). Moment methods for structural reliability. *Structural Safety*, 23(1), 47-75.
- Zheng, Y., Dong, Y., and Li, Y. (2018). Resilience and life-cycle performance of smart bridges with shape memory alloy (SMA)-cable-based bearings. *Construction and Building Materials*, 158, 389-400.
- Zhong, J., Gardoni, P., and Rosowsky, D. (2010). Stiffness degradation and time to cracking of cover concrete in reinforced concrete structures subject to corrosion. *Journal of engineering mechanics*, 136(2), 209-219.
- Zhou, X., and Zhang, X. (2019). Thoughts on the development of bridge technology in China. *Engineering*, 5(6), 1120-1130.
- Zhu, B., and Frangopol, D. M. (2016). Time-variant risk assessment of bridges with partially and fully closed lanes due to traffic loading and scour. *Journal of Bridge Engineering*, 21(6), 04016021.
- Zhu, D., and Dong, Y. (2020). Experimental and 3D numerical investigation of solitary wave forces on coastal bridges. *Ocean Engineering*, 209, 107499.